Computational Modelling of Singlet Fission

Wibowo, Meilani Kurniawati

Computational Modelling of Singlet Fission

From the static picture to fission dynamics

Meilani Wibowo

Computational Modelling of Singlet Fission

From the static picture to fission dynamics

Zernike Institute PhD thesis series 2019-12
ISSN: 1570-1530
ISBN: 978-94-034-1511-6 (printed version)
ISBN: 978-94-034-1510-9 (electronic version)

The research presented in this thesis has been performed in the Theoretical Chemistry Group of the Zernike Institute for Advanced Materials at the University of Groningen, The Netherlands and in the Department of Chemistry and Industrial Chemistry, University of Pisa, Italy. This PhD project is a part of the Innovative Training Network–European Joint Doctorate (ITN–EJD) in Theoretical Chemistry and Computational Modelling (TCCM) programme, funded by the European Union's Horizon 2020 research and innovation programme under the Marie Skłodowska–Curie Actions grant agreement No. 642294 (ITN–EJD–642294–TCCM).

university of groningen / faculty of science and engineering / zernike institute for advanced materials

MARIE CURIE ACTIONS TCCM

Cover designed by Meilani Wibowo and finalised by Peggy Sanjaya.

Printed by Gildeprint – Enschede.

university of groningen

UNIVERSITÀ DI PISA

Computational Modelling of Singlet Fission

From the static picture to fission dynamics

PhD thesis

to obtain the degree of PhD at the
University of Groningen
on the authority of the
Rector Magnificus Prof. E. Sterken
and in accordance with
the decision by the College of Deans,

and

to obtain the degree of PhD at the
University of Pisa
on the authority of the
Rector Prof. P.M. Mancarella
and in accordance with
the decision by the Council of the Doctorate in Chemistry and Materials Science.

Double PhD degree

This thesis will be defended in public on

Friday 10 May 2019 at 16.15 hours

by

Meilani Kurniawati Wibowo

born on 19 May 1989
in Surabaya, Indonesia

Supervisors

Prof. R. Broer

Prof. M. Persico

Prof. G. Granucci

Co-supervisor

Dr. R.W.A. Havenith

Assessment committee

Prof. S. Faraji

Prof. F.C. Grozema

Prof. N. Guihéry

Prof. B. Mennucci

For my late mother, Linawati Tjio, who had never given up,

&

for my father, Agus Wibowo Jong, who always be there for us.

Success and failure is a lifetime's journey.
We need initiative and courage to start and to decide what we want to do.
We need enthusiasm, hard work, perseverance, and sacrifice to achieve the goal.
Enjoy everything that we are doing and learning to do.

Contents

Chapter 1 Introduction

A brief introduction to the research topic in this thesis—singlet fission—and thesis outline are presented. This brief introduction includes a short history on singlet fission, singlet fission chromophores, singlet fission mechanisms, fission dynamics, and applications of singlet fission in solar cells. It starts from the theory of singlet fission, follows with some experimental measurements used to detect the occurrence of singlet fission, and concludes with the development of theoretical chemistry and computational modelling for unveiling the mechanism and dynamics of singlet fission–which is the aim of the research conducted in this thesis. With the aid of static quantum chemical calculations and nonadiabatic excited state dynamics simulations, a comprehensive understanding of singlet fission will potentially be achieved.

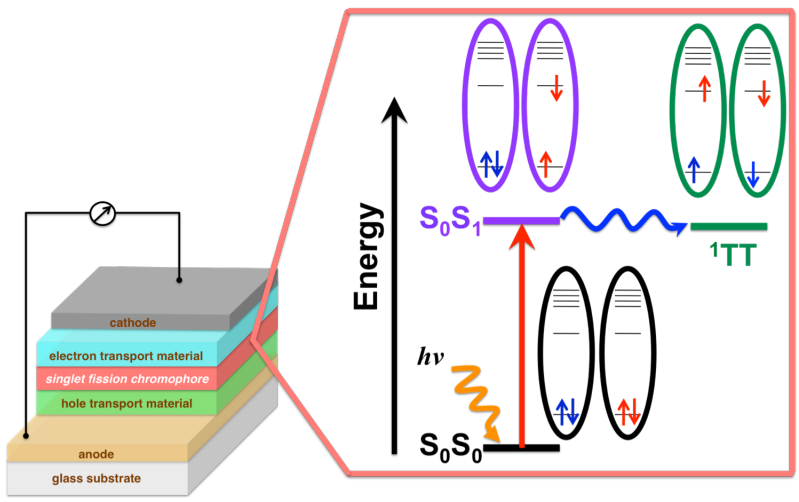

1.1 Singlet Fission

Singlet fission (SF) is a process whereby a photogenerated excited singlet state (S_1) of a chromophore transfers part of its energy to a neighbouring ground state (S_0) chromophore, and both are converted into two (local) triplets, coupled into a total spin singlet (^{1}TT), $S_1 + S_0 \rightarrow {}^1\text{TT}$.[1,2] It was first observed in 1965[3] in the course of a study of delayed fluorescence of anthracene single crystals. In 1968[4] the SF phenomenon was invoked to interpret the temperature dependence of the radiationless decay in crystalline tetracene and one year later the occurrence of singlet exciton fission was proven in the study of magnetic field effects on crystalline tetracene.[5,6] This phenomenon was neglected until 2004,[7] when it was suggested that SF could actually improve the efficiency of photovoltaic cells: then this hardly known subject became popular.

The detailed balance limit efficiency (theoretical efficiency) of a single junction solar cell is defined as the ratio of the generated electrical energy to the incident solar energy. It was first calculated in the seminal paper by Shockley and Queisser.[8] Under ideal conditions for photovoltaic cells with an optimal band gap energy (E_g) of about 1.34 eV, this theoretical efficiency limit is only about 30% due to four unavoidable loss mechanisms:[9] (i) lack of absorption of low-energy photons ($E \leq E_g$), (ii) thermalisation of high-energy photons ($E \geq E_g$), (iii) thermodynamic loss, and (iv) radiative recombination of the excited state with the ground state. The first two-loss mechanisms—known as spectral mismatch—contribute the most to limit this theoretical efficiency.

To minimise the spectral mismatch, two strategies have been proposed: (i) transforming the incoming solar spectrum to match the semiconductor features of single band gap solar cells, and (ii) combining several semiconductor materials to better exploit the available solar spectrum. The first strategy can be attained by the up- and down-conversion processes of low- and high-energy photons.[10,11] In the up-conversion process, the sub-band gap photons are converted into supra-band gap photons, which then can be absorbed by the solar cells. In down-conversion, on the other hand, one high-energy photon is cut into two low-energy photons. If both low-energy photons are absorbed by the solar cell, its efficiency increases up to 40%.[11] The second strategy has been successfully applied in the so-called multi junction (tandem) solar cells,[12] where multiple cells made from different semiconductor materials with

different band gaps are stacked and each cell absorbs a different fraction of the solar spectrum. With an infinite number of junctions, the theoretical efficiency will reach about 85%.[12] The theoretical efficiency of a multi junction solar cell with a finite number of junctions, which contains a light harvesting material capable of exhibiting SF could increase up to 45%.[13,14]

Since it was suggested that SF could improve the efficiency of photovoltaic cells,[7,14] the main goal of the research on SF is, of course, to apply it in the third generation of organic solar cells.[12,15,16] The promising potential to incorporate SF chromophores in solar cells is to decrease the energy losses due to spectral mismatch by absorbing high-energy photons in order to generate multiple electron-hole pairs, which are capable of charge separation.[12]

The SF solar cells require at least two light harvesting materials: (i) a SF chromophore that is able to absorb the high-energy photons, and (ii) a semiconductor material for converting each low-energy photon into a single electron-hole pair.[14,17] The first application of SF solar cells used the combination of poly(3-hexylthiophene) and pentacene (SF chromophore) as an electron donor and C_{60} as an electron acceptor in the active layer.[18] The architecture of this SF solar cell—like that of the tandem solar cell—is very complex. For instance, for a maximum triplet exciton dissociation of SF chromophore—a critical process for engineering a high performance SF solar cell—the incorporation of a thin blocking layer at the interface between the transparent conducting film indium tin oxide and pentacene is required.[16,19,20] This additional requirement makes the engineering of SF solar cells is a challenging task. Despite its complexity, this SF solar cell has been reported to achieve an external quantum efficiency, which is defined as the ratio between the number of electrons collected by the solar cell to the number of incident photons, of 126% and an internal quantum efficiency—the number of electrons collected per absorbed photon—of about 200%; this cannot be achieved with a single junction solar cell.[19,20] Since then, different combinations of SF chromophores, electron donors, electron acceptors, and blocking layer materials have been proposed and tested in order to boost the performance of SF solar cells.[17,19-22] Alternatively, to improve the performance of solar cells one can use SF chromophores as sensitizers, for instance, in the applications of SF quantum dot solar cells,[23] SF dye-sensitised solar cells,[24] silicon SF parallel tandem solar cells,[25] and SF perovskite solar cells.[26]

SF can also be seen as an internal conversion (IC) process, *i.e.* a radiationless process between states with the same spin multiplicity, and it is a spin-allowed process. SF can be a

very fast process, occurring on a picosecond (ps) or even a sub-ps time scale. SF can occur efficiently in pairs of certain molecules (chromophores) in which the energy of the molecular S_1 state is equal to or higher than twice the energy of the T_1 state, $\Delta E(S_1) \geq 2\Delta E(T_1)$, so that SF is exoergic.[1,2] These energy differences can be evaluated as vertical transition energies (at the equilibrium geometry of the S_0 state) or, better, as adiabatic transition energies (minimum-to-minimum) in order to take into account the vibrational relaxation.

One plausible interfering path to SF is the recombination of the ^{1}TT state into a single-molecule excited state, for instance, the T_2 state. To avoid the occurrence of this recombination, an additional energetic criterion for SF chromophores is required, *i.e.* the energy of the T_2 state should be higher than twice the energy of the T_1 state, $\Delta E(T_2) > 2\Delta E(T_1)$, and preferably also higher than that of the S_1 state, $\Delta E(T_2) > \Delta E(S_1)$.[1,2] The former guarantees that the triplet-triplet annihilation process is energetically forbidden, while the latter requirement ensures no fast intersystem crossing (ISC) transition takes place after the initial photoexcitation.

1.2 Singlet Fission Chromophores

For a chromophore to show efficient SF, the $S_1 + S_0 \rightarrow {}^1$TT process should be exoergic, isoergic, or at least not significantly endoergic, and no other processes should compete with it significantly. Therefore, SF has to be faster than other intra- and inter-molecular relaxation processes such as fluorescence, IC, ISC, excimer formation, and exciton dissociation that may occur in a dimer, in an aggregate, or in a crystal. In addition, the chemical stability of the chromophore, particularly under solar irradiation, should be considered. For the application of SF in solar cells, one can start to search for potential SF chromophores from molecules with a fluorescence quantum yield close to unity and that have a high absorption coefficient in the visible solar spectrum. Most organic molecules with a conjugated π-system usually exhibit broad absorption bands. Depending on the nature of their ground state, two main classes of potential SF chromophores have been identified: alternant hydrocarbons and biradicaloids.[1,2] The ground state of the former class is a closed-shell state, whereas the latter has a partial open-shell ground state character.

1.2.1 Alternant Hydrocarbons

The ground state (S_0) wave function of alternant hydrocarbons can be approximated by a closed-shell single Slater determinant, while the lowest singlet and triplet excited states (S_1 and T_1) can be represented by singlet and triplet excitations from the highest occupied molecular orbital (HOMO, ϕ_h) to the lowest unoccupied molecular orbital (LUMO, ϕ_l). The S_0, S_1, and T_1 (for each m_s component) wave functions can be approximated as $\Psi(S_0) \simeq \left(\left|\phi_1\phi_2 \ldots \phi_h\bar{\phi}_h\right|\right)$, $\Psi(S_1) \simeq \frac{1}{\sqrt{2}}\left(\left|\phi_1\phi_2 \ldots \phi_h\bar{\phi}_l\right| - \left|\phi_1\phi_2 \ldots \bar{\phi}_h\phi_l\right|\right)$, $\Psi\left(T_{1,m_s=1}\right) \simeq \left(\left|\phi_1\phi_2 \ldots \phi_h\phi_l\right|\right)$, $\Psi\left(T_{1,m_s=0}\right) \simeq \frac{1}{\sqrt{2}}\left(\left|\phi_1\phi_2 \ldots \phi_h\bar{\phi}_l\right| + \left|\phi_1\phi_2 \ldots \bar{\phi}_h\phi_l\right|\right)$, and $\Psi\left(T_{1,m_s=-1}\right) \simeq \left(\left|\phi_1\phi_2 \ldots \bar{\phi}_h\bar{\phi}_l\right|\right)$, respectively, where $\phi_1\phi_2 \ldots$ represent other occupied molecular orbitals that are not involved in the excitation and the overbar sign indicates the β spin of HOMO and LUMO.

The energy splitting $\Delta E(S_1) - \Delta E(T_1)$ is approximately twice the exchange integral $2K_{hl}$. It will be maximised if the HOMO and LUMO occupy the same region of space. As the size of conjugated π-system increases, this exchange integral does not change significantly, whereas the S_1–S_0 energy gap, $\Delta E(S_1)$, decreases. To obtain alternant hydrocarbons for which the energy splitting between the S_1 and T_1 states is nearly equal to one half of the S_1–S_0 energy gap, that is, $\Delta E(S_1) - \Delta E(T_1) \simeq \frac{1}{2}\Delta E(S_1)$, one can increase the size of the conjugated π-systems. This situation is (nearly) fulfilled in a conjugated π-system with about 20 carbon atoms as, for instance, pentacene ($C_{22}H_{14}$).[27-29] Some examples of alternant hydrocarbons for which SF has been observed experimentally (**1**–**3**)[4,6,27-32] and have been proposed as potential SF chromophores (**4**–**9**)[33-35] are presented in Figure 1.1.

In a polycrystalline film of pentacene (**1**), the experimental measured S_1 energy is about 1.83 eV,[28,29] and twice the T_1 energy is about 1.62 eV.[27] This measurement makes **1** as the shortest polyacene for which SF is exoergic by about 0.2 eV. In shorter polyacenes, such as anthracene (**3**)[30,31] and tetracene (**2**),[4,6,32] SF has been observed, although it is slightly endoergic by about 0.5 eV and 0.2 eV, respectively. Several experimental and computational studies have tried to modify the anthracene, tetracene and pentacene structures either by replacing some carbon atoms with other heteroatoms or by chemical functionalization (**4**–**9**),

as shown in Figure 1.1, in order to match better the low-lying singlet and triplet energies with the optimal conditions for SF chromophores and to further improve their photochemical stabilities.[33,34,36]

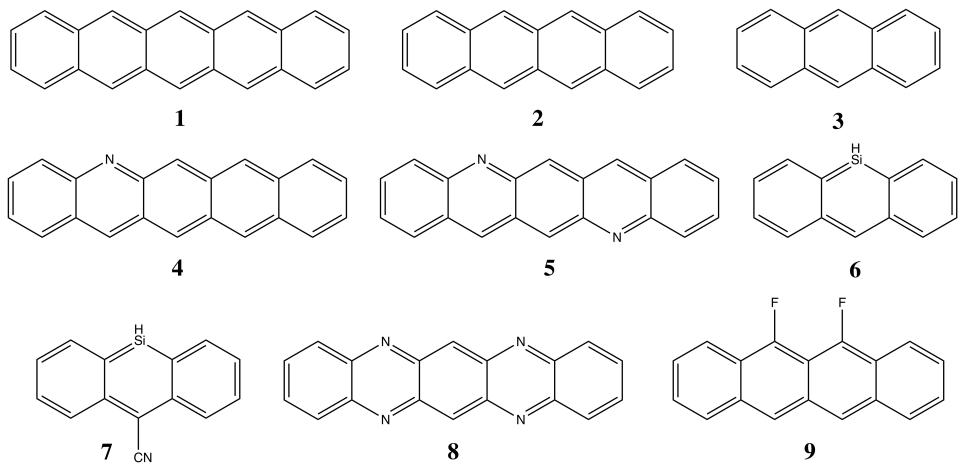

Figure 1.1 Chemical structures of alternant hydrocarbons for which SF has been observed (**1**–**3**) and which have been proposed as potential SF chromophores (**4**–**9**).

1.2.2 Biradicaloids

For a perfect biradical structure that can be described with two unpaired electrons in two (nearly) degenerate orbitals ϕ_a and ϕ_b, four approximate low-energy states can be constructed: open-shell ground state (S_0), open-shell triplet state (T_1), and two closed-shell excited singlet states (S_1 and S_2). The wave function for each state can be written as $\Psi(S_0) \simeq \frac{1}{\sqrt{2}}\left(|\phi_a\bar{\phi}_b| - |\bar{\phi}_a\phi_b|\right)$, $\Psi(T_1) \simeq \frac{1}{\sqrt{2}}\left(|\phi_a\bar{\phi}_b| + |\bar{\phi}_a\phi_b|\right)$, $\Psi(S_1) \simeq \frac{1}{\sqrt{2}}\left(|\phi_a\bar{\phi}_a| + |\bar{\phi}_b\phi_b|\right)$, and $\Psi(S_2) \simeq \frac{1}{\sqrt{2}}\left(|\phi_a\bar{\phi}_a| - |\bar{\phi}_b\phi_b|\right)$, where the overbar sign indicates the β spin of ϕ_a and ϕ_b orbitals. The two closed-shell states (S_1 and S_2) are typically found at higher energy than the two open-shell states (S_0 and T_1). The energy splitting between the T_1 and S_0 states as well as between the S_2 and S_1 states is relatively small and is approximated by twice the exchange integral $2K_{ab}$.

There are two types of biradicals: disjoint and nondisjoint biradicals. In disjoint biradicals, the two (nearly) degenerate orbitals are localised. This localisation decreases the $2K_{ab}$ value, produces quasi-degenerate S_0 and T_1 states, and keeps the higher-lying S_1 and S_2 states unchanged. On the contrary, in nondisjoint biradicals, the localisation is less perfect and the T_1 energy is significantly decreased, resulting in a triplet ground state. Only a few molecules belong to these two extreme types, for example, tetramethyleneethane (disjoint biradical) and trimethylenemethane (nondisjoint biradical), and many biradicals are intermediate between these two and typically are unstable molecules.

To produce a stable molecule starting from a perfect biradical structure, one needs to break the degeneracy of the two (nearly) degenerate molecular orbitals. Structural perturbation of perfect biradical structures can lift the degeneracy of ϕ_a and ϕ_b orbitals and gives place to more stable molecules—known as biradicaloids. Such perturbation may be used to tune the energy levels of the singlet and triplet states, which will result in the proper low-lying singlet and triplet energies for SF chromophores. Some examples of biradicaloids that have been proposed as potential SF chromophores are presented in Figure 1.2.[13,37-41]

Among the most extensively studied SF chromophores derived from a parent biradical structure are 1,3-diphenyl-isobenzofuran (**10**) and its derivative (**11**) in which more than 100% triplet yield has been observed.[13,38,39] So far, most of the SF chromophores are typically quite large molecules.[1,2,13,39,42] This challenges computational chemists to perform accurate calculations in order to understand the electronic nature of those molecules and to study their fission dynamics. Inspired by the captodative effect—combination of an electron-withdrawing (captor) and an electron-releasing (donor or dative) in radical centres—that leads to an enhanced stabilisation of radicals,[43] several computational studies have tried to find relatively small and stable molecules having low-lying singlet and triplet energies that match with the energetic criteria for SF chromophores. Michl and co-workers[37] pioneered this work by joining two small captodatively stabilised biradicaloids into a single conjugated system. They proposed five biradicaloids and computed their low-lying singlet and triplet energies. Based on the quantum chemical calculations, one of the proposed biradicaloids, which is derived from the structure of 2,5-diketopiperazine, namely the bis(inner salt) of 2,5-dihydroxy-1,4-dimethyl-pyrazinium (**12**) is expected to satisfy the energetic conditions for SF chromophores, $\Delta E(S_1) \approx 2\Delta E(T_1)$.[37] Therefore, this biradicaloid had been chosen as a potential SF chromophore studied in this thesis. A plausible crystal structure and the electronic couplings

between the initial and final diabatic states in three different pairs taken from this plausible crystal structure were computed, and in addition, its possible fission dynamics were explored.

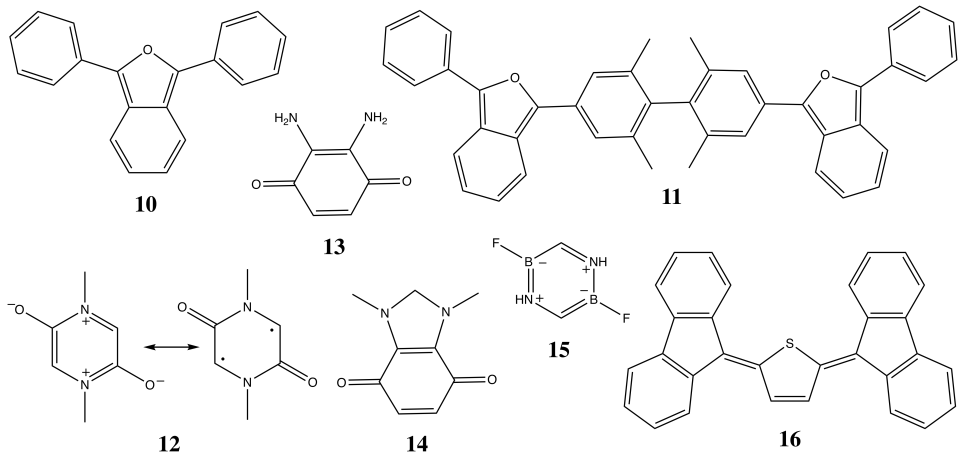

Figure 1.2 Chemical structures of biradicaloids that have been proposed as potential SF chromophores.

Several other biradicaloids have also been proposed and investigated theoretically. Some of their chemical structures (**13**–**15**) are shown in Figure 1.2.[40,41] Recently, some non-polycyclic aromatic molecules have been designed and synthesised as potential SF chromophores. These molecules are designed based on the biradicaloid character of thienoquinoid molecules, which have been previously reported as organic transistor molecules. These molecules show a resonance structure between a closed-shell quinoid and an open-shell biradical structure. One of these newly synthesised molecules is 2,5-bis(fluorene-9-ylidene)-2,5-dihydrothiophene (**16**).[22] Its SF character was examined by means of the magnetic field response on the photocurrent measurements of the organic photovoltaic devices that used these molecules as electron donor in the active layer. Besides, on the basis of quantum chemical calculations, these molecules also satisfy the basic energetic conditions for SF chromophores. However, its SF mechanism, fission dynamics, SF quantum yield, and the excited state lifetimes are hitherto unknown. Therefore, this molecule had also been chosen as a potential SF chromophore studied in this thesis for which the fission dynamics and the time scales involved in each process were investigated in detail.

1.3 Chromophore Couplings

The kinetic scheme of SF and subsequent dissociation of singlet coupled triplet states can be written as

$$S_1 + S_0 \underset{k_{-1}}{\overset{k_1}{\rightleftharpoons}} {}^1TT \underset{k_{-2}}{\overset{k_2}{\rightleftharpoons}} T_1 + T_1, \tag{1.1}$$

where k_1 and k_{-1} correspond to the rate constants of interconversion of the $S_1 + S_0$ and the ^1TT states, while k_2 and k_{-2} correspond to the rate constants of interconversion of the ^1TT and the $T_1 + T_1$ states. The former, which is the primary process of SF, can be modelled as a first-order reaction. In the limit of weak coupling between initial and final states, the SF rate constant can be expressed by Fermi's golden rule,[1,2]

$$k_{SF} = \frac{2\pi}{\hbar} \left|V_{if}\right|^2 \rho\left(E_i \simeq E_f\right), \tag{1.2}$$

where V_{if} is the coupling between initial (i) and final (f) electronic states, and $\rho\left(E_i \simeq E_f\right)$ is the Franck-Condon weighted density of states. The argument of $\rho\left(E_i \simeq E_f\right)$ ascertains the isoergicity of the process. Eq. (1.2) associates the SF rate constant with the coupling between initial and final states V_{if}. The magnitude of $\left|V_{if}\right|^2$ is approximately proportional to the SF rate in the weak coupling limit, but it remains a crucial parameter to determine the SF probability even when it is an ultrafast process, which cannot be described by a kinetic rate law. In fact, ultrafast transitions normally occur at surface crossings, and in the SF context, this occurs when the S_1 and ^1TT states are close in energy. In such cases, simplified treatments of the nonadiabatic dynamics such as the Landau-Zener rule give a realistic description of the dynamics at the surface crossing and emphasise the role of this coupling parameter $\left|V_{if}\right|^2$.[44,45]

To describe the states involved in SF with well-defined electronic character, the diabatic state representation is often used. In the diabatic picture, the coupling—electronic coupling—is just a matrix element of the electronic Hamiltonian between electronic diabatic states η_I and η_J,

$$V_{IJ} = \left\langle \eta_I \left| \hat{\mathcal{H}}_{el} \right| \eta_J \right\rangle, \tag{1.3}$$

whereas in the adiabatic state representation the interaction between states is given by the dynamics or derivative coupling, which is a differential Hamiltonian operator in the space of vibrational states.

1.3.1 Electronic Coupling

Based on the SF mechanisms, the electronic coupling can be computed by taking into account the contributions either from the direct mechanism or from the mediated mechanism, depicted in Figure 1.3. In the direct mechanism, the electronic coupling V_{if} in Eq. (1.2) involves the electronic Hamiltonian matrix element between the initial $\left|\mathrm{S_1S_0}\right\rangle$ and final $\left|{}^1\mathrm{TT}\right\rangle$ diabatic states of the pair of chromophores, which can be expressed as

$$\left|V_{if}\right|^2 = \left|\left\langle \mathrm{S_1S_0}\left|\hat{\mathcal{H}}_{el}\right|{}^1\mathrm{TT}\right\rangle\right|^2 . \tag{1.4}$$

In the mediated mechanism, on the other hand, the charge transfer states are formed either as virtual or intermediate states through the superexchange mechanism or through the transfer of an electron from one chromophore to its neighbour. The virtual charge transfer states, which typically higher in energy, may interact with both the initial $\left|\mathrm{S_1S_0}\right\rangle$ and final $\left|{}^1\mathrm{TT}\right\rangle$ diabatic states, facilitating the fission process. Besides, the ^{1}TT state can also be formed through the formation of intermediate charge transfer states whereby an electron from the excited singlet state is transferred to the neighbouring ground state, forming singlet coupled cation-anion $\left|{}^1\mathrm{CA}\right\rangle$ and anion-cation $\left|{}^1\mathrm{AC}\right\rangle$ pairs, illustrated in Figure 1.3 with red arrows. The electronic coupling matrix element V_{if} , which appears in Eq. (1.2), contains also contributions from these intermediate states. Then, Eq. (1.2) can be expressed as

$$k_{SF} = \frac{2\pi}{\hbar}\left|V_{if} - \sum_{m\neq i,f}\frac{V_{im}V_{mf}}{E_m - E_{i,f}}\right|^2 \rho\left(E_i \simeq E_f\right), \tag{1.5}$$

where V_{im} (and V_{mf}) are the electronic couplings between the initial (and final) and intermediate charge transfer states, and $E_m - E_{i,f}$ is the energy difference between the intermediate charge transfer states and the nearly degenerate $\left|\mathrm{S_1S_0}\right\rangle$ and $\left|{}^1\mathrm{TT}\right\rangle$ states.

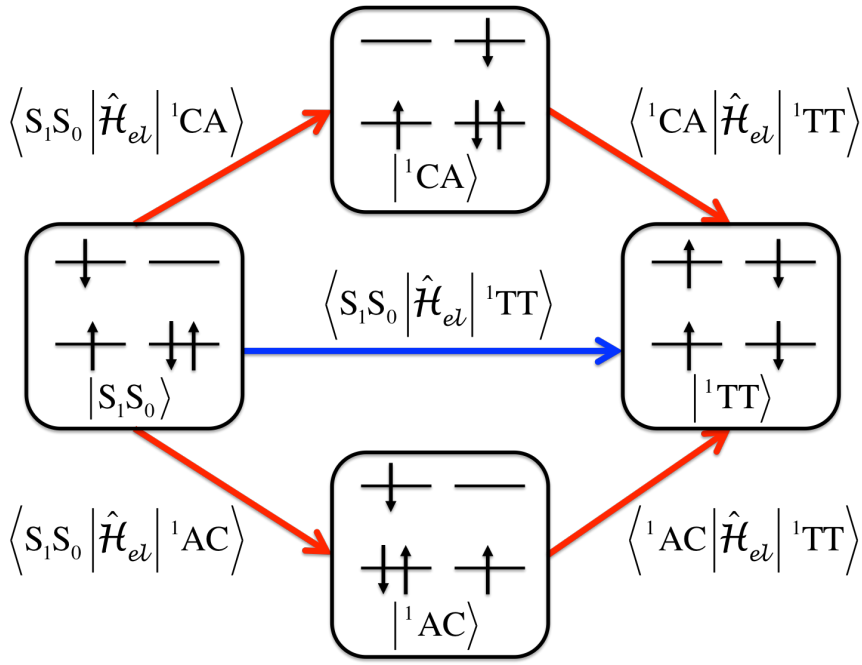

Figure 1.3 Diagrammatic representations of the SF mechanisms in a pair of two molecules within the HOMO/LUMO model. The charge-transfer configurations are indicated as a singlet coupled cation-anion (^{1}CA) and anion-cation (^{1}AC). The direct and mediated mechanisms are represented as blue and red arrows, respectively.

The electronic couplings entering Eq. (1.5) can also be written in terms of the electronic Hamiltonian matrix elements such that,[2,46]

$$\left|V_{if}-\sum_{m\neq i,f}\frac{V_{im}V_{mf}}{E_m-E_{i,f}}\right|^2=\left|\langle S_1S_0|\hat{\mathcal{H}}_{el}|{}^1TT\rangle-\left\{\frac{\langle S_1S_0|\hat{\mathcal{H}}_{el}|{}^1CA\rangle\langle {}^1CA|\hat{\mathcal{H}}_{el}|{}^1TT\rangle}{\Delta E({}^1CA)}+\frac{\langle S_1S_0|\hat{\mathcal{H}}_{el}|{}^1AC\rangle\langle {}^1AC|\hat{\mathcal{H}}_{el}|{}^1TT\rangle}{\Delta E({}^1AC)}\right\}\right|^2. \quad (1.6)$$

The electronic couplings are typically used to describe various photophysical processes, such as electron transfer and excitation energy transfer processes,[47,48] which occur in many organic, inorganic, and biochemical systems. Many different approaches have been developed to simplify the computation of electronic couplings.[1,2,46,49,50] The scheme described by Michl *et al*. in their review papers[1,2] is perhaps the most well known approach to compute electronic

couplings in SF. It has been employed to search for the mutual orientations between two chromophores that yield optimal couplings for an efficient SF.[42,46,51] Moreover, this scheme has also been used to build an effective electronic Hamiltonian for exploring the fission dynamics.[52-54]

The scheme described by Michl and co-workers[1,2] is based on the HOMO/LUMO model. In this scheme, the diabatic wave functions of a pair of two molecules are described by single Slater determinants, constructed from one orthonormal set of the MOs for each molecule, with the assumption that the two sets are strongly orthogonal. Hence, the matrix elements can be expressed in terms of one- and two-electron integrals such that,

$$\left\langle \mathrm{S_1S_0}\left|\hat{\mathcal{H}}_{el}\right|{}^1\mathrm{TT}\right\rangle = \sqrt{\frac{3}{2}}\left[\left\langle l_A l_B\left|\frac{1}{r_{12}}\right|h_B l_A\right\rangle - \left\langle h_A h_B\left|\frac{1}{r_{12}}\right|l_B h_A\right\rangle\right], \tag{1.7}$$

$$\left\langle \mathrm{S_1S_0}\left|\hat{\mathcal{H}}_{el}\right|{}^1\mathrm{CA}\right\rangle = \left\langle l_A\left|\hat{F}\right|l_B\right\rangle + 2\left\langle h_A l_A\left|\frac{1}{r_{12}}\right|l_B h_A\right\rangle - \left\langle h_A l_A\left|\frac{1}{r_{12}}\right|h_A l_B\right\rangle, \tag{1.8}$$

$$\left\langle {}^1\mathrm{CA}\left|\hat{\mathcal{H}}_{el}\right|{}^1\mathrm{TT}\right\rangle = \sqrt{\frac{3}{2}}\left[\left\langle l_A\left|\hat{F}\right|h_B\right\rangle + 2\left\langle l_A l_B\left|\frac{1}{r_{12}}\right|h_B l_B\right\rangle - \left\langle l_A h_A\left|\frac{1}{r_{12}}\right|h_B h_A\right\rangle\right], \tag{1.9}$$

$$\left\langle \mathrm{S_1S_0}\left|\hat{\mathcal{H}}_{el}\right|\mathrm{S_0S_1}\right\rangle = 2\left\langle h_A l_B\left|\frac{1}{r_{12}}\right|l_A h_B\right\rangle - \left\langle h_A l_B\left|\frac{1}{r_{12}}\right|h_B l_A\right\rangle, \tag{1.10}$$

$$\left\langle {}^1\mathrm{CA}\left|\hat{\mathcal{H}}_{el}\right|{}^1\mathrm{AC}\right\rangle = 2\left\langle h_A l_A\left|\frac{1}{r_{12}}\right|l_B h_B\right\rangle - \left\langle h_A l_A\left|\frac{1}{r_{12}}\right|h_B l_B\right\rangle, \tag{1.11}$$

where *h* and *l* correspond to the HOMO and LUMO, the subindices *A* and *B* indicate different molecules, and $\left\langle i\left|\hat{F}\right|j\right\rangle$ is a Fock matrix element. Because only the HOMO and LUMO of each molecule appear in the expressions for the matrix elements, hence the name is HOMO/LUMO model. This simple model suggests that larger couplings may arise from the contributions of one-electron integrals, which are present in the electronic couplings between initial (final) and intermediate states.

If the two molecules are equivalent by symmetry, the equalities $E\left(\mathrm{S_1S_0}\right) = E\left(\mathrm{S_0S_1}\right)$ and $E\left({}^1\mathrm{CA}\right) = E\left({}^1\mathrm{AC}\right)$ hold, and therefore, the excitations are delocalised over two molecules. In fact, the linear combinations $2^{-1/2}\left(c_1\left|\mathrm{S_1S_0}\right\rangle \pm c_2\left|\mathrm{S_0S_1}\right\rangle\right)$ and $2^{-1/2}\left(c_1\left|{}^1\mathrm{CA}\right\rangle \pm c_2\left|{}^1\mathrm{AC}\right\rangle\right)$ will be approximate eigenstates of the electronic Hamiltonian. In a situation when the $\left|\mathrm{S_1S_0}\right\rangle$ and

$|S_0S_1\rangle$ states are equivalent, the energy splitting of the linear combinations of $2^{-1/2}\left(|S_1S_0\rangle \pm |S_0S_1\rangle\right)$ equals to $2\left\langle S_1S_0\middle|\hat{\mathcal{H}}_{el}\middle|S_0S_1\right\rangle$, and it is known as the Davydov splitting. If the signs of the $|S_1S_0\rangle$ and $|S_0S_1\rangle$ states are chosen such that, $\left\langle S_1S_0\middle|\hat{\mathcal{H}}_{el}\middle|{}^1TT\right\rangle = \left\langle S_0S_1\middle|\hat{\mathcal{H}}_{el}\middle|{}^1TT\right\rangle$, the combination with the minus sign does not interact with the $|{}^1TT\rangle$ state, while the one with the plus sign does. It is then interesting to know which ones are the bright and dark combination states and their energy ordering (see Section 5.3 for more details).

An approach based on the localisation of this HOMO/LUMO model followed by transformation of the Fock matrix to this basis has also been employed to study the vibrational effects on the computed electronic couplings.[49] Alternatively, an approach based on the diabatisation of low-lying adiabatic excited states, the so-called fragment spin difference (FSD) method,[55] has also been proposed for the evaluation of electronic couplings in SF. This approach is originally developed for the calculation of triplet-triplet energy transfer couplings.[56-58] In the FSD method, which is a generalisation of the fragment charge difference method,[59] the diabatic states are constructed as a pair of linear combinations of the two lowest eigenstates $|1\rangle$ and $|2\rangle$ with an energy difference ΔE_{12} and the largest values of the spin difference Δs_{12}. Then, the FSD coupling V_{FSD} is computed as

$$V_{FSD} = \frac{\Delta s_{12}\,\Delta E_{12}}{\sqrt{\left(\Delta s_1 - \Delta s_2\right)^2 + 4\Delta s_{12}^2}}. \tag{1.12}$$

Since the diabatisation in the FSD method focuses on the localisation of spin population of the two lowest eigenstates, the formed diabatic states do not necessarily exhibit pure $|S_1S_0\rangle$ or $|S_0S_1\rangle$ and $|{}^1TT\rangle$ in character. As a consequence, these diabatic states might contain contributions from the charge transfer configurations. A rigorous approach based on the nonorthogonal configuration interaction (NOCI) method[60,61] has also been developed to accurately calculate the electronic couplings in a potential SF chromophore and will be presented in details in Chapter 3.

1.3.2 Derivative Coupling

In the adiabatic picture, the electronic couplings vanish. Instead, the nonadiabatic couplings, which are also called vibronic couplings (see Section 2.1), govern the transitions between states. Recent experimental studies using transient spectroscopy have shown the existence of strong vibronic coupling and coherent nuclear vibration in the 5,12-bis(triisopropylsilylethynyl)-tetracene (TIPS-tetracene) and 6,13-bis(triisopropylsilylethynyl)-pentacene (TIPS-pentacene). These studies demonstrated that a strong vibronic coupling between the S_1 and ^{1}TT states induces the ultrafast IC of $S_1 \rightarrow {}^1$TT .[62,63]

In practice, the calculation of nonadiabatic couplings is not a standard option in many quantum chemical packages. However, analytical expressions for the calculations of nonadiabatic couplings within the Frenkel-Davydov exciton model have been developed and have been employed to study excited states in molecular crystals and in aggregates.[64] This methodology has also been applied to investigate the importance of vibronic couplings for a coherent SF mechanism that proceeds spontaneously despite the endoergicity of SF in crystalline tetracene.[65]

A theoretical model based on the concept of vibronic coupling density has been proposed to analyse the role of vibronic couplings in SF.[66] In this model, the derivatives of the electronic Hamiltonian are expressed in terms of electron densities $\rho_n(\mathbf{r})$, transition densities $\rho_{mn}(\mathbf{r})$, and a potential derivative $v_i(\mathbf{r})$ such that,

$$\left.\frac{\partial \hat{\mathcal{H}}_{nn}(\mathbf{Q})}{\partial Q_i}\right|_{\mathbf{Q}=\mathbf{0}} = \int d\mathbf{r}\left(\rho_n(\mathbf{r}) - \rho_0(\mathbf{r})\right) v_i(\mathbf{r})$$
$$\left.\frac{\partial \hat{\mathcal{H}}_{mn}(\mathbf{Q})}{\partial Q_i}\right|_{\mathbf{Q}=\mathbf{0}} = \int d\mathbf{r}\, \rho_{mn}(\mathbf{r})\, v_i(\mathbf{r}) \quad , \tag{1.13}$$

with

$$v_i(\mathbf{r}) = \sum_A^{N_{atom}} \left(\frac{\partial}{\partial Q_i} \frac{-Z_A}{|\mathbf{r}-\mathbf{R}_A|} \right)_{\mathbf{Q}=\mathbf{0}} . \tag{1.14}$$

This model has been applied to study the frequency dependence of Holstein and Peierls vibronic couplings in each electronic excited state of a tetracene dimer model in order to determine specific vibrational modes that influence the spontaneous SF.[67]

A simple approach based on the reduced one-particle transition density matrix between the initial and final adiabatic states, γ_{pq}^{if}, has also been developed to estimate the nonadiabatic couplings.[68] In this approach, the norm of the one-particle transition density matrix $||\gamma||^2$ is assumed to be proportional to the nonadiabatic coupling such that,

$$\gamma_{pq}^{if} \equiv \left\langle \Psi_i \middle| p^+ q \middle| \Psi_f \right\rangle$$
$$||\gamma||^2 \equiv \sum_{pq} \left(\gamma_{pq}^{if}\right)^2 \quad , \tag{1.15}$$

where p^+ and q are the one-particle creation and annihilation operators. This approach has been used to qualitatively evaluate the nonadiabatic couplings, and in particular, to study the trend of nonadiabatic couplings along structural distortions in tetracene and in pentacene.[68] This approach has also been applied to further understand the effect of the morphology on SF rates in different polymorphs of 1,3-diphenylisobenzofuran and its derivatives.[69]

1.4 Singlet Fission Dynamics

The experimental measurements using transient absorption, delayed fluorescence, two dimensional electronic and time-resolved two-photon photoemission spectroscopies have shed light on a more complete understanding of the SF mechanisms and time scales involved. These techniques have also guided some experimental investigations to determine key parameters that control the efficiency of SF, for example, the chemical structure and topology of organic crystals, the polarity of solvents, and the influence of environments.[62,70-72] Besides, the theoretical simulations of the time evolution of fission dynamics help to rationalise the experimental measurements and to complement the static quantum chemical calculations. These investigations will ultimately provide a comprehensive understanding of SF, aid to the design of a molecular structure for efficient SF, and to guide in solar cell engineering. The time evolution of the SF process can be studied either by full quantum dynamics or by mixed quantum-classical (semiclassical) dynamics, for instance, by employing the quantum master equation, wave packet propagation, or trajectory surface hopping approach.

Berkelbach and co-workers[53,54] described a quantum dynamics model based on the Redfield theory and applied it to the Liouville-von Neumann equation. They considered the

coupling of electronic and nuclear degrees of freedom by employing a system-bath type Hamiltonian as the sum of the electronic, phonon, and electron-phonon Hamiltonians such that,

$$\hat{\mathcal{H}}_{tot} = \hat{\mathcal{H}}_{el} + \hat{\mathcal{H}}_{ph} + \hat{\mathcal{H}}_{el-ph}. \tag{1.16}$$

In the description of the electronic Hamiltonian, a set of diabatic states, which consists of the local Frenkel singlet excitation, the intermolecular charge-transfer excitation, and a singlet coupled pair of intramolecular triplet excitations, is used. This electronic Hamiltonian is computed at the ground state geometry, while the phonon Hamiltonian takes into account both the intra- and inter-molecular ground state normal modes of the system, and the electron-phonon Hamiltonian takes into account the interaction between the electronic system and bath. Then, the dynamics of this system-bath Hamiltonian $\hat{\mathcal{H}}_{tot}$, is given by the Liouville-von Neumann equation for the total density matrix $\rho(t)$,

$$\frac{d\rho(t)}{dt} = -\frac{i}{\hbar}\left[\hat{\mathcal{H}}_{tot}, \rho(t)\right]. \tag{1.17}$$

In general, this approximation can either be written in its Markovian or non-Markovian form. If the bath relaxation takes place faster than that of the electronic system, the Markovian form of this time-dependent Redfield equation can be safely applied. On the contrary, if the bath relaxes within the same (or longer) time scale as the electronic system, the non-Markovian form should be used instead. However, the accuracy and applicability of this approximation to study a process of interest in each situation involved should be carefully checked. The application of the Redfield theory to study the SF mechanism in pentacene has been compared with the numerically exact hierarchical equation of motion. The obtained results clarify the role of high-energy (virtual) charge transfer states to mediate the fission process in pentacene dimers.[73] The Markovian form of the Redfield theory has also been applied to understand the role of charge transfer states by taking into account both the coherent and incoherent fission dynamics and to investigate the dependence of different electronic couplings on the displacements along the molecular stacking of perylenediimide, pentacene, and 1,3-diphenylisobenzofuran dimers.[74] In addition, the non-Markovian quantum jump technique within the Redfield theory has been used to explore the role of Holstein and Peierls vibrations in the SF mechanism of perylenediimide and its derivatives.[75]

Tamura *et al*.[76] developed the first principles nonadiabatic quantum dynamical model, which uses the multiconfigurational time-dependent Hartree (MCTDH) method to solve the time-dependent Schrödinger equation (TDSE) of the vibronic coupling Hamiltonian in the diabatic representation. This model has been employed to study the coherent versus thermally activated SF mechanisms in the dimer model of TIPS-pentacene and in rubrene. This study provides evidence that the slip-stacked packing of TIPS-pentacene enhances ultrafast SF by a coherent superexchange mechanism *via* charge transfer states, in contrast to the thermally activated SF mechanism in rubrene where the symmetry breaking vibrations are needed in order to guarantee a non-vanishing coupling between the initial and final states. An improved description using a three-state model combined with the multilayer MCTDH method has also been employed to describe the fission dynamics in pentacene. The results agree well with the previous dynamics simulations based on the Redfield theory.[77]

Prezhdo and co-workers[78] employed a mixed quantum-classical approach based on the self-consistent fewest switches surface hopping (FSSH) technique to investigate the time evolution of fission dynamics in pentacene dimers placed over a large range of mutual orientations. To describe the fission dynamics in pentacene, five electronic diabatic states, *i.e*. the singlet excitation on one of the chromophores (S_1S_0 and S_0S_1), the charge transfer states (^{1}CA and ^{1}AC), and the singlet coupled triplet states (^{1}TT) are included in the description of the electronic Hamiltonian. Additionally, to characterise the electron–phonon interactions the Holstein Hamiltonian is adopted in this approach. The results provide detailed two-dimensional mappings of both instantaneous and long-term triplet yields, characterising the favourable stacking arrangements of pentacene dimers. This study also shows how to increase electronic couplings by tuning the inter-molecular packing. Moreover, the simulations indicate that SF in pentacene is most likely driven by thermal electron-phonon fluctuations at the ambient temperature and at high temperature rather than having a large charge transfer character in the description of photoexcited states. Another semiclassical approach based on the original idea of Tully FSSH approach[79] combined with the floating occupation molecular orbital–configuration interaction (FOMO–CI) method[80-82] has been developed and has been adopted to study not only the fission dynamics of SF chromophores but also other processes that may occur during the dynamics. The details and application of this approach are presented in Chapter 4 and Chapter 5.

1.5 Thesis Outline

The aim of the research performed and described in this thesis is to investigate the SF mechanism and to rationalise the fission dynamics of several potential SF chromophores with the aid of theoretical chemistry and computational modelling. To understand the electronic nature of SF chromophores and their fission dynamics, both static quantum chemical calculations based on the NOCI approach have been performed and the nonadiabatic excited state dynamics simulations based on the trajectory surface hopping approach have been adopted and applied. Then, the results are presented in the following chapters of this thesis and some important aspects and potential directions of the research on SF that have not been touched yet in this thesis are proposed in the last chapter of this thesis.

Chapter 2 introduces briefly the electronic structure and direct semiclassical dynamics simulations methods, which are the main tools used in this thesis. Chapter 3 presents the static quantum chemical calculations based on the NOCI approach for the accurate computations of electronic couplings applied to a potential SF chromophore, namely the bis(inner salt) of 2,5-dihydroxy-1,4-dimethyl-pyrazinium. This chromophore has been designed and proposed as a potential SF chromophore, by showing that the energy levels of the S_1 and T_1 states match with the energetic criteria of SF chromophores, according to quantum chemical calculations. The electronic coupling, in addition, is one important key parameter that can be used to determine the spontaneous SF. Following the results obtained from the static quantum chemical calculations based on the NOCI approach of this potential chromophore, the exploration of its possible fission dynamics employing the direct semiclassical dynamics simulations is presented in Chapter 4.

Chapter 5 presents the SF mechanism, fission dynamics, and time scales involved in each process of the recently synthesised chromophore derived from a resonance structure between closed-shell quinoid and open-shell biradical structures of the thienoquinoidal molecules, namely 2,5-bis(fluorene-9-ylidene)-2,5-dihydrothiophene. This chromophore has been used as the electron donor in organic photovoltaic devices. On the basis of the quantum chemical calculations, this chromophore satisfies the basic energetic conditions of SF chromophores. Besides, based on the magnetic field response of the photocurrent measurements this chromophore shows SF character, although its fission dynamics and mechanisms are unknown.

Chapter 6, the last chapter of this thesis, proposes some important aspects of future research on SF and some potential directions related to the overall process of SF that can be considered and applied not only for the study of SF but also for its application in high-performance solar cells.

1.6 References

(1) Smith, M. B.; Michl, J. Singlet fission. *Chem. Rev.* **2010**, *110*, 6891.

(2) Smith, M. B.; Michl, J. Recent advances in singlet fission. *Annu. Rev. Phys. Chem.* **2013**, *64*, 61.

(3) Singh, S.; Jones, W. J.; Siebrand, W.; Stoicheff, B. P.; Schneider, W. G. Laser generation of excitons and fluorescence in anthracene crystals. *J. Chem. Phys.* **1965**, *42*, 330.

(4) Swenberg, C. E.; Stacy, W. T. Bimolecular radiationless transitions in crystalline tetracene. *Chem. Phys. Lett.* **1968**, *2*, 327.

(5) Merrifield, R. E.; Avakian, P.; Groff, R. P. Fission of singlet excitons into pairs of triplet excitons in tetracene crystals. *Chem. Phys. Lett.* **1969**, *3*, 155.

(6) Geacintov, N.; Pope, M.; Vogel, F. Effect of magnetic field on the fluorescence of tetracene crystals: Exciton fission. *Phys. Rev. Lett.* **1969**, *22*, 593.

(7) Nozik, A. J.; Ellingson, R. J.; Mićić, O. I.; Blackburn, J. L.; Yu, P.; Murphy, J. E.; Beard, M. C.; Rumbles, G. Unique approaches to solar photon conversion based on semiconductor nanostructures and novel molecular chromophores; dynamics of electron relaxation, interfacial charge transfer, and carrier multiplication. Proceedings of the 27th DOE Solar Photochemistry Research Conference, Airline Conference Center, Warrentron, Virginia, 2004.

(8) Shockley, W.; Queisser, H. J. Detailed balance limit of efficiency of p-n junction solar cells. *J. Appl. Phys.* **1961**, *32*, 510.

(9) Archer, M. D.; Bolton, J. R. Requirements for ideal performance of photochemical and photovoltaic solar energy converters. *J. Phys. Chem.* **1990**, *94*, 8028.

(10) Trupke, T.; Green, M. A.; Würfel, P. Improving solar cell efficiencies by up-conversion of sub-band-gap light. *J. Appl. Phys.* **2002**, *92*, 4117.

(11) Trupke, T.; Green, M. A.; Würfel, P. Improving solar cell efficiencies by down-conversion of high-energy photons. *J. Appl. Phys.* **2002**, *92*, 1668.

(12) Green, M. A. *Third Generation Photovoltaics*; Springer-Verlag Berlin Heidelberg: Berlin, Germany, 2003.

(13) Paci, I.; Johnson, J. C.; Chen, X.; Rana, G.; Popovic, D.; David, D. E.; Nozik, A. J.; Ratner, M. A.; Michl, J. Singlet fission for dye-sensitized solar cells: Can a suitable sensitizer be found? *J. Am. Chem. Soc.* **2006**, *128*, 16546.

(14) Hanna, M. C.; Nozik, A. J. Solar conversion efficiency of photovoltaic and photoelectrolysis cells with carrier multiplication absorbers. *J. Appl. Phys.* **2006**, *100*, 074510.

(15) Beard, M. C.; Luther, J. M.; Semonin, O. E.; Nozik, A. J. Third generation photovoltaics based on multiple exciton generation in quantum confined semiconductors. *Acc. Chem. Res.* **2013**, *46*, 1252.

(16) Xia, J.; Sanders, S. N.; Cheng, W.; Low, J. Z.; Liu, J.; Campos, L. M.; Sun, T. Singlet fission: Progress and prospects in solar cells. *Adv. Mater.* **2017**, 1601652.

(17) Lee, J.; Jadhav, P.; Reusswig, P. D.; Yost, S. R.; Thompson, N. J.; Congreve, D. N.; Hontz, E.; Van Voorhis, T.; Baldo, M. A. Singlet exciton fission photovoltaics. *Acc. Chem. Res.* **2013**, *46*, 1300.

(18) Rao, A.; Wilson, M. W. B.; Hodgkiss, J. M.; Albert-Seifried, S.; Bässler, H.; Friend, R. H. Exciton fission and charge generation via triplet excitons in pentacene/C_{60} bilayers. *J. Am. Chem. Soc.* **2010**, *132*, 12698.

(19) Congreve, D. N.; Lee, J.; Thompson, N. J.; Hontz, E.; Yost, S. R.; Reusswig, P. D.; Bahlke, M. E.; Reineke, S.; Van Voorhis, T.; Baldo, M. A. External quantum efficiency above 100% in a singlet-exciton-fission-based organic photovoltaic cell. *Science* **2013**, *340*, 334.

(20) Thompson, N. J.; Congreve, D. N.; Goldberg, D.; Menon, V. M.; Baldo, M. A. Slow light enhanced singlet exciton fission solar cells with a 126% yield of electrons per photon. *Appl. Phys. Lett.* **2013**, *103*, 263302.

(21) Ehrler, B.; Walker, B. J.; Bôhm, M. L.; Wilson, M. W. B.; Vaynzof, Y.; Friend, R. H.; Greenham, N. C. In situ measurement of exciton energy in hybrid singlet-fission solar cells. *Nat. Commun.* **2012**, *3:1019*.

(22) Kawata, S.; Pu, Y.-J.; Saito, A.; Kurashige, Y.; Beppu, T.; Katagiri, H.; Hada, M.; Kido, J. Singlet fission of non-polycyclic aromatic molecules in organic photovoltaics. *Adv. Mater.* **2016**, *28*, 1585.

(23) Ehrler, B.; Wilson, M. W. B.; Rao, A.; Friend, R. H.; Greenham, N. C. Singlet exciton fission-sensitized infrared quantum dot solar cells. *Nano Lett*. **2012**, *12*, 1053.

(24) Schrauben, J. N.; Zhao, Y.; Mercado, C.; Dron, P. I.; Ryerson, J. L.; Michl, J.; Zhu, K.; Johnson, J. C. Photocurrent enhanced by singlet fission in a dye-sensitized solar cell. *ACS Applied Materials & Interfaces* **2015**, *7*, 2286.

(25) Pazos, L. M.; Lee, J. M.; Kirch, A.; Tabachnyk, M.; Friend, R. H.; Ehrler, B. A silicon-singlet fission parallel tandem solar cell exceeding 100% external quantum efficiency. *arXiv preprint* **2015**, *arXiv:1512.07466*.

(26) Lee, S.; Hwang, D.; Jung, S. I.; Kim, D. Electron transfer from triplet state of TIPS-pentacene generated by singlet fission processes to $CH_3NH_3PbI_3$ perovskite. *J. Phys. Chem. Lett*. **2017**, *8*, 884.

(27) Geacintov, N. E.; Burgos, J.; Pope, M.; Strom, C. Heterofission of pentacene excited singlets in pentacene-doped tetracene crystals. *Chem. Phys. Lett*. **1971**, *11*, 504.

(28) Lee, K. O.; Gan, T. T. Influence of substrate temperature on the optical properties of evaporated films of pentacene. *Chem. Phys. Lett*. **1977**, *51*, 120.

(29) Sebastian, L.; Weiser, G.; Bässler, H. Charge transfer transitions in solid tetracene and pentacene studied by electroabsorption. *Chem. Phys*. **1981**, *61*, 125.

(30) Avakian, P.; Abramson, E.; Kepler, R. G.; Caris, J. C. Indirect observation of singlet-triplet absorption in anthracene crystals. *J. Chem. Phys*. **1963**, *39*, 1127.

(31) Wolf, H. C. The electronic spectra of aromatic molecular crystals. *Solid State Phys*. **1959**, *9*, 1.

(32) Tomkiewicz, Y.; Groff, R. P.; Avakian, P. Spectroscopic approach to energetics of exciton fission and fusion in tetracene crystals. *J. Chem. Phys*. **1971**, *54*, 4504.

(33) Kaur, I.; Jia, W.; Kopreski, R. P.; Selvarasah, S.; Dokmeci, M. R.; Pramanik, C.; McGruer, N. E.; Miller, G. P. Substituent effects in pentacenes: Gaining control over HOMO—LUMO gaps and photooxidative resistances. *J. Am. Chem. Soc*. **2008**, *130*, 16274.

(34) Chen, Y.; Shen, L.; Li, X. Effects of heteroatoms of tetracene and pentacene derivatives on their stability and singlet fision. *J. Phys. Chem. A* **2014**, *118*, 5700.

(35) Bhattacharyya, K.; Datta, A. Polymorphism controlled singlet fission in TIPS-anthracene: Role of stacking orientation. *J. Phys. Chem. C* **2017**, *121*, 1412.

(36) Bhattacharyya, K.; Pratik, S. M.; Datta, A. Small organic molecules for efficient singlet fission: Role of silicon substitution. *J. Phys. Chem. C* **2015**, *119*, 25696.

(37) Akdag, A.; Havlas, Z.; Michl, J. Search for a small chromophore with efficient singlet fission: Biradicaloid heterocycles. *J. Am. Chem. Soc.* **2012**, *134*, 14624.

(38) Johnson, J. C.; Michl, J. 1,3-diphenylisobenzofuran: A model chromophore for singlet fission. *Topics in Current Chemistry (Z)* **2017**, *375*, 1.

(39) Johnson, J. C.; Nozik, A. J.; Michl, J. High triplet yield from singlet fission in a thin film of 1,3-diphenylisobenzofuran. *J. Am. Chem. Soc.* **2010**, *132*, 16302.

(40) Wen, J.; Havlas, Z.; Michl, J. Captodatively stabilized biradicaloids as chromophores for singlet fission. *J. Am. Chem. Soc.* **2015**, *137*, 165.

(41) Zeng, T.; Ananth, N.; Hoffmann, R. Seeking small molecules for singlet fission: A heteroatom substitution strategy. *J. Am. Chem. Soc.* **2014**, *136*, 12638.

(42) Johnson, J. C.; Akdag, A.; Zamadar, M.; Chen, X.; Schwerin, A. F.; Paci, I.; Smith, M. B.; Havlas, Z.; Miller, J. R.; Ratner, M. A.; Nozik, A. J.; Michl, J. Toward designed singlet fission: Solution photophysics of two indirectly coupled covalent dimers of 1,3-diphenylisobenzofuran. *J. Phys. Chem. B* **2013**, *117*, 4680.

(43) Viehe, H. G.; Janousek, Z.; Merenyi, R.; Stella, L. The captodative effect. *Acc. Chem. Res.* **1985**, *18*, 148.

(44) Cattaneo, P.; Persico, M. Wave packet dynamics in the presence of a conical intersection. *J. Phys. Chem. A* **1997**, *101*, 3454.

(45) Ferretti, A.; Granucci, G.; Lami, A.; Persico, M.; Villani, G. Quantum mechanical and semiclassical dynamics at a conical intersection. *J. Chem. Phys.* **1996**, *104*, 5517.

(46) Havlas, Z.; Michl, J. Guidance for mutual disposition of chromophores for singlet fission. *Isr. J. Chem.* **2016**, *56*, 96.

(47) Hsu, C.-P. The electronic couplings in electron transfer and excitation energy transfer. *Acc. Chem. Res.* **2009**, *42*, 509.

(48) Newton, M. D. Quantum chemical probes of electron-transfer kinetics: The nature of donor-acceptor interactions. *Chem. Rev.* **1991**, *91*, 767.

(49) Alguire, E. C.; Subotnik, J. E.; Damrauer, N. H. Exploring non-condon effects in a covalent tetracene dimer: How important are vibrations in determining the electronic coupling for singlet fission? *J. Phys. Chem. A* **2015**, *119*, 299.

(50) Kawatsu, T.; Coropceanu, V.; Ye, A.; Brédas, J.-L. Quantum-chemical approach to electronic coupling: Application to charge separation and charge recombination pathways in a

model molecular donor-acceptor system for organic solar cells. *J. Phys. Chem. C* **2008**, *112*, 3429.

(51) Buchanan, E. A.; Havlas, Z.; Michl, J. Singlet fission: Optimization of chromophore dimer geometry, In *Adv. Quantum Chem.*; Zoe Kruze: 2017; Vol. 75, p 175.

(52) Busby, E.; Berkelbach, T. C.; Kumar, B.; Chernikov, A.; Zhong, Y.; Hlaing, H.; Zhu, X.-Y.; Heinz, T. F.; Hybertsen, M. S.; Sfeir, M. Y.; Reichman, D. R.; Nuckolls, C.; Yaffe, O. Multiphonon relaxation slows singlet fission in crystalline hexacene. *J. Am. Chem. Soc.* **2014**, *136*, 10654.

(53) Berkelbach, T. C.; Hybertsen, M. S.; Reichman, D. R. Microscopic theory of singlet exciton fission. I. General formulation. *J. Chem. Phys.* **2013**, *138*, 114102.

(54) Berkelbach, T. C.; Hybertsen, M. S.; Reichman, D. R. Microscopic theory of singlet exciton fission. II. Application to pentacene dimers and the role of superexchange. *J. Chem. Phys.* **2013**, *138*, 114103.

(55) Yang, C.-H.; Hsu, C.-P. First-principle characterization for singlet fission couplings. *J. Phys. Chem. Lett.* **2015**, *6*, 1925.

(56) You, Z.-Q.; Hsu, C.-P. Ab initio study on triplet excitation energy transfer in photosynthetic light-harvesting complexes. *J. Phys. Chem. A* **2011**, *115*, 4092.

(57) You, Z.-Q.; Hsu, C.-P. The fragment spin difference scheme for triplet-triplet energy transfer coupling. *J. Chem. Phys.* **2010**, *133*, 074105.

(58) You, Z.-Q.; Hsu, C.-P. Theory and calculation for the electronic coupling in excitation energy transfer. *Int. J. Quantum Chem.* **2014**, *114*, 102.

(59) Voityuk, A. A.; Rösch, N. Fragment charge difference method for estimating donor-acceptor electronic coupling: Application to DNA phi-stacks. *J. Chem. Phys.* **2002**, *117*, 5607.

(60) Havenith, R. W. A.; De Gier, H. D.; Broer, R. Explorative computational study of the singlet fission process. *Mol. Phys.* **2012**, *110*, 2445.

(61) Wibowo, M.; Broer, R.; Havenith, R. W. A. A rigorous nonorthogonal configuration interaction approach for the calculation of electronic couplings between diabatic states applied to singlet fission. *Comput. Theor. Chem.* **2017**, *1116*, 190.

(62) Bakulin, A. A.; Morgan, S. E.; Kehoe, T. B.; Wilson, M. W. B.; Chin, A. W.; Zigmantas, D.; Egorova, D.; Rao, A. Real-time observation of multiexcitonic states in ultrafast singlet fission using coherent 2D electronic spectroscopy. *Nat. Chem.* **2016**, *8*, 16.

(63) Musser, A. J.; Liebel, M.; Schnedermann, C.; Wende, T.; Kehoe, T. B.; Rao, A.; Kukura, P. Evidence for conical intersection dynamics mediating ultrafast singlet exciton fission. *Nat. Phys.* **2015**, *11*, 352.

(64) Morrison, A. F.; You, Z.-Q.; Herbert, J. M. Ab initio implementation of the Frenkel-Davydov exciton model: A naturally parallelizable approach to computing collective excitations in crystals and aggregates. *J. Chem. Theory Comput.* **2014**, *10*, 5366.

(65) Morrison, A. F.; Herbert, J. M. Evidence for singlet fission driven by vibronic coherence in crystalline tetracene. *J. Phys. Chem. Lett.* **2017**, *8*, 1442.

(66) Sato, T.; Tokunaga, K.; Tanaka, K. Vibronic coupling in cyclopentadienyl radical: A method for calculation of vibronic coupling constant and vibronic coupling density analysis. *J. Chem. Phys.* **2006**, *124*, 024314.

(67) Ito, S.; Nagami, T.; Nakano, M. Density analysis of intra- and intermolecular vibronic couplings toward bath engineering for singlet fission. *J. Phys. Chem. Lett.* **2015**, *6*, 4972.

(68) Feng, X.; Luzanov, A. V.; Krylov, A. I. Fission of entangled spins: An electronic structure perspective. *J. Phys. Chem. Lett.* **2013**, *4*, 3845.

(69) Feng, X.; Kolomeisky, A. B.; Krylov, A. I. Dissecting the effect of morphology on the rates of singlet fission: Insights from theory. *J. Phys. Chem. C* **2014**, *118*, 19608.

(70) Chan, W.-L.; Tritsch, J. R.; Zhu, X.-Y. Harvesting singlet fission for solar energy conversion: One- versus two-electron transfer from the quantum mechanical superposition. *J. Am. Chem. Soc.* **2012**, *134*, 18295.

(71) Monahan, N. R.; Sun, D.; Tamura, H.; Williams, K. W.; Xu, B.; Zhong, Y.; Kumar, B.; Nuckolls, C.; Harutyunyan, A. R.; Chen, G.; Dai, H.-L.; Beljonne, D.; Rao, Y.; Zhu, X.-Y. Dynamics of the triplet-pair state reveals the likely coexistence of coherent and incoherent singlet fission in crystalline hexacene. *Nat. Chem.* **2017**, *9*, 341.

(72) Montero, R.; Martínez-Martínez, V.; Longarte, A.; Epelde-Elezcano, N.; Palao, E.; Lamas, I.; Manzano, H.; Agarrabeitia, A. R.; López-Arbeloa, Í.; Ortiz, M. J.; Garcia-Moreno, I. Singlet fission mediated photophysics of BODIPY dimers. *J. Phys. Chem. Lett.* **2018**, *9*, 641.

(73) Berkelbach, T. C.; Hybertsen, M. S.; Reichman, D. R. Microscopic theory of singlet exciton fission. III. Crystalline pentacene. *J. Chem. Phys.* **2014**, *141*, 074705.

(74) Mirjani, F.; Renaud, N.; Gorczak, N.; Grozema, F. C. Theoretical investigation of singlet fission in molecular dimers: The role of charge transfer states and quantum interference. *J. Phys. Chem. C* **2014**, *118*, 14192.

(75) Renaud, N.; Grozema, F. C. Intermolecular vibrational modes speed up singlet fission in perylenediimide crystals. *J. Phys. Chem. Lett.* **2015**, *6*, 360.

(76) Tamura, H.; Huix-Rotllant, M.; Burghardt, I.; Olivier, Y.; Beljonne, D. First-principles quantum dynamics of singlet fission: Coherent versus thermally activated mechanisms governed by molecular phi stacking. *Phys. Rev. Lett.* **2015**, *115*, 107401.

(77) Zheng, J.; Xie, Y.; Jiang, S.; Lan, Z. Ultrafast nonadiabatic dynamics of singlet fission: Quantum dynamics with the multilayer muticonfigurational time-dependent Hartree (ML-MCTDH) method. *J. Phys. Chem. C* **2016**, *120*, 1375.

(78) Wang, L.; Olivier, Y.; Prezhdo, O. V.; Beljonne, D. Maximizing singlet fission by intermolecular packing. *J. Phys. Chem. Lett.* **2014**, *5*, 3345.

(79) Tully, J. C.; Preston, R. K. Trajectory surface hopping approach to nonadiabatic molecular collisions: The reaction of H^+ with D_2. *J. Chem. Phys.* **1971**, *55*, 562.

(80) Granucci, G.; Persico, M.; Toniolo, A. Direct semiclassical simulation of photochemical processes with semiempirical wave functions. *J. Chem. Phys.* **2001**, *114*, 10608.

(81) Granucci, G.; Toniolo, A. Molecular gradients for semiempirical CI wavefunctions with floating occupation molecular orbitals. *Chem. Phys. Lett.* **2000**, *325*, 79.

(82) Persico, M.; Granucci, G. An overview of nonadiabatic dynamics simulations methods, with focus on the direct approach versus the fitting of potential energy surfaces. *Theor. Chem. Acc.* **2014**, *133*, 1.

Chapter 2 A Brief Introduction to Electronic Structure and Direct Semiclassical Dynamics Simulations Methods

The stages of human development are to strive for: besitz (possession), wissen (knowledge), können (ability), sein (being). ~ Erwin Schrödinger, August 1918 ~

Theoretical chemistry is an area of chemistry, which aims to figure out the solutions of mathematical problems underlying the chemical phenomena. For example, to study electron motion in atoms or molecules we solve either the Schrödinger or Dirac equation for the non-relativistic or relativistic cases, respectively. The Schrödinger equation can be solved exactly only for very simple systems, for instance, two particles with Coulombic interactions as in hydrogen-like atoms. For systems consisting of more than two particles, we solve the Schrödinger equation with some additional approximations. The electronic structure methods play important roles in providing viable approximate solutions of the Schrödinger equation for atoms, molecules, and solids. Solving the Schrödinger equation employing a specific electronic structure method for a given nuclear configuration in a stationary state results in approximate electronic wave functions and energies. This procedure can be repeated for the same system in different stationary states and the obtained energies are functions of one or more reaction coordinates, called the potential energy surface (PES). The PESs present, in principle, all the information needed to devise mechanisms for reactions occurring on a single

PES. Theoretical models, such as those embodied in the Transition State theories, allow making quantitative predictions. However, in some cases an explicit treatment of the nuclear dynamics is necessary. To study the time evolution of the system we can apply classical or quantum dynamics simulations. Classical molecular dynamics simulations, using force fields to compute the ground state PES, can be used to treat very large systems such as proteins or enzymes. In dealing with excited state dynamics, it is necessary to consider the interplay of nuclear dynamics and electronic transitions, and the latter must be treated quantum mechanically. Full quantum dynamics simulations are normally limited to 20–30 nuclear coordinates and to short propagation times (< 1 picosecond). However, a combination of quantum mechanics (QM) for the electrons and classical molecular mechanics (MM) for the nuclei, known as the semiclassical approach, enables us to study large systems as well. This chapter will briefly introduce the main tools used in this thesis, *i.e.* the electronic structure and direct semiclassical dynamics simulations methods. This chapter is written based on the book of Modern Quantum Chemistry: Introduction to Advanced Electronic Structure Theory by Attila Szabo and Neil S. Ostlund,[1] Introduction to Computational Chemistry by Frank Jensen,[2] European Summerschool in Quantum Chemistry book I, II, and III by Trond Saue and Simene Reine (Editors),[3-5] lecture notes on "Excited State Dynamics" by Maurizio Persico,[6] lecture notes on "Semiclassical Methods for Excited State Dynamics" by Giovanni Granucci, Maurizio Persico, and Alessandro Toniolo,[7] and lecture notes entitled "An Overview of Nonadiabatic Dynamics Simulations Methods, with Focus on the Direct Approach versus the Fitting of Potential Energy Surface" by Maurizio Persico and Giovanni Granucci.[8]

2.1 Nonadiabatic Couplings

All possible information about the electronic structure of a molecule in a stationary state can be derived from a wave function $\Psi(\mathbf{r},\mathbf{R})$, where $\mathbf{r}$ and $\mathbf{R}$ represent the set of electronic and nuclear coordinates, respectively. This wave function can be obtained by solving the time-independent Schrödinger equation,

$$\hat{\mathcal{H}}\,\Psi(\mathbf{r},\mathbf{R}) = E\,\Psi(\mathbf{r},\mathbf{R}), \tag{2.1}$$

where $\hat{\mathcal{H}}$ is the Hamiltonian operator and E is the eigenvalue of the Hamiltonian operator. Neglecting the relativistic effects, but including the spin-orbit interactions, the non-relativistic Hamiltonian operator for a molecule in its stationary state is a sum of five terms (in atomic units),

$$\hat{\mathcal{H}} = -\sum_A \frac{1}{2M_A}\nabla_A^2 - \frac{1}{2}\sum_i \nabla_i^2 - \sum_{A,i}\frac{Z_A}{r_{Ai}} + \sum_{A>B}\frac{Z_A Z_B}{R_{AB}} + \sum_{i>j}\frac{1}{r_{ij}}, \tag{2.2}$$

where i and j refer to electrons i and j with distance of r_{ij}, A and B refer to nuclei with atomic numbers Z_A and Z_B that are separated at a distance of R_{AB}, and r_{Ai} is the distance between electron i and nucleus A. The terms ∇_i^2 and ∇_A^2 are the Laplacian operators with respect to the coordinates of electron i and nucleus A, respectively. This Hamiltonian operator represents the total energy of the system, *i.e.* the sum of the kinetic energy operator of electrons, the kinetic energy operator of nuclei, and the potential energies due to the electron-nuclear attraction, nuclear-nuclear and electron-electron repulsions, respectively. In a compact way, this Hamiltonian operator can be written as

$$\hat{\mathcal{H}} = \hat{T}_N(\mathbf{R}) + \hat{\mathcal{H}}_{el}(\mathbf{R}). \tag{2.3}$$

Here, $\hat{\mathcal{H}}_{el}$ is the electronic Hamiltonian operator for a fixed set of nuclear coordinates, defined as

$$\hat{\mathcal{H}}_{el}(\mathbf{R}) = \hat{T}_e(\mathbf{r}) + \hat{V}_{eN}(\mathbf{r},\mathbf{R}) + \hat{V}_{NN}(\mathbf{R}) + \hat{V}_{ee}(\mathbf{r}). \tag{2.4}$$

Assuming that a complete set of electronic wave functions $\psi_k(\mathbf{r},\mathbf{R})$ is available, and therefore, the full set of solutions to the electronic Schrödinger equation is accessible,

$$\hat{\mathcal{H}}_{el}(\mathbf{R})\psi_k(\mathbf{r},\mathbf{R}) = E_k(\mathbf{R})\psi_k(\mathbf{r},\mathbf{R}); \quad k = 1,2,\ldots,\infty. \tag{2.5}$$

Without introducing any approximations,[9] the total (exact) wave function can be written as a product of the complete set of electronic wave functions $\psi_k(\mathbf{r},\mathbf{R})$ and the nuclear wave function $\chi_{nk}(\mathbf{R})$,

$$\Psi_{tot}(\mathbf{r},\mathbf{R}) = \sum_{k=1}^{\infty}\chi_{nk}(\mathbf{R})\psi_k(\mathbf{r},\mathbf{R}). \tag{2.6}$$

Inserting Eqs. (2.6) and (2.3) into the time-independent Schrödinger equation, Eq. (2.1), gives the total time-independent Schrödinger equation which then can be expressed as

$$\sum_{k=1}^{\infty}\left(\hat{T}_N+\hat{\mathcal{H}}_{el}\right)\chi_{nk}(\mathbf{R})\psi_k(\mathbf{r},\mathbf{R})=E_{tot}\sum_{k=1}^{\infty}\chi_{nk}(\mathbf{R})\psi_k(\mathbf{r},\mathbf{R}). \tag{2.7}$$

Rewriting the nuclear kinetic energy operator as $\hat{T}_N=-\sum_A\frac{1}{2M_A}\nabla_A^2=\nabla_n^2$ and expanding Eq. (2.7) gives (the symbol $(\mathbf{R})$ and $(\mathbf{r},\mathbf{R})$ in the nuclear and electronic wave functions are dropped)

$$\begin{aligned}
\sum_{k=1}^{\infty}\left(\nabla_n^2+\hat{\mathcal{H}}_{el}\right)\chi_{nk}\psi_k&=E_{tot}\sum_{k=1}^{\infty}\chi_{nk}\psi_k\\
\sum_{k=1}^{\infty}\left\{\nabla_n^2\chi_{nk}\psi_k+\hat{\mathcal{H}}_{el}\chi_{nk}\psi_k\right\}&=E_{tot}\sum_{k=1}^{\infty}\chi_{nk}\psi_k\\
\sum_{k=1}^{\infty}\left\{\nabla_n\left(\psi_k\nabla_n\chi_{nk}+\chi_{nk}\nabla_n\psi_k\right)+\chi_{nk}\hat{\mathcal{H}}_{el}\psi_k\right\}&=E_{tot}\sum_{k=1}^{\infty}\chi_{nk}\psi_k\\
\sum_{k=1}^{\infty}\left\{\begin{array}{l}\psi_k\left(\nabla_n^2\chi_{nk}\right)+2\left(\nabla_n\chi_{nk}\right)\left(\nabla_n\psi_k\right)+\\ \left(\nabla_n^2\psi_k\right)\chi_{nk}+\chi_{nk}E_k\psi_k\end{array}\right\}&=E_{tot}\sum_{k=1}^{\infty}\chi_{nk}\psi_k
\end{aligned}. \tag{2.8}$$

By multiplying from the left by another specific electronic wave function ψ_l^* and integrating over the electron coordinates, Eq. (2.8) becomes

$$\nabla_n^2\chi_{nl}+E_l\chi_{nl}+\sum_{k=1}^{\infty}\left\{\begin{array}{l}2\left\langle\psi_l\middle|\nabla_n\middle|\psi_k\right\rangle\left(\nabla_n\chi_{nk}\right)+\\ \left\langle\psi_l\middle|\nabla_n^2\middle|\psi_k\right\rangle\chi_{nk}\end{array}\right\}=E_{tot}\chi_{nl}, \tag{2.9}$$

where the curly bracket contains two terms that couple different electronic states. These terms correspond to the matrix elements called the first and second derivatives of ‘nonadiabatic’ (or ‘dynamic’ or ‘derivative’ or ‘vibronic’) couplings. The first derivatives of the nonadiabatic coupling do not couple different vibrational states belonging to the same electronic states. The second derivatives of the nonadiabatic coupling, on the other hand, when $k=l$ they give a small correction to the E_k potential and are independent of the nuclear masses. These nonadiabatic couplings are important for describing processes that involve more than one electronic PES.

2.2 Born Oppenheimer Approximation

The Born-Oppenheimer approximation (BOA) relies on the fact that the nuclei are much more massive than electrons, and thus, the nuclei are assumed to be nearly fixed with respect to the electron motion. Hereby, the separation of the electronic and nuclear wave functions is approximately correct. Since the nuclear configuration is fixed at some value of $\mathbf{R}$, the electronic wave function $\psi_{el}(\mathbf{r};\mathbf{R})$ depends parametrically on $\mathbf{R}$, and therefore, the time-independent Schrödinger equation for the 'clamped-nuclei' electronic Hamiltonian can be written as

$$\hat{\mathcal{H}}_{el}\,\psi_{el}(\mathbf{r};\mathbf{R}) = E_{el}(\mathbf{R})\,\psi_{el}(\mathbf{r};\mathbf{R}), \tag{2.10}$$

where the electronic energy $E_{el}(\mathbf{R})$ is a function of $\mathbf{R}$. The term $\hat{V}_{NN}(\mathbf{R})$ in the electronic Hamiltonian, Eq. (2.4), shifts all the eigenvalues by the same amount that only depends on $\mathbf{R}$, and does not affect the electronic wave functions.

In the BOA, the total time-independent Schrödinger equation, Eq. (2.7), turns into a set of eigenvalue equations that depend only on the nuclear coordinates,

$$\left[\hat{T}_N(\mathbf{R}) + E_{el}(\mathbf{R})\right]\chi_n(\mathbf{R}) = E_{tot}\,\chi_n(\mathbf{R}), \tag{2.11}$$

where $\chi_n(\mathbf{R})$ is the nuclear wave function. This equation clearly shows that the nuclei move in a potential field generated by the electrons for each nuclear geometry $\mathbf{R}$. The BOA is justified when the energy gap between two electronic states, for instance, the ground and excited states, is larger than the energy scale of nuclear motion.

The Schrödinger equation for the electronic Hamiltonian can be solved analytically only for a few systems, for example, the hydrogen atom, H_2^+, and He^+. To get an exact solution for a system with more than one electron is a very challenging task, and thus, some approximations are applied to find approximate solutions for *N*-electron (*many*-electron) systems such as atoms, molecules, or solids.

2.3 One- and *N*-electron Basis Approximation

The most common approach to describe the electronic wave function in the time-independent Schrödinger equation is to use one-particle functions (atomic orbitals). A linear combination of atomic orbitals (AOs) is used to construct the molecular orbitals (MOs). For *N*-electron systems, and according to Pauli's principle, the *N*-electron wave functions must be antisymmetric with respect to the exchange of space and spin coordinates of any two electrons. Therefore, these *N*-electron wave functions are constructed as antisymmetrised products (ASPs) of MOs written in the form of determinants, the so-called Slater determinants. A spin and symmetry adapted linear combination of Slater determinants, which is an eigenfunction of the $\hat{S}^2$ and $\hat{S}_z$ operators, is called a configuration state function (CSF).

The exact solution of the time-independent Schrödinger equation can be found if the unknown wave function is expanded in a complete *N*-electron basis functions, *i.e*. all possible CSFs are used, and a complete set of one-electron functions is used to generate the *N*-electron basis functions. In practice, the MOs are expanded in a finite one-electron basis; therefore, the solution of the time-independent Schrödinger equation is still approximate even though one uses a complete *N*-electron basis functions. Based on the variational principle,[10] the expectation value (energy) of an approximate wave function is above the exact energy or it can be equal to the exact energy only if the exact wave function is used. Therefore, both the size and quality of the basis set are crucial to get an accurate solution.

The AOs can be described using Slater-type orbitals (STOs), Gaussian-type orbitals (GTOs), numerical atomic orbitals, or plane waves. The plane wave basis is mainly used in the solid-state calculations. For most molecular calculations, the GTOs and STOs bases are usually used. The STOs are hydrogen-like orbitals, at least for the 1*s* orbital, and show correct short- and long-range behaviours even though they lack the radial nodes and cannot represent efficiently orbitals with different principal quantum numbers, for example, 1*s* and 2*s*. On the contrary, the GTOs do not represent the hydrogen-like orbitals. However, a linear combination of enough Gaussian functions, which was first proposed by Boys,[11] can mimic one STO and can provide an approximately accurate solution.

2.4 Hartree-Fock Method

A way to approximately solve the time-independent Schrödinger equation is by the Hartree-Fock (HF) method. This method applies the BOA and uses a single Slater determinant to describe the *N*-electron wave function. It is solved using the variational principle[10] by finding an approximate wave function that minimises the expectation value of the energy. The resulting wave function is an approximate wave function to the ground state wave function, and the corresponding energy is an upper bound to the exact ground state energy.

Recalling the electronic Hamiltonian given in Eq. (2.4), the HF energy E_{HF} can be expressed as

$$E_{HF} = \left\langle \Psi_{HF} \middle| \hat{\mathcal{H}}_{el} \middle| \Psi_{HF} \right\rangle, \tag{2.12}$$

where Ψ_{HF} is a single Slater determinant HF wave function, composed from MOs, ϕ_i. The HF energy can be further written in terms of one- and two-electron integrals,

$$E_{HF} = \sum_i h_{ii} + \frac{1}{2}\sum_{ij}\left(J_{ij} - K_{ij}\right) + V_{NN}, \tag{2.13}$$

where

$$h_{ii} = \left\langle \phi_i(1) \middle| -\frac{1}{2}\nabla_1^2 - \sum_A \frac{Z_A}{r_{1A}} \middle| \phi_i(1) \right\rangle. \tag{2.14}$$

The h_{ii} term describes the kinetic energy of electron 1 and its attraction to all nuclei. The two-electron integrals J_{ij} and K_{ij} in the second term of Eq. (2.13) represent the Coulomb and exchange interactions between electrons, while the last term is the potential energy due to the nuclear-nuclear interaction.

The HF equation may be solved numerically (exact HF), but it is a very challenging task and computationally complicated. Most of the time, the HF equation is solved in a space spanned by a set of basis functions, using the so-called Hartree-Fock-Roothaan-Hall equation.[12,13] The HF equations imply that each electron interacts with the average field generated by the other electrons. This approximation yields a sufficiently accurate description of the ground state properties of most organic molecules near their equilibrium geometries. Furthermore, it recovers almost 99% of the total energy of the systems.[2]

2.5 Electron Correlation Methods

The HF wave function is an approximation to the solution of the time-independent Schrödinger equation albeit one uses a complete basis since it assumes that each electron interacts with the average potential generated from the other electrons, while in reality electrons repel each other according to Coulomb's law with the repulsion energy of $\frac{1}{r_{ij}}$. This assumption introduces an error in the wave function and energy. This error in energy is called the correlation energy, E_{corr}, *i.e.* the energy difference between the total exact non-relativistic energy of the system and the HF energy in a complete basis,

$$E_{corr} = \varepsilon_{exact} - E_{HF}^{\infty}. \tag{2.15}$$

The electron correlation effects can be divided into two, *i.e.* static (nondynamical) and dynamical electron correlations. The static electron correlation reflects the inadequacy of a single Slater determinant used to describe the wave function in the HF method. This becomes important in a situation when two or more states are (nearly) degenerate, for example, when bonds are broken, and hence open-shell configurations become important. The dynamical electron correlation comes from the fact that electrons repel each other instantaneously due to Coulomb repulsion. The instantaneous interaction between electrons has to be taken into account in order to recover the dynamical electron correlation effect and its correlation energy.

2.5.1 Configuration Interaction Method

One way to recover the electron correlation is to include more than one Slater determinant in the wave function, *i.e.* a linear combination of CSFs. In the configuration interaction (CI) method, the wave function is written as

$$\Psi_{CI} = \sum_i C_i \Phi_i, \tag{2.16}$$

where Φ_i is the CSFs, and the expansion coefficients C_i are determined variationally while the MOs are fixed.[14,15]

The advantage of using CSFs rather than individual Slater determinants in the CI wave function is to reduce the dimension of the CI space because only functions with the correct eigenvalues of $\hat{S}^2$ and $\hat{S}_z$ operators are included. The first CSF, representing the ground state configuration, consists usually of only one Slater determinant. The dimension of the full CI space for a system with N electrons in M orbitals and total spin of S can be calculated by Weyl's formula,[16]

$$D_{CSFs}(N,M,S) = \frac{2S+1}{M+1}\begin{pmatrix} M+1 \\ N/2-S \end{pmatrix}\begin{pmatrix} M+1 \\ N/2+S+1 \end{pmatrix}. \tag{2.17}$$

For a small system such as the Li_2 molecule with 6 electrons in 30 orbitals, the dimension of full CI space in CSFs is approximately 5×10^6. As the number of CSFs grows factorially with the number of electrons and orbitals, this makes a full CI calculation that yields the total 'exact' energy of a given system computationally impractical for large systems using large basis set. Although some large full CI calculations including a few billion determinants have been reported,[17-19] the computational expense is currently still too great for this size.

Since a full CI calculation for a large system with a large basis set is an intractable computation, one has to truncate the CI expansions up to a certain level. This results in the truncated CI methods, namely CIS, CID, CISD, CISDT, and so on, where S, D, T, represent singly, doubly, triply excited CSFs. Based on the Brillouin theorem,[20] the singly excited CSFs do not interact with the reference HF wave function. Therefore, the double excitation is the smallest truncation that can provide an improved wave function and energy with respect to the HF reference. The truncated CI methods are neither size consistent nor size extensive. A method is called size consistent if the total energy of two fragments equals the sum of the energies for well-separated fragments A and B, $\left(E_{AB} = E_A + E_B\right)$. Size consistency implies also the correct description of the dissociation process. A method is called size extensive if the calculated energy scales linearly with the number of (interacting or non-interacting) particles in a given system. As the size of a given system increases, the percentage of correlation energy recovered by the truncated CI methods will be diminished. Some efforts have been dedicated to correct this problem depending on whether the correction applies to the modification of the original CI equation or only to the CI energy. The former is known as coupled electron pair approximation,[21-23] while the latter is known as Davidson correction.[24]

2.5.2 Multiconfigurational Self-Consistent Field Methods

The multiconfigurational self-consistent field (MCSCF) methods are general approaches for describing molecular systems in which a single electron configuration (a single CSF) is inadequate to describe their electronic structures. The MCSCF wave function is written in the CI form, *i.e.* as a linear combination of CSFs, where the MOs are those that minimise the CI energy with respect to the MCSCF wave function and the CI coefficients are determined variationally.

In some cases, it is quite common to select all possible CSFs in a given set of 'active' orbitals, called the active space, and to keep the remaining orbitals either doubly occupied orbitals or empty (inactive orbitals). This method is called complete active space SCF (CASSCF) that has been popularised by Roos *et al*.[25] It has also been called a fully optimised reaction space (FORS) method by Ruedenberg *et al*.[26,27] An intermediate solution is to use the restricted active space SCF (RASSCF) approach by Malmqvist *et al*.[28] In this method, the active space is divided into three sub-spaces, namely RAS1, RAS2, and RAS3. All possible CSFs (excitations) are allowed in the RAS2 sub-space like in the CASSCF method, and limited numbers of holes and particles are allowed in the RAS1 and RAS3 sub-spaces, respectively. All the aforementioned methods require a careful consideration of the choice of the active space, and one has to include the most important orbitals that are involved in the chemical or physical process into the active space.

To account for both the static and the dynamical electron correlations, a combination of the MCSCF and CI or perturbation theory (PT) methods has also been developed, namely the multireference CI or multireference PT methods.[29] These methods use the MCSCF wave function as the reference wave function, and then apply the CI or PT method on the reference MCSCF wave function. These methods provide accurate results, but they are computationally demanding and are limited for the calculations of a system with an active space of no more than 18 electrons in 18 orbitals.

2.5.3 Many-Body Perturbation Theory

Another way to improve the HF method and to recover the electron correlation energy is by employing the Rayleigh-Schrödinger perturbation theory (RSPT).[30] The idea of RSPT is to divide the Hamiltonian operator into two Hermitian operators, *i.e.* the reference or unperturbed Hamiltonian $\hat{\mathcal{H}}^{(0)}$ for which its solution is known and a small perturbation $\hat{\mathcal{V}}$ that depends on a parameter λ, which has a value between 0 and 1,

$$\hat{\mathcal{H}} = \hat{\mathcal{H}}^{(0)} + \lambda \hat{\mathcal{V}} . \tag{2.18}$$

When $\lambda = 0$, the total Hamiltonian equals the unperturbed Hamiltonian $\hat{\mathcal{H}}^{(0)}$ for which one knows how to obtain its eigenfunctions and eigenvalues. As the value of the parameter λ increases, a small perturbation is introduced in the expressions of the energy and wave function, and the system will be fully perturbed if $\lambda = 1$. When the perturbation is introduced, the expressions for both the energy E and the wave function Ψ are dependent on the parameter λ. They can be written in terms of an expansion of power series,

$$E = E^{(0)} + \lambda E^{(1)} + \lambda^2 E^{(2)} + \lambda^3 E^{(3)} + \ldots \tag{2.19}$$

and

$$\Psi = \Psi^{(0)} + \lambda \Psi^{(1)} + \lambda^2 \Psi^{(2)} + \lambda^3 \Psi^{(3)} + \ldots, \tag{2.20}$$

where $E^{(0)}$ is the eigenvalue of the zeroth order wave function $\Psi^{(0)}$. The other terms are the first order, second order, third order, and so on, corrections to the energies and wave functions.

A particular formulation of RSPT is Møller-Plesset perturbation theory (MPPT),[31] which uses the sum of the Fock operator for each electron as the unperturbed Hamiltonian $\hat{\mathcal{H}}^{(0)}$ and the corresponding HF wave function as the zeroth order wave function $\Psi^{(0)}$. The MPPT treats the electron correlation as a small perturbation to the unperturbed Hamiltonian. It is size extensive since the total energy for every order of perturbation scales linearly with the number of (interacting or non-interacting) particles in a given system. However, the total energy is not determined variationally.

It is quite common to apply the perturbation up to a certain order, which can be denoted as MPn, where $n = 2, 3, 4, \cdots$, for example, MP2, MP3, MP4, *etc*. The MP2 method is the most widely used method to improve the HF energy. It recovers more than 80% of the

correlation energy. Higher-order perturbation methods, such as MP3 and MP4, do not always perform as well as the MP2 method. Also, their calculations are computationally demanding.

In the cases that require more than one Slater determinant in the zeroth order wave function, one can use the MCSCF or CASSCF wave function as the reference wave function, and then apply the perturbation up to the certain order (commonly up to the second order) to this reference wave function. This method is known as the CASPT2 method.[29] It recovers most of the static and dynamical electron correlation energies. It has been widely used for computing electronic structures of various systems, from small to large systems including organic and inorganic molecules as well as transition metals, both in their ground and excited states.[32,33] It gives a balanced compromise between the accuracy and computational cost.

2.5.4 Coupled Cluster Method

The essential idea in the coupled cluster (CC) theory is to describe the wave function by the exponential ansatz,

$$\Psi_{CC} = e^{\hat{T}}\,\Phi_0, \tag{2.21}$$

where the $e^{\hat{T}}$ is given by a Taylor series expansion,

$$e^{\hat{T}} = \left(1 + \hat{T} + \frac{1}{2!}\hat{T}^2 + \frac{1}{3!}\hat{T}^3 + \cdots\right). \tag{2.22}$$

The $\hat{T}$ operator is defined as the sum of one-, two-, three-particle, and so on, up to *N*-particle excitations,

$$\hat{T} = \hat{T}_1 + \hat{T}_2 + \hat{T}_3 + \cdots + \hat{T}_N. \tag{2.23}$$

As in the CI method, the truncation of the CC wave function is also done up to a certain level of excitations. The most common one is to truncate the $\hat{T}$ operator up to the two-particle excitations, where $\hat{T} = \hat{T}_1 + \hat{T}_2$, which gives rise to the CCSD method. The truncated CC wave function also contains contributions from the determinants corresponding to the higher-order excitations, which makes the CC method size extensive. Higher-order excitations such as three-particle excitations are usually estimated using perturbation theory, which leads to the CCSD(T) method. The energy of the CC method is solved by projecting the

Schrödinger equation onto the manifold of all *N*-particle excited determinants, then by solving it self-consistently. The obtained approximate energy can be above or below the total exact energy of a system. If all possible excitations operators $\hat{T}_N$ are included, this method becomes equivalent to the full CI method and gives the exact non-relativistic energy of the system.

2.6 Valence Bond Method

All of the previously discussed methods describe the MOs as linear combinations of AOs. These MOs are mutually orthogonal and in general they span the entire molecule, *i.e.* they are delocalised rather than being localised on atoms or in the bonding regions. The valence bond (VB) theory uses a different approach. It is designed to agree with the idea of a chemical bond as a shared pair of electrons between two particular atoms. Bonding is described in terms of overlap between orbitals from adjacent atoms. This overlap gives a two-electron bond wave function. The simplest VB wave function was first introduced by Heitler and London.[34] It shows how shared electrons form a chemical bond in the H_2 molecule, and is written as

$$\Psi_{HL} = \mathcal{N}\left\{\left|1s_a(1)\ \overline{1s_b(2)}\right| - \left|\overline{1s_a(1)}\ 1s_b(2)\right|\right\}, \tag{2.24}$$

where $\mathcal{N}$ is the normalisation constant, $1s_a(1)$ is the $1s$ orbital of hydrogen a with an α spin, $\overline{1s_b(2)}$ is the $1s$ orbital of hydrogen b with a β spin, and so on. This VB wave function shows that the $1s$ orbital of hydrogen a is singlet coupled with the $1s$ orbital of hydrogen b by a covalent interaction.

The Heitler-London approach restricts the atomic orbitals to be localised on each atom. Coulson and Fischer[35] suggested the use of optimal orbitals and to adopt the orbitals shape, *i.e.* slightly distorted atomic orbitals. For the H_2 molecule, the Coulson-Fischer wave function can be written as

$$\Psi_{CF} = \mathcal{N}\left\{\left|\phi_1\ \overline{\phi}_2\right| - \left|\overline{\phi}_1\ \phi_2\right|\right\}, \tag{2.25}$$

where $\mathcal{N}$ is the normalisation constant, ϕ_1 and ϕ_2 are distorted atomic orbitals with a small distortion parameter λ,

$$\phi_1 = 1s_a + \lambda\, 1s_b \ \text{ and } \ \phi_2 = 1s_b + \lambda\, 1s_a\,. \tag{2.26}$$

The resulting orbitals are still predominantly atomic in character, but they can be slightly delocalised.

The generalisation of the Coulson-Fischer approach is well known as the spin-coupled VB (SCVB) method.[36,37] In this method, the number of electrons involved in the bonding are described by N singly occupied nonorthogonal orbitals, which are then spin-coupled in all possible combinations in order to give the total spin. The general SCVB wave function is written as

$$\Psi_{SCVB} = \mathcal{N} \sum_{i=1}^{f_S^N} C_{Si} \hat{\mathcal{A}} \left[\phi_1 \phi_2 \phi_3 \cdots \phi_N \Theta_{S,i}^N \right], \tag{2.27}$$

with

$$\phi_i = \sum_{j=1}^{M_{basis}} c_{ji} \chi_j , \tag{2.28}$$

where $\mathcal{N}$ is the normalisation constant, C_{Si} is the spin-coupling coefficient, $\hat{\mathcal{A}}$ is the antisymmetriser, and $\Theta_{S,i}^N$ describes the i-th possible combination of spin coupling of N electrons to give an overall spin S with f_S^N number of ways to make the combinations. The value of f_S^N can be calculated as

$$f_S^N = \frac{(2S+1)N!}{(N/2+S+1)!(N/2-S)!} . \tag{2.29}$$

The SCVB wave function is optimised variationally with respect to the VB-orbital coefficients c_{ji} and the spin-coupling coefficients C_{Si}.

The VBSCF method[38,39] is the most general form of the modern VB approaches. The VBSCF wave function can be constructed using a number of VB structures with a number of nonorthogonal orbitals. Both the orbitals and VB structure coefficients are optimised. The main advantage of VBSCF is that the resulting wave functions are compact and can be chemically interpreted in a straightforward way. To determine the importance of each structure in the VB wave function, the weight of each term can be calculated based on the Gallup and Norbeck scheme,[40]

$$W_i = \frac{\mathcal{N} |C_i|^2}{\mathbf{S}_{ii}^{-1}} , \tag{2.30}$$

where $\mathcal{N}$ is the normalisation constant, C_i are the VB coefficients, and $\mathbf{S}_{ii}^{-1}$ is the inverse of the overlap matrix.

2.7 Nonorthogonal Configuration Interaction

In practice, it is quite common to use in the *many*-electron basis functions one orbital set for all CSFs. Also, it is quite common to use the same orbital set for the wave functions describing more than one electronic state. For instance, the same set of orbitals is used in the calculations of the ground and excited states. This choice facilitates the calculations of the electronic Hamiltonian matrix elements and overlap integrals between different electronic states of the same symmetry. However, it may lead to rather long CI expansions in the wave functions, and the optimal orbitals for the ground state configuration may be quite different from the optimal orbitals for the electronic excited configurations; this is especially true for the so-called charge-transfer configurations.[41]

Alternatively, one may describe the molecular wave function of each electronic state with its own optimised orbital set. In principle, the molecular wave function can be of any type, from the simplest HF wave function to a correlated one such as the CASSCF wave function. These molecular wave functions form *many*-electron basis functions Φ_k for the NOCI expansion, *i.e.* the NOCI wave function is written as a linear combination of *many*-electron basis functions Φ_k. For the special case of an *ensemble* of molecules, which is relevant for the work described in this thesis, the *many*-electron basis functions Φ_k are each constructed as ASPs of the molecular HF, CASSCF, *etc*. wave functions for various molecular electronic states.

The NOCI wave function can be written as

$$\Psi_{NOCI} = \sum_k C_k \Phi_k \,, \tag{2.31}$$

where the expansion coefficients C_k are obtained by solving the secular equations. To determine the expansion coefficients C_k, the computation of both the Hamiltonian matrix element $\left\langle \Phi_k \middle| \hat{\mathcal{H}}_{el} \middle| \Phi_l \right\rangle$ and overlap integral $\left\langle \Phi_k \middle| \Phi_l \right\rangle$ are required.

The use of different optimised orbital sets for each molecular wave function has the consequence that the *many*-electron basis functions in the NOCI wave function are not orthogonal, and hence, the CI that produces the optimised linear combination of the *many*-electron basis functions is a NOCI. Such transparent (NOCI) wave function makes a clear interpretation of the state of interests, and also the use of optimised orbital sets has the advantage that orbital relaxation effects can be properly taken into account.

2.8 Density Functional Theory

The density functional theory (DFT) method improves the limitation of the HF method by including an approximate treatment of the correlated motions of electrons. It has become one of the most applied methods to compute properties of molecules, albeit there is no exact hierarchy of the density functionals nor systematic ways to improve them. Its computation is very similar to the HF method.

The DFT method conceptually originated from the Thomas-Fermi model, but it is rigorously based on the two Hohenberg-Kohn (H-K) theorems, that were published in 1964.[42] The original H-K theorems hold only for non-degenerate ground states in the absence of a magnetic field. The first H-K theorem states that the ground state properties of an *N*-electron system depend only on the electronic density in three spatial coordinates $\rho(x,y,z)$, which can also be written as $\rho(\vec{r})$. The second H-K theorem states that the correct ground state electron density for a system is the one that minimises the total energy functional of the electron density $E\left[\rho(\vec{r})\right]$.

Recalling the electronic Hamiltonian introduced earlier, Eq. (2.4), the corresponding energy functional can be written as

$$E[\rho] = T[\rho] + E_{eN}[\rho] + E_{ee}[\rho] + V_{NN}. \tag{2.32}$$

The electron-nuclear attraction energy functional can be expressed as

$$E_{eN}[\rho] = -\sum_{A}^{N_{nuclei}} \int \frac{Z_A \rho(\vec{r})}{\left|\vec{R}_A - \vec{r}\right|} d\vec{r} \,. \tag{2.33}$$

The electron-electron repulsion energy functional, $E_{ee}[\rho]$, can be represented as the classical Coulomb repulsion between two electron densities,

$$E_{ee}[\rho] = J[\rho] = \frac{1}{2} \iint \frac{\rho(\vec{r})\rho(\vec{r}')}{\left|\vec{r} - \vec{r}'\right|} d\vec{r}\, d\vec{r} \,. \tag{2.34}$$

It is less obvious how to compute the exchange energy contribution, which is derived from the fact that electrons must satisfy the antisymmetry principle. It is also unclear how to compute the kinetic energy functional as a function of the electron density and how to evaluate the electron correlation energy.

Kohn and Sham[43] suggested a way to compute the kinetic energy functional by assuming that a system of non-interacting electrons can generate the same density as the interacting ones. This formulation becomes the common approach in the DFT method, known as the Kohn-Sham DFT (KS-DFT) method. This method uses the HF expression of the kinetic energy operator applied to the MOs ϕ_i to determine the kinetic energy functional,

$$T_s[\rho] = \sum_{i=1}^{N} \left\langle \phi_i \left| -\frac{1}{2}\nabla^2 \right| \phi_i \right\rangle . \tag{2.35}$$

The connection between electron density and orbitals can be written as

$$\rho(\vec{r}) = \sum_{i=1}^{N} \left|\phi_i(\vec{r})\right|^2 . \tag{2.36}$$

In the H-K approach, the exchange term together with the correlation energy is included in the exchange-correlation energy functional $E_{xc}[\rho]$. With this additional term, the expression of the total energy functional of the KS-DFT method becomes

$$E_{KS-DFT}[\rho] = T_s[\rho] + E_{eN}[\rho] + J[\rho] + E_{xc}[\rho] + V_{NN} \,, \tag{2.37}$$

where the exchange-correlation energy functional $E_{xc}[\rho]$ is defined as

$$E_{xc}[\rho] = \left(T[\rho] - T_s[\rho]\right) + \left(E_{ee}[\rho] - J[\rho]\right). \tag{2.38}$$

The KS-DFT equations, where the one-electron KS operator $\hat{h}_{KS}$ is applied to the MOs and gives the orbital energies ε_i, are solved self-consistently. This procedure can be written as

$$\hat{h}_{KS}(\vec{r})\,\phi_i(\vec{r}) = \varepsilon_i\,\phi_i(\vec{r}), \tag{2.39}$$

where

$$\hat{h}_{KS}(\vec{r}) = -\frac{1}{2}\nabla^2(\vec{r}) + V_{eff}(\vec{r}). \tag{2.40}$$

The effective potential is defined as

$$V_{eff}(\vec{r}) = V_{eN}(\vec{r}) + \int \frac{\rho(\vec{r}')}{|\vec{r}-\vec{r}'|}\,d\vec{r}' + V_{xc}(\vec{r}). \tag{2.41}$$

All terms in the one-electron KS operator are known except for the $V_{xc}(\vec{r})$ term. This term is the functional derivative of the exchange-correlation energy functional with respect to the electron density, $\frac{\partial E_{xc}[\rho]}{\partial \rho}$. This term is unknown, and its value is determined from an approximate expression for the exchange-correlation energy. The exchange-correlation energy functional is usually divided into exchange and correlation terms. The simplest exchange-correlation functional approximation is the Local Density Approximation (LDA), which is based on the uniform electron gas model. This functional depends only on the local density at a given point. Its accuracy is poor because the electron density is approximated as a constant, and it cannot capture the situation where the electron density can vary rapidly over a small region of space such as in a molecule or an extended system. To improve the LDA functional, one can include either the first derivative of the density or both the first and the second derivatives of the density. If one includes only the local density and the first derivative (gradient), it leads to the so-called Generalised Gradient Approximation (GGA). Other functionals that include the local density, the gradient, and the second derivative are called meta-GGA or semi-local functionals. Moreover, another way to improve the performance of the functional is to add a percentage of the HF exchange. This leads to the well-known hybrid functionals, for instance, B3LYP, PBE0, HSE, *etc*. Over the years many other exchange-correlation functionals[44,45] have been developed to answer the big challenges of the KS-DFT method, for instance, van der Waals (dispersive) interactions that are also known as the non-local correlation effects, self-interaction error that often appears in charge-transfer and in excited states, and the multireference character of a given system such as a strongly correlated system. These new exchange-correlation functionals perform quite well in some cases, but

they may fail in the other cases. Therefore, one has to be careful in choosing the functional beforehand.

2.9 Direct Semiclassical Dynamics Simulations

This section and its subsequent subsections briefly discuss the main idea of the direct semiclassical dynamics simulations. First, the word 'semiclassical' means that the nuclear motion is treated classically by solving Newton's equation, while the electrons are treated quantum mechanically. Second, the word 'direct' can be regarded as the synonym of 'on-the-fly' meaning that the electronic problem is solved at every time step of the molecular dynamics. This procedure allows us to avoid two preliminary steps in the dynamics simulations: (i) determining the PES and other relevant matrix elements between electronic states for a large number of molecular geometries, and (ii) fitting those quantities as functions of the nuclear coordinates. However, this procedure can also be quite expensive since the computational cost scales linearly with the number of trajectories and with the time length of the simulated process.

To reduce the computational burden of the direct semiclassical dynamics simulations, semiempirical methods, which perform faster than the so-called *ab initio* and DFT methods, are chosen for the electronic structure calculations. Semiempirical methods have been widely used for various computational studies of organic molecules in the ground state, but the quality of the results strongly depend on the calibration of empirical parameters with respect to the experimental or theoretical reference data. Hence, there is a need to improve the semiempirical methods concerning their accuracy and applicability to treat not only the ground state but also excited states. With this respect, modifications of standard semiempirical methods have been developed. The semiempirical method used in this thesis is a modification of standard semiempirical methods and is based on the floating occupation molecular orbital–configuration interaction (FOMO–CI) approach.[46] This approach compromises the accuracy of the results and its computational viability to treat both the ground and excited states.

2.9.1 Semiempirical Methods

Semiempirical methods have the same conceptual formulation as *ab initio* quantum chemical methods, but to reduce the computational costs these methods neglect many integrals necessary for constructing the Fock matrix, consider only the valence electrons, and use a minimal basis set. For example, a hydrogen atom has one basis function, *i.e.* one *s*-orbital, while all atoms in the second and third rows of the periodic table have four basis functions (one *s*- and three *p*-orbitals). The most widely used class of semiempirical methods is based on the Zero Differential Overlap (ZDO) approximation. It neglects all integrals over products of basis functions that depend on the same electron coordinates when located on different atoms, $\langle \mu_A | \upsilon_B \rangle = 0 \; \forall \; A \neq B$. As the consequences: (i) the overlap matrix **S** is reduced to a unit matrix, (ii) one-electron integrals involving three centres are set to zero, $\langle \mu_A | V_C | \upsilon_B \rangle = 0$, and (iii) all three- and four-centre two-electron integrals are neglected, $\langle \mu_A \upsilon_B | \lambda_C \sigma_D \rangle = \delta_{AC} \delta_{BD} \langle \mu_A \upsilon_B | \lambda_A \sigma_B \rangle$.

Since these methods neglect many integrals, three different levels of approximation are made in addition to the ZDO approximation, namely Complete Neglect of Differential Overlap (CNDO), Intermediate Neglect of Differential Overlap (INDO), and Neglect of Diatomic Differential Overlap (NDDO). The CNDO approximation considers only all two-centre two-electron integrals of the Coulomb type, $\langle \mu_A \upsilon_B | \mu_A \upsilon_B \rangle$. The INDO approximation considers not only two-centre two-electron integrals of the Coulomb type, but also one-centre two-electron integrals of the type $\langle \mu_A \upsilon_A | \mu_A \upsilon_A \rangle$. While the CNDO and INDO approximations only consider some of the two-electron integrals, all one- and two-electron integrals are computed in the NDDO approximation. These remaining integrals can be calculated from the function of atomic orbitals or through formulas containing parameters, the values of which are assigned on the basis of experimental data.

The MNDO model is probably the most popular procedure to parameterise the semiempirical methods. The derivation of this model is similar to that of NDDO and a minimal basis set of Slater type AOs for valence electrons is used. Some of the one- and two-electron integrals are the same as in NDDO. First, the electrostatic core-electron attraction is

parameterised in terms of a reduced nuclear charge Z_B and of the one-centre two-electron integral $\langle \mu_A \mu_A | \upsilon_A \upsilon_A \rangle$, which can be written as

$$h_{\mu_A \upsilon_A} = U_\mu \delta_{\mu_A \upsilon_A} - \sum_{B \neq A}^{N_{nuclei}} Z_B \langle \mu_A \mu_A | \upsilon_A \upsilon_A \rangle . \tag{2.42}$$

Second, two-centre one-electron integrals are written as a product of the corresponding overlap integral $S_{\mu\upsilon}$, multiplied by the average of two atomic resonance parameters β,

$$h_{\mu_A \upsilon_B} = \frac{1}{2} S_{\mu_A \upsilon_B} \left(\beta_{\mu_A} + \beta_{\upsilon_B} \right). \tag{2.43}$$

The overlap integral entering this formula is calculated explicitly (this is an exception to the NDDO approximation). Third, one-centre two-electron integrals of type $\langle \mu_A \upsilon_A | \lambda_A \sigma_A \rangle$ are represented by empirical parameters. There are five empirical parameters needed for the *s*- and *p*-orbitals (they will not be explained in details here). Fourth, two-centre two-electron integrals of the type $\langle \mu_A \upsilon_A | \lambda_B \sigma_B \rangle$ are modelled as interactions between multipoles. They are evaluated based on the electrostatic interactions and empirical parameters ζ (atomic orbital exponents). Lastly, the two-centre core-core repulsion is determined as the sum of the electrostatic term and an additional effective term that can be written as

$$E_{AB}^{core} = Z_A \, Z_B \langle s_A s_A | s_B s_B \rangle + E_{AB}^{eff} . \tag{2.44}$$

The standard implementation of the MNDO model including MNDO, AM1, PM3, and PM5 is parameterised employing the HF wave function by taking into account only the ground-state properties of organic molecules. As a result, the calculation of excited states using semiempirical methods employing the CIS method cannot be accurate. In the direct semiclassical dynamics simulations, all electronic states have to be treated in a balanced way. The method used to calculate electronic states has to behave correctly for all nuclear configurations explored in the dynamics, for example, state degeneracies and bond breaking. For this reason, a modification of the standard semiempirical procedure with the FOMO–CI approach has been developed.[46]

The idea of using the FOMO–CI approach is to describe the typical homolytic bond breaking process correctly by avoiding the use of an expensive multiconfigurational method, such as CASSCF. In the FOMO–CI method, the MOs are obtained from the SCF calculation

of the closed-shell type, and then occupation numbers O_k that differ from 0 or 2 are introduced in the density matrix **P**,

$$\mathbf{P} = \mathbf{C}\,\mathbf{O}\,\mathbf{C}^{+}, \tag{2.45}$$

where **O** is the diagonal matrix of the occupation numbers O_k.

To introduce the floating occupation numbers in the MOs, which will adapt smoothly due to the changes of nuclear geometry during the dynamics simulations, the electron distribution in an orbital with energy ε is determined using the Gaussian function,

$$f_k(\varepsilon) = \frac{\sqrt{2}}{\omega\sqrt{\pi}} \exp\left[-\frac{(\varepsilon - \varepsilon_k)^2}{2\omega^2} \right], \tag{2.46}$$

where ω is an arbitrary orbital energy width parameter such that,

$$\int_{-\infty}^{\infty} f_k(\varepsilon)\, d\varepsilon = 1. \tag{2.47}$$

The occupation numbers O_k are given in each SCF step following the expression

$$O_k = \int_{-\infty}^{\varepsilon_F} f_k(\varepsilon)\, d\varepsilon, \tag{2.48}$$

where ε_F indicates the Fermi energy determined by imposing the condition that the sum of occupation numbers must give the total number of electrons. For low-lying orbitals with $\varepsilon_F - \varepsilon \gg \omega$, one gets the occupation number $O_k = 2$, while the high-energy virtual orbitals will be empty.

The use of floating occupation numbers in the MOs of a SCF calculation has as a consequence that the obtained energy loses its meaning because it depends on the electron distribution in the virtual orbitals and also on the orbital energy width parameter ω. Therefore, a subsequent CI calculation is required to obtain a correct description of the various states of the system. In the CI calculation the orbitals are divided into inactive, active, and virtual orbitals. All the orbitals with floating occupation must be included, at least formally, in the active subspace. The excitations are allowed only within the active MOs. Moreover, it is advisable to use an active space as small as possible, *i.e.* to include only important orbitals that are involved in the chemical reactivity, for two reasons. First, electron correlation effects in the semiempirical calculations are taken into account primarily *via* the parameterisation, thus there is no need to use long CI expansions. Second, two-electron integrals in the CI

calculation must be transformed from the AO to MO basis, which will become impractical for large molecules with a large active space.

2.9.2 Hybrid QM/MM Simulations

The idea of the hybrid QM/MM simulations is to partition the system into two parts, *i.e.* QM and MM subsystems. The QM subsystem usually contains the active part of the system studied where its electronic structure is very important, and it is treated quantum mechanically. It can be a molecule dissolved in the solvent, a group of molecules, or a fragment of a big system. The MM subsystem is known as the environment. It does not participate directly in the chemical or physical process, but it interacts with the active part of the system studied. A simple MM force field model is usually used to treat this subsystem. It can be a number of solvent molecules, a solid surface, a crystal structure, a DNA strand, or the non-reactive parts of an enzyme.

The hybrid QM/MM potential energy comprises three classes of interactions, *i.e.* interactions between atoms in the QM subsystem, interactions between atoms in the MM subsystem, and interactions between QM and MM atoms. The interactions within the QM and MM subsystems are relatively straightforward to describe, while the interaction between two subsystems are more difficult to describe. The common approach to determine the electronic Hamiltonian of the whole system is by using the additive coupling scheme,

$$\hat{\mathcal{H}}_{el} = \hat{\mathcal{H}}_{QM} + \hat{\mathcal{H}}_{MM} + \hat{\mathcal{H}}_{QM/MM} . \tag{2.49}$$

Then, the total energy of the whole system can be expressed as

$$E = E_{QM} + E_{MM} + E_{QM/MM} . \tag{2.50}$$

The term E_{MM} simply coincides with $\hat{\mathcal{H}}_{MM}$, while E_{QM} and $E_{QM/MM}$ are expectation values of $\hat{\mathcal{H}}_{QM}$ and $\hat{\mathcal{H}}_{QM/MM}$, respectively. Hereby, the total energy of the whole system can also be written as

$$E = \left\langle \psi \middle| \hat{\mathcal{H}}_{QM} + \hat{\mathcal{H}}_{QM/MM} \middle| \psi \right\rangle + E_{MM} . \tag{2.51}$$

The term E_{MM} is the MM energy obtained using a classical force field, which contains both the bonded terms (bonds, bond angles, torsions) and non-bonded terms (electrostatic and van

der Waals) for the MM interactions. The bonded terms are implemented in many MM force fields as Morse or harmonic bonds, harmonic bond angles, and truncated Fourier expansions. The van der Waals terms are usually represented by Lennard-Jones potentials.[47] The term $\hat{\mathcal{H}}_{QM}$ uses forms adopted either from the semiempirical, *ab initio*, or DFT methods. The last (and critical) term $\hat{\mathcal{H}}_{QM/MM}$ represents the interactions of MM atoms with electrons and nuclei of the QM subsystem. A simple and reasonably accurate description of this term includes electrostatic interactions and Lennard-Jones repulsion-dispersion terms,[48]

$$\hat{\mathcal{H}}_{QM/MM} = -\sum_{i,m}\frac{q_m}{R_{im}} + \sum_{\alpha,m}\frac{Z_\alpha q_m}{R_{\alpha m}} + \sum_{\alpha,m}\varepsilon_{\alpha m}\left[\left(\frac{\sigma_{\alpha m}}{R_{\alpha m}}\right)^{12} - \left(\frac{\sigma_{\alpha m}}{R_{\alpha m}}\right)^{6}\right], \tag{2.52}$$

where q_m is the atomic point charge on the m-th MM atom, R_{im} is the distance between QM electron i and MM atom m, Z_α is the core charge of the QM atom α, $R_{\alpha m}$ is the distance between QM atom α to MM atom m, $\varepsilon_{\alpha m}$ and $\sigma_{\alpha m}$ are the Lennard-Jones parameters for QM atom α interacting with MM atom m.

The most important term in Eq. (2.52) that allows the QM and MM subsystems to interact is the first term. It corresponds to all interactions between MM atoms and QM electrons. This term is incorporated into the QM Hamiltonian explicitly and treated like the electron-nucleus electrostatic interactions within the QM region. This scheme—called 'electrostatic embedding'—allows the QM electronic structure to respond to its environment through the interaction of its electrons with the surrounding molecules. Moreover, it also gives rise to a specific change in the electronic distribution of each electronic state. The addition of $\hat{\mathcal{H}}_{QM/MM}$ and $\hat{\mathcal{H}}_{QM}$ has to be done before diagonalising the electronic Hamiltonian in order to take into account the differences between electronic states. Hence, it correctly represents the spectral shifts due to interactions with the environment and the displacement of conical intersections or avoided crossings along the reaction coordinate and energy axes. The last two terms in Eq. (2.52) are added to the total energy once the electronic energy has been determined. They do not affect the electronic distribution of the system directly, but they affect the PES and the dynamics of the system.

2.9.3 Semiclassical Dynamics

The simulations of the dynamics of photochemical reactions such as photosensitisation, photoisomerisation, *etc*., which usually involve more than one electronic PES, are important tools to unravel their mechanisms, which may not be easily discernable in the experiments, as well as to associate the experimental measurements with the theory. Most of the photochemical reactions are fast processes in which the nuclear and electron motions are strongly coupled. In such processes, the BOA is no longer valid and one needs to solve the time-dependent Schrödinger equation (TDSE) and to compute the nonadiabatic couplings (Section 2.1). The simulations presented in this thesis make use of the surface hopping (SH) method based on Tully's fewest switches SH (FSSH).[49] In this approach, a swarm of trajectories is usually run with the same (or different) initial conditions in which each trajectory, representing the time evolution of the classical degrees of freedom, evolves independently on a single PES with an occasional possibility to hop from one PES to another. Before going into details about the SH method, a brief review on the TDSE and on the nuclear trajectories for solving the electronic and nuclear motions will be presented.

2.9.3.1 Time-Dependent Schrödinger Equation

Suppose a classical trajectory $Q(t)$ in the nuclear configuration space has been defined. Then, the electronic Hamiltonian $\hat{\mathcal{H}}_{el}\big(Q(t)\big)$, its eigenstates $\psi_k\big(Q(t)\big)$ and eigenvalues $U_k\big(Q(t)\big)$ are implicitly time-dependent such that, for each state *k*,

$$\hat{\mathcal{H}}_{el}\big(Q(t)\big)\Big|\psi_k\big(Q(t)\big)\Big\rangle = U_k\big(Q(t)\big)\Big|\psi_k\big(Q(t)\big)\Big\rangle. \tag{2.53}$$

The TDSE for the electrons is written as (in atomic units, $\hbar = 1$)

$$i\frac{d}{dt}\Big|\psi_{el}(t)\Big\rangle = \hat{\mathcal{H}}_{el}\Big|\psi_{el}(t)\Big\rangle, \tag{2.54}$$

where $\psi_{el}(t)$ is the time-dependent electronic wave function that will be expanded in the adiabatic basis,

$$\Big|\psi_{el}(t)\Big\rangle = \sum_l A_l(t)\, e^{-i\gamma_l(t)}\Big|\psi_l\big(Q(t)\big)\Big\rangle, \tag{2.55}$$

with $\gamma_l(t) = \int_0^t U_l\big(Q(t')\big)\,dt'$.

The probability to be in the state l at time t is $P_l(t) = \left|A_l(t)\right|^2$ and the time derivative of $\left|\psi_{el}(t)\right\rangle$ is expressed as

$$\begin{aligned}\frac{d}{dt}\left|\psi_{el}(t)\right\rangle &= \sum_l \left[\left(\dot{A}_l - iU_l A_l\right)\left|\psi_l\right\rangle + A_l\left|\frac{d\psi_l}{dt}\right\rangle\right] e^{-i\gamma_l(t)} \\ &= \sum_l \left[\left(\dot{A}_l - iU_l A_l\right)\left|\psi_l\right\rangle + A_l \sum_r \left|\frac{\partial\psi_l}{\partial Q_r}\right\rangle \dot{Q}_r\right] e^{-i\gamma_l(t)}\end{aligned} . \tag{2.56}$$

Substituting into the TDSE in Eq. (2.54), and multiplying by $\left\langle\psi_k\right|$ yields

$$\dot{A}_k = -\sum_{l\neq k} A_l(t)\, e^{i(\gamma_k-\gamma_l)} \sum_r \dot{Q}_r G_{kl}^{(r)}\,, \tag{2.57}$$

where $G_{kl}^{(r)}$ is the nonadiabatic coupling matrix element between states k and l. When the two electronic states are the same, $k = l$, the nonadiabatic coupling matrix element vanishes, $G_{kk}^{(r)} = 0$. The transition probabilities depend on the scalar product of nuclear velocity vector $\dot{\mathbf{Q}}$ and nonadiabatic coupling vector $\mathbf{G}_{kl}$. These vectors become large in the proximity of a surface crossing where $U_l - U_k \simeq 0$, while when the two surfaces are well separated the phase factors $e^{i(\gamma_k-\gamma_l)}$ oscillate rapidly in time, thus effectively reduce the transition probability.

Differentiating Eq. (2.53), one gets

$$\frac{\partial\hat{\mathcal{H}}_{el}}{\partial Q_r}\left|\psi_l\right\rangle + \hat{\mathcal{H}}_{el}\frac{\partial\left|\psi_l\right\rangle}{\partial Q_r} = \frac{\partial U_l}{\partial Q_r}\left|\psi_l\right\rangle + U_l\frac{\partial\left|\psi_l\right\rangle}{\partial Q_r}, \tag{2.58}$$

and pre-multiplying by $\left\langle\psi_l\right|$ yields Hellmann-Feynman's equation,

$$\frac{\partial U_l}{\partial Q_r} = \left\langle\psi_l\left|\frac{\partial\hat{\mathcal{H}}_{el}}{\partial Q_r}\right|\psi_l\right\rangle. \tag{2.59}$$

Using the condition of $\left\langle\psi_k\right|\left(k\neq l\right)$ one gets a useful relationship of the nonadiabatic couplings,

$$G_{kl}^{(r)} = \left\langle\psi_k\left|\frac{\partial}{\partial Q_r}\right|\psi_l\right\rangle = \frac{\left\langle\psi_k\left|\frac{\partial\hat{\mathcal{H}}_{el}}{\partial Q_r}\right|\psi_l\right\rangle}{U_l - U_k}. \tag{2.60}$$

This equation clearly shows that in general the nonadiabatic couplings between two states are large if the two states are close in energy. Eqs. (2.59) and (2.60) are only valid for exact eigenfunctions of the electronic Hamiltonian $\hat{\mathcal{H}}_{el}$, or of any other Hamiltonian with a parametric dependence on a variable Q_r. They cannot be used to compute the energy gradients and couplings for approximate wave functions. However, they may be applied for the model Hamiltonian in the diabatic representation.

Alternatively, it is possible to calculate explicitly the nonadiabatic couplings of Eq. (2.57) based on the approximate equality,[50]

$$\sum_r \dot{Q}_r G_{kl}^{(r)} = \left\langle \psi_k \left| \frac{\partial}{\partial t} \right| \psi_l \right\rangle \simeq \frac{\left\langle \psi_k(t) \middle| \psi_l(t+\Delta t) \right\rangle}{\Delta t}. \tag{2.61}$$

This equation shows the most direct way a basic trend in nonadiabatic transitions, *i.e.* the minimisation of electronic change or maximum overlap of the initial and final electronic states.

2.9.3.2 Nuclear Trajectories

One of the simplest methods to integrate Newton's equation of motion is the Verlet integration algorithm.[51] This algorithm updates both positions Q and velocities $\dot{Q}$ from time t to time $t+\Delta t$. In a given potential energy function $V(Q)$, the force and acceleration are defined as $F_r = -\dfrac{\partial V}{\partial Q_r}$ and $\ddot{Q}_r = \dfrac{F_r}{m_r}$, respectively, where m_r is the mass of the atom associated with the coordinate Q_r. Applying Newton's equations and computing the Taylor expansions at time interval $t+\Delta t$ and time t, one gets

$$Q(t+\Delta t) = Q(t) + \dot{Q}(t)\Delta t + \frac{1}{2}\ddot{Q}(t)\Delta t^2 + \frac{1}{6}\dddot{Q}(t)\Delta t^3 + O\left(\Delta t^4\right) \tag{2.62}$$

and

$$Q(t) = Q(t+\Delta t) - \dot{Q}(t+\Delta t)\Delta t + \frac{1}{2}\ddot{Q}(t+\Delta t)\Delta t^2 \pm \frac{1}{6}\dddot{Q}(t+\Delta t)\Delta t^3 + O\left(\Delta t^4\right). \tag{2.63}$$

Adding these two equations yields

$$\dot{Q}(t+\Delta t) = \dot{Q}(t) + \frac{\Delta t}{2}\left[\ddot{Q}(t) - \ddot{Q}(t+\Delta t)\right] + \frac{\Delta t^2}{6}\left[\dddot{Q}(t) - \dddot{Q}(t+\Delta t)\right] + O\left(\Delta t^3\right). \tag{2.64}$$

By introducing the first order approximation to the third derivatives $\dddot{Q}(t)$, one gets

$$\dddot{Q}(t) = \frac{\ddot{Q}(t) - \ddot{Q}(t-\Delta t)}{\Delta t} + O\left(\Delta t^2\right) \tag{2.65}$$

and similarly to $\dddot{Q}(t+\Delta t)$. Using this approximation, Eqs. (2.62) and (2.64) become

$$Q(t+\Delta t) = Q(t) + \dot{Q}(t)\Delta t + \Delta t^2\left[\frac{2}{3}\ddot{Q}(t) - \frac{1}{6}\ddot{Q}(t-\Delta t)\right] + O\left(\Delta t^4\right) \tag{2.66}$$

and

$$\dot{Q}(t+\Delta t) = \dot{Q}(t) + \Delta t\left[\frac{5}{6}\ddot{Q}(t) + \frac{1}{3}\ddot{Q}(t+\Delta t) - \frac{1}{6}\ddot{Q}(t-\Delta t)\right] + O\left(\Delta t^3\right). \tag{2.67}$$

These two equations define Verlet's algorithm with accuracy on the order of Δt^4 for each time step, *i.e.* Δt^3 for a given time interval.

2.9.4 Surface Hopping

SH is an approach that combines the classical and quantum mechanical methods for the treatment of nuclei and electrons, respectively. In this approach, the molecule is considered in a given electronic state *k* at any time, even though the probability of any other state $P_l(t)$ may be different from zero. In this adiabatic state $|\psi_k\rangle$ the nuclear trajectory is driven by its potential energy function, $V(Q) = U_k(Q)$. As the probability of state *l* increases, there is a possibility for a transition (or a 'hop') from surface U_k to surface U_l, which is determined by a stochastic algorithm according to the time evolution of the $P_l(t)$ value. However, at the end of the trajectory the molecule may be in any state and possibly not in the one with the largest probability. To obtain the converged results from the SH approach one needs to run many trajectories independently from each starting point in a region of the phase space.

One of the best and most commonly used methods applied to the SH approach is Tully's FSSH method.[49] It compromises the conceptual simplicity, accuracy of the results, and computational efficiency applied from medium to large molecules. In this method, the electronic density matrix is propagated coherently along with the trajectory and the transition probability is evaluated during the trajectory run. The transitions only occur when the

coupling between electronic states is non negligible and the number of state switches is minimised by enforcing that the total flux of probability between two states is obtained by one-way transitions at each integration time step.

Considering the quantity $\Pi_k(t)$ as the fraction of trajectories that are found in surface U_k at time *t*, each trajectory has a different probability $P_k(t)$ and the average probability over all trajectories $\overline{P}_k(t)$. Ideally, the quantity $\Pi_k(t)$ should coincide with $\overline{P}_k(t)$ at any time *t*. This ideal condition can be fulfilled by random hopping from one state to another one according to the $P_k(t)$. However, this random hopping would be unphysical because surface hops would also take place in the regions of the phase space where the transition probability is negligible. In addition, for theoretical and practical reasons, it is preferable to rely on the probabilities $P_k(t)$ that are computed on a single trajectory rather than on averages over many trajectories $\overline{P}_k(t)$.

The first derivative of $P_k(t)$ can be derived from Eq. (2.57) such that,

$$\dot{P}_k = \dot{A}_k A_k^* + A_k \dot{A}_k^* = -\sum_{l \neq k} B_{kl} \,, \tag{2.68}$$

where

$$B_{kl} = 2\Re\left[A_l A_k^* e^{i(\gamma k - \gamma l)} \right] \sum_r \dot{Q}_r G_{kl}^{(r)} \tag{2.69}$$

(notice that $B_{lk} = -B_{kl}$). Considering $|\psi_k\rangle$ as the current electronic state, in a given time step its probability will change by a sum of positive or negative contributions $B_{kl}\Delta t$. The negative B_{kl} values correspond to positive increments of P_k and are ignored. Thus, the transition probabilities of this state to hop to another state are put equal to

$$P(k \to l) = \max\left\{0, \frac{B_{kl}\Delta t}{P_k}\right\}. \tag{2.70}$$

A hop from state *k* to state *l* at time *t* occurs if two conditions are simultaneously fulfilled: (i) a uniformly selected random number x in the $[0,1]$ interval is, such that,

$$\sum_{l=1}^{n-1} P(k \to l) < x \leq \sum_{l=1}^{n} P(k \to l), \tag{2.71}$$

and (ii) the energy gap between state *k* and state *l* satisfies the condition $U_l - U_k \leq T$, where T is the nuclear kinetic energy. The latter condition allows the adjustment of the nuclear

velocities after the hop and to ensure the energy conservation. If only the former condition is fulfilled, Eq. (2.71), the situation is called frustrated hopping because the system does not have enough energy to hop from the current state to a higher one. Moreover, if both conditions are not fulfilled the usual choice is to give up the surface hopping.

The FSSH method describes very well fast transitions that occur when the two PESs cross or are close in energy. However, it faces a problem, namely decoherence, in the regions where the energy gap between two PESs is large. It occurs because the semiclassical TDSE implies a fully coherent propagation of the electronic wave function for all the states, while it is propagated along a single trajectory that runs on a specific electronic PES *k*. To resolve this problem a decoherence correction applied to FSSH method based on the energy difference between two electronic states has been proposed.[52] The important point of this correction is to correct the coefficients A_k at each integration time step and to use those coefficients in order to obtain the transition probabilities $P_k(t)$ in the current state *k* such that,

$$\begin{aligned} A_l' &= A_l\, e^{-\frac{\Delta t}{\tau_{kl}}} \qquad \forall\ l \neq k \\ A_k' &= A_k \left[\frac{1 - \sum_{l \neq k} |A_l'|^2}{|A_k|^2} \right]^{1/2} \\ \tau_{kl} &= \frac{\hbar}{|U_l - U_k|}\left(1 + \frac{C}{T}\right) \end{aligned} \quad , \tag{2.72}$$

where *T* is the nuclear kinetic energy and *C* is a constant with a value of 0.1 Hartree.[53,54] This correction tends to equate the populations of the average probabilities $\overline{P}_k(t)$ to the $\Pi_k(t)$ distributions of the trajectories in the quantum states and progressively cancels the coherence effects. However, this correction is negligible when the energy gap between two electronic states is small or when the two PESs cross. Another way to include a decoherence correction in the FSSH method is based on the overlap between two wave packets.[55] In this correction, 'ancillary' points in the coordinate and momentum spaces are attributed to every other electronic state except the current one, and they are propagated independently. The electronic populations computed by the TDSE are modified accordingly, taking into account the distance of each phase space point from the current one. This scheme can be realised by assigning frozen Gaussian wave packets to the representative points and evaluating the

overlap between the two wave packets in the ancillary points and in the current one, which depend on their phase space distance.

2.9.4.1 Sampling of Initial Conditions

As mentioned in the previous section, the SH approach, which is based on a stochastic algorithm, requires many trajectories to be launched in order to obtain reliable statistics of the state populations. These many trajectories can be obtained by sampling of initial conditions, which can take into account the quantum and/or statistical distributions of nuclear coordinates and momenta. The number of trajectories depends on the photochemical processes of interest. If less than 10–50 trajectories are launched; the final probability (quantum yield) of the state of interest cannot be assessed (semi-) quantitatively. Considering N_T is the number of trajectories and P is the probability of the event to occur, the average of 'interesting' events will be $x = N_T P$ with a standard deviation of $\sigma = \sqrt{N_T P(1-P)}$. For a small value of P with $x = 10$, the average relative error $\sigma / x = \sqrt{(1-P)/x}$ is in the order of 30%.

A canonical distribution of initial conditions in the ground state can be obtained by Monte Carlo sampling or by running a molecular dynamics trajectory with a thermostat. The sampling of the initial conditions in the excited states, on the other hand, can be done based on the assumption that the field-induced transition probability is proportional to the squared transition dipole moment between the initial and final states, $\mu_{i,f}^2$, and the resonance condition $\left|U_f - U_i\right| \simeq h\nu$ holds approximately depending on the shape and length of the pulse. This sampling of the initial conditions in the excited states can be summarised as follows: (i) setting up a transition energy interval $\left[\Delta E_{\min}, \Delta E_{\max}\right]$ according to the excitation wavelengths one wants to consider; (ii) choosing a reference value of the squared transition dipole moment μ_{ref}^2 that regulates how many trajectories will be launched from the same initial phase space point; (iii) sampling a set of coordinate and momentum phase space points $\left(\mathbf{Q}_j, \mathbf{P}_j\right)$ from the desired distribution $\rho(\mathbf{Q}, \mathbf{P})$ for the initial PES U_i; (iv) computing the transition energies $U_f(\mathbf{Q}_j) - U_i(\mathbf{Q}_j)$ and their corresponding dipole moments $\mu_{i,f}(\mathbf{Q}_j)$ for each point; (v)

calculating the sum of the squared transition dipole moments of the eligible states $\mu_{tot}^2 = \sum_f \mu_{i,f}^2$ and computing the maximum number of trajectories to be launched from the $(\mathbf{Q}_j, \mathbf{P}_j)$ initial conditions as $N_{\max} = \mu_{tot}^2 / \mu_{ref}^2$, approximated to the next integer (if there are no eligible states, $N_{\max} = 0$); and (vi) generating $N_{\max}$ random numbers x_r in the interval $[0,1]$ and for each x_r launching a trajectory by vertical excitation to state f if $\sum_l^{f-1} \mu_{i,l}^2 < x_r \, N_{\max} \, \mu_{ref}^2 \leq \sum_l^{f} \mu_{i,l}^2$ (no trajectory is launched if $x_r \, N_{\max} \, \mu_{ref}^2 > \mu_{tot}^2$).[56]

2.10 References

(1) Szabo, A.; Ostlund, N. S. *Modern Quantum Chemistry: Introduction to Advanced Electronic Structure Theory*; Dover Publications, Inc.: Mineola, New York, 1996.

(2) Jensen, F. *Introduction to Computational Chemistry*; Second ed.; John Wiley & Sons Ltd. : West Sussex, England, 2007.

(3) *European Summerschool in Quantum Chemistry Book I* Palermo, Italy, 2017.

(4) *European Summerschool in Quantum Chemistry Book II* Palermo, Italy, 2017.

(5) *European Summerschool in Quantum Chemistry Book III* Palermo, Italy, 2017.

(6) Persico, M. Excited State Dynamics. Dipartimento di Chimica e Chimica Industriale Università di Pisa.

(7) Granucci, G.; Persico, M.; Toniolo, A. Semiclassical methods for excited state dynamics. Dipartimento di Chimica e Chimica Industriale Università di Pisa.

(8) Persico, M.; Granucci, G. An overview of nonadiabatic dynamics simulations methods, with focus on the direct approach versus the fitting of potential energy surfaces. Dipartimento di Chimica e Chimica Industriale Università di Pisa.

(9) Helgaker, T.; Jørgensen, P.; Olsen, J. *Molecular electronic structure theory*; John Wiley & Sons Ltd.: England, 2000.

(10) Levine, I. N. *Quantum Chemistry*; 5th ed.; Prentice Hall: Upper Saddle River, New Jersey, 2000.

(11) Boys, S. F. Electronic wave functions. I. A general method of calculation for the stationary states of any molecular system. *Proceedings of The Royal Society A* **1950**, *200*, 542.

(12) Hall, G. G. The molecular orbital theory of chemical valency VIII. A method of calculating ionization potentials. *Proceedings of The Royal Society A* **1951**, *205*, 541.

(13) Roothaan, C. C. J. New developments in molecular orbital theory. *Rev. Mod. Phys.* **1951**, *23*, 69.

(14) Foster, J. M.; Boys, S. F. Canonical configuration interaction procedure. *Rev. Mod. Phys.* **1960**, *32*, 300.

(15) Löwdin, P.-O. Quantum theory of many-particle systems. I. Physical interpretations by means of density matrices, natural spin-orbitals, and convergence problems in the method of configurational interaction. *Phys. Rev.* **1955**, *97*, 1474.

(16) Weyl, H. *The Theory of Groups and Quantum Mechanics*; Dover Publications, Inc.: New York, 1950.

(17) Knowles, P. J.; Handy, N. C. Unlimited full configuration interaction calculations. *J. Chem. Phys.* **1989**, *91*, 2396.

(18) Mitrushenkov, A. O. Passing the several billions limit in FCI calculations on a mini-computer. *Chem. Phys. Lett.* **1994**, *217*, 559.

(19) Olsen, J.; Jørgensen, P.; Simons, J. Passing the one-billion limit in full configuration-interaction (FCI) calculations. *Chem. Phys. Lett.* **1990**, *169*, 463.

(20) Surján, P. R. The Brillouin theorem, In *Second Quantized Approach to Quantum Chemistry*; Springer, Berlin: Heidelberg, 1989.

(21) Meyer, W. PNO-CI studies of electron correlation effects. 1. Configuration expansion by means of nonorthogonal orbitals, and application to ground-state and ionized states of methane. *J. Chem. Phys.* **1973**, *58*, 1017.

(22) Ahlrichs, R. Many-body perturbation calculations and coupled electron pair models. *Comput. Phys. Commun.* **1979**, *17*, 31.

(23) Ahlrichs, R.; Driessler, F.; Lischka, H.; Staemmler, V.; Kutzelnigg, W. PNO-CI (pair natural orbital configuration interaction) and CEPA-PNO (coupled electron pair approximation with pair natural orbitals) calculation of molecular systems. 2. Molecules BeH_2, BH, BH_3, CH_4, CH_3^-, NH_3 (planar and pyramidal), H_2O, OH^{+3}, HF, and Ne atom. *J. Chem. Phys.* **1975**, *62*, 1235.

(24) Langhoff, S. R.; Davidson, E. R. Configuration interaction calculations on the nitrogen molecule. *Int. J. Quantum Chem.* **1974**, *8*, 61.

(25) Roos, B. O.; Taylor, P. R.; Siegbahn, P. E. M. A complete active space SCF method (CASSCF) using a density matrix formulated super-CI approach. *Chem. Phys.* **1980**, *48*, 157.

(26) Ivanic, J.; Ruedenberg, K. Identification of deadwood in configuration spaces through general direct configuration interaction. *Theor. Chem. Acc.* **2001**, *106*, 339.

(27) Ruedenberg, K.; Schmidt, M. W.; Gilbert, M. M.; Elbert, S. Are atoms intrinsic to molecular electronic wavefunctions? I. The FORS model. *Chem. Phys.* **1982**, *71*, 41.

(28) Malmqvist, P.-Å.; Rendell, A.; Roos, B. O. The restricted active space self-consistent field method: Implemented with a split graph unitary group approach. *J. Phys. Chem.* **1990**, *94*, 5477.

(29) Andersson, K.; Malmqvist, P.-Å.; Roos, B. O.; Sadlej, A. J.; Wolinski, K. Second-order perturbation theory with a CASSCF reference function. *J. Phys. Chem.* **1990**, *94*, 5483.

(30) Surján, P. R.; Ángyán, J. Perturbation theory for nonlinear time-independent Schrödinger equations. *Phys. Rev. A* **1983**, *28*, 45.

(31) Møller, C.; Plesset, M. S. Note on an approximation treatment for many-electron systems. *Phys. Rev.* **1934**, *46*, 618.

(32) Serrano-Andrés, L.; Merchán, M. Quantum chemistry of the excited state: 2005 overview. *J. Mol. Struc.-THEOCHEM* **2005**, *729*, 99.

(33) Serrano-Andrés, L.; Serrano-Pérez, J. J. Calculation of excited states: Molecular photophysics and photochemistry on display, In *Handbook of Computational Chemistry*; Leszczynski, J., Ed.; Springer Dordrecht Heidelberg: London, New York, 2012; Vol. 1, p 483.

(34) Heitler, W.; London, F. Wechselwirkung neutraler atome und homöopolare bindung nach der quantenmechanik. *Z. Phys.* **1927**, *44*, 455.

(35) Coulson, C. A.; Fischer, I. XXXIV. Notes on the molecular orbital treatment of the hydrogen molecule. *Philos. Mag.* **1949**, *40*, 386.

(36) Copper, D. L.; Gerratt, J.; Raimondi, M. Studies of molecular states using spin-coupled valence-bond theory. *Faraday Symp. Chem. Soc.* **1984**, *19*, 149.

(37) Cooper, D. L.; Karadakov, P. B. Bonding in benzodicyclobutadiene isomers: Insights from modern valence bond theory. *Mol. Phys.* **2014**, *112*, 2840.

(38) Van Lenthe, J. H.; Balint-Kurti, G. G. The valence-bond SCF (VBSCF) method. Synopsis of theory and test calculation of OH potential energy curve. *Chem. Phys. Lett.* **1980**, *76*, 138.

(39) Van Lenthe, J. H.; Balint-Kurti, G. G. The valence-bond self-consistent field method (VB-SCF): Theory and test calculations. *J. Chem. Phys.* **1983**, *78*, 5699.

(40) Gallup, G. A.; Norbeck, J. M. Population analyses of valence-bond wavefunctions and BeH_2. *Chem. Phys. Lett.* **1973**, *21*, 495.

(41) Broer, R.; Van Oosten, A. B.; Nieuwpoort, W. C. Nonorthogonal CI description of localized excitations in ionic transition metal compounds. *Rev. Solid State Sci.* **1991**, *5*, 79.

(42) Hohenberg, P.; Kohn, W. Inhomogeneous electron gas. *Phys. Rev.* **1964**, *136*, B864.

(43) Kohn, W.; Sham, L. J. Self-consistent equations including exchange and correlation effects. *Phys. Rev.* **1965**, *140*, A1133.

(44) Dion, M.; Rydberg, H.; Schröder, E.; Langreth, D. C.; Lundqvist, B. I. Van der Waals density functional for general geometries. *Phys. Rev. Lett.* **2004**, *92*, 246401.

(45) Grimme, S. Semiempirical GGA-type density functional constructed with a long-range dispersion correction. *J. Comput. Chem.* **2006**, *27*, 1787.

(46) Granucci, G.; Toniolo, A. Molecular gradients for semiempirical CI wavefunctions with floating occupation molecular orbitals. *Chem. Phys. Lett.* **2000**, *325*, 79.

(47) Gao, J.; Xia, X. A priori evaluation of aqueous polarization effects through Monte Carlo QM-MM simulations. *Science* **1992**, *258*, 631.

(48) Field, M. J.; Bash, P. A.; Karplus, M. A combined quantum mechanical and molecular mechanical potential for molecular dynamics simulations. *J. Comput. Chem.* **1990**, *11*, 700.

(49) Tully, J. C.; Preston, R. K. Trajectory surface hopping approach to nonadiabatic molecular collisions: The reaction of H^+ with D_2. *J. Chem. Phys.* **1971**, *55*, 562.

(50) Granucci, G.; Persico, M.; Toniolo, A. Direct semiclassical simulation of photochemical processes with semiempirical wave functions. *J. Chem. Phys.* **2001**, *114*, 10608.

(51) Verlet, L. Computer "Experiments" on classical fluids. I. Thermodynamical properties of Lennard-Jones molecules. *Phys. Rev.* **1967**, *159*, 98.

(52) Granucci, G.; Persico, M. Critical appraisal of the fewest switches algorithm for surface hopping. *J. Chem. Phys.* **2007**, *126*, 134114.

(53) Zhu, C.; Nangia, S.; Jasper, A. W.; Truhlar, D. G. Coherent switching with decay of mixing: An improved treatment of electronic coherence for non-Born-Oppenheimer trajectories. *J. Chem. Phys.* **2004**, *121*, 7658.

(54) Zhu, C.; Jasper, A. W.; Truhlar, D. G. Non-Born-Oppenheimer Liouville-von Neumann dynamics. Evolution of a subsystem controlled by linear and population-driven decay of mixing with decoherent and coherent switching. *J. Chem. Theory Comput.* **2005**, *1*, 527.

(55) Granucci, G.; Persico, M.; Zoccante, A. Including quantum decoherence in surface hopping. *J. Chem. Phys.* **2010**, *133*, 134111.

(56) Persico, M.; Granucci, G. An overview of nonadiabatic dynamics simulations methods, with focus on the direct approach versus the fitting of potential energy surfaces. *Theor. Chem. Acc.* **2014**, *133*, 1.

Chapter 3 Nonorthogonal Configuration Interaction for the Calculation of Electronic Couplings in Singlet Fission

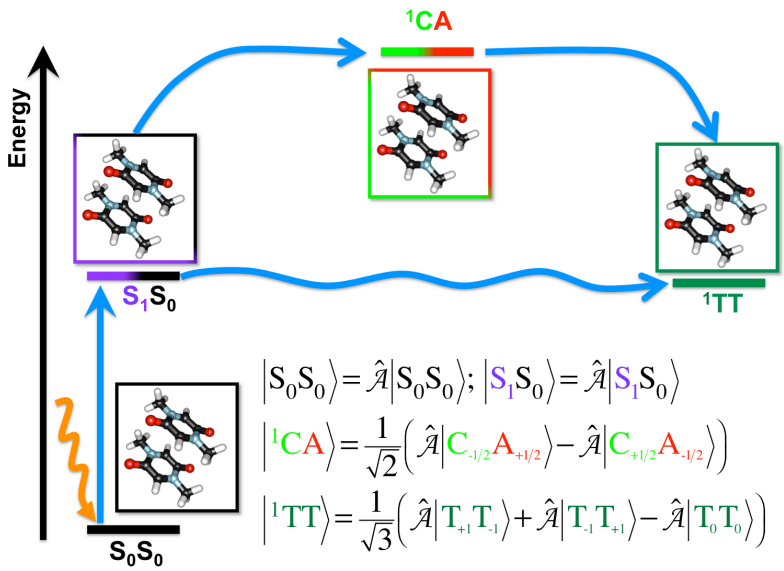

Part of the work presented in this chapter has been published as M. Wibowo, R. Broer, and R.W.A. Havenith, *Comput. Theor. Chem.*, **2017**, *1116*, 190-194, DOI: 10.1016/j.comptc.2017.03.013.

The applicability of a rigorous nonorthogonal configuration interaction approach for the evaluation of electronic couplings in singlet fission is presented. The magnitude of electronic couplings is a crucial parameter to determine the spontaneous singlet fission, mainly for the conversion from the initially photoexcited singlet state to the ^1TT state. Compared to the simplified model for the calculation of electronic couplings in singlet fission described by Michl et al. in their review papers,[1,2] this rigorous approach enables the direct calculation of the diabatic states, the inclusion of static electron correlation and orbital relaxation effects, and a clear chemical interpretation in terms of molecular states. This approach has been applied to compute the electronic couplings for a biradicaloid molecule, namely the bis(inner salt) of 2,5-dihydroxy-1,4-dimethyl-pyrazinium. This molecule is, on the basis of the quantum chemical calculations of its excitation energies, a promising candidate for singlet fission. We show that the electronic couplings between the initial and final diabatic states of this molecule are sufficiently large for singlet fission to occur.

3.1 Introduction

The magnitude of electronic couplings is an important parameter to predict the rate constant of an electron transfer process. As mentioned in Chapter 1, the rate constant of an isoergic singlet fission (SF) is commonly described by using Fermi's golden rule in which the SF rate is approximately proportional to the square of the electronic coupling between the initial (*i*) and final (*f*) diabatic states, $\left|V_{if}\right|^2 = \left|\left\langle \Psi_i \left| \hat{\mathcal{H}}_{el} \right| \Psi_f \right\rangle\right|^2$. The study presented in this chapter focuses on the calculation of this matrix element based on a rigorous nonorthogonal configuration interaction (NOCI) approach. This matrix element can be evaluated in various ways, for example, by employing the ZINDO/CISD approximation,[3] or the simplified model which consider only frontier molecular orbitals of interacting chromophores,[1,2] or even by DFT calculations.[4] Several approaches using orthogonal orbitals have also been developed to

calculate electronic couplings in an excitation energy transfer process.[5,6] An approach based on the localisation of frontier molecular orbitals followed by transformation of the Fock matrix to this basis has been used to study the vibrational effects on the computed electronic couplings in covalent tetracene dimers.[7] Recently, the calculation of electronic couplings has been performed using nonorthogonal orbitals, albeit employing the simplified model described earlier,[1] to determine the mutual orientation between two chromophores that results in maximum electronic couplings in ethene dimer models.[8,9] Another approach based on the Frenkel-Davydov exciton model has also been developed to compute molecular excited states and aggregates at the single CI level.[10] In this approach, an excitonic basis is constructed as the direct products of fragment configuration state functions (CSFs) of the ground and excited states, which are computed independently. As a result, the CSFs on different fragments are generally not orthogonal. This approach has been further applied to study the vibrational effects on a coherent fission dynamics in crystalline tetracene.[11] These existing approaches do not take into account orbital relaxation and static electron correlation effects.

In this study, we introduce a rigorous NOCI approach that enables us to calculate the electronic coupling matrix elements explicitly. We do not introduce any approximations to calculate this matrix element, and in addition, our approach is able to incorporate important orbital relaxation and static electron correlation effects. It is based on the use of a scheme introduced earlier,[12,13] in which we express the diabatic states of an ensemble of molecules in terms of NOCI wave functions. In the previous study,[12] due to technical limitations, the NOCI wave functions were approximated by computing the CASCI wave function of an ensemble of molecules with the orbitals obtained from CASSCF calculations on the individual molecules. The resulting CASCI wave function contains unwanted, contaminating, charge transfer contributions that thwart the interpretation of the NOCI wave function as being composed of several molecular states. Moreover, these charge transfer contributions lead to rather long CI expansions, especially when many molecules are included in the ensemble. Furthermore, the CASCI calculation requires an unwanted intermediate (Löwdin) orthogonalization of molecular orbitals, which also obscures the interpretation of the state. Contrary to this previous approximate ansatz, in the present study the *many*-electron basis functions for which the NOCI wave functions are expanded are spin adapted proper antisymmetrised products (ASPs) of molecular wave functions of the CASSCF type. The

orbitals in these *many*-electron basis functions are the molecular orbitals without any orthogonalizations, as the CASCI step to obtain the CI coefficients is no longer needed.

The main advantages of this rigorous implementation compared to the previous models, using orthogonal approaches, for the calculation of electronic couplings between diabatic states are: (i) the explicit computation of the electronic Hamiltonian matrix elements, (ii) the systematic inclusion of non-dynamical electron correlation and orbital relaxation effects, (iii) a clear chemical interpretation of the states involved, and (iv) the compactness of the wave function.

To illustrate the applicability of this approach, we discuss the calculation of electronic coupling matrix elements between the nonorthogonal diabatic S_0S_1 and ^1TT states for a molecule proposed by Michl and co-workers as a potential SF chromophore.[14] This so-called biradicaloid molecule, namely the bis(inner salt) of 2,5-dihydroxy-1,4-dimethyl-pyrazinium (DHDMPY), shown in Figure 3.1, has been selected and proposed to be synthesized because on the basis of quantum chemical calculations, it has been found to fulfil the basic excitation energy criteria for a potential SF chromophore, *i.e.* $\Delta E(S_1) \approx 2\Delta E(T_1)$ and $\Delta E(T_2) > 2\Delta E(T_1)$.[14]

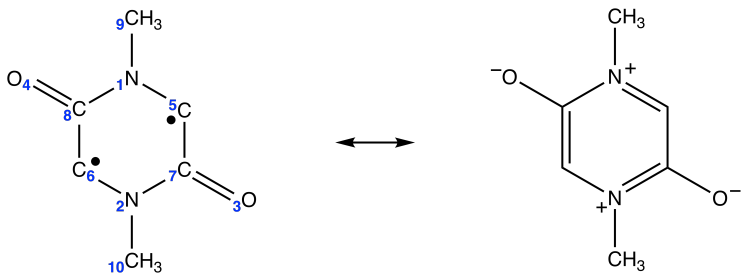

Figure 3.1 The resonance structures of DHDMPY.

In addition, we show for this system the effect of the arrangement between neighbouring chromophores on the computed electronic couplings. In our previous work on tetracene,[12] it was shown that only the nearest neighbour couplings are significant, and these are insensitive to the cluster size. In addition, efficient SF was observed in solution of one photoexcited state and one ground state of TIPS-pentacene, showing that the involvement of two chromophores

is sufficient to detect the evidence of singlet exciton fission.[15] Therefore, for the present purpose it suffices to use small clusters consisting of only two neighbouring molecules.

3.1.1 Electronic States in Singlet Fission

The main electronic states in SF are the ones described in Eq. (1.1), *i.e.* the singlet ground state (S_0), the lowest singlet and triplet excited states (S_1 and T_1), and the singlet coupled triplet states (^{1}TT). However, other states might contribute as well, *i.e.* the intermediate charge transfer states, ^{1}CA and ^{1}AC, as already mentioned in Section 1.3.

The very first process in SF before it goes to the formation of the ^{1}TT state is the initial photoexcitation of the ground state SF chromophore to an optically active singlet excited state (S_n), carrying the largest oscillator strength. If the optically active singlet excited state is not the lowest one (S_1), it is commonly assumed that the chromophore will rapidly decay to the S_1 state by internal conversion (Kasha's rule).[16] Moreover, in the limit of weakly interacting chromophores, the optically active singlet excited state is usually the bright state with higher energy rather than the lower dark one. The character of this bright state and other low-lying energy states for SF chromophores has been discussed in terms of chromophore classes.[1] The final product of the whole process is the T_1 state, which can be populated after the dissociation of the ^{1}TT state occurred. The ^{1}TT state corresponds to the triplet-pair states coupled into an overall spin singlet. The electronic character of this state is multiconfigurational in nature. Providing a good description of this state (^{1}TT) and other spin-pair states (^{1}CA and ^{1}AC) is a challenging task from the theoretical and computational point of view. However, in principle, these pure spin-pair states can be expressed as spin adapted ASPs between molecular wave functions such that,

$$\left|\Phi_n\right\rangle = \sum_{\sigma} C_{\sigma}\, \hat{\mathcal{A}} \left|\Psi_I^{M_I}\Psi_J^{M_J}\Psi_K^{M_K}\ldots\right\rangle_{\sigma}, \tag{3.1}$$

where C_σ is the spin-coupling coefficients and the summation over σ indicates several combinations of ASPs of molecular wave functions $\left|\Psi_I^{M_I}\Psi_J^{M_J}\Psi_K^{M_K}\ldots\right\rangle$ with different spin quantum numbers m_s. Therefore, the ^{1}TT and ^{1}CA wave functions for two weakly interacting chromophores can be written as

$$\left|{}^1\mathrm{TT}\right\rangle = \frac{1}{\sqrt{3}}\left(\hat{\mathcal{A}}\left|\Psi_I^{m_s=+1}\Psi_J^{m_s=-1}\right\rangle - \hat{\mathcal{A}}\left|\Psi_I^{m_s=0}\Psi_J^{m_s=0}\right\rangle + \hat{\mathcal{A}}\left|\Psi_I^{m_s=-1}\Psi_J^{m_s=+1}\right\rangle\right) \tag{3.2}$$

and

$$\left|{}^1\mathrm{CA}\right\rangle = \frac{1}{\sqrt{2}}\left(\hat{\mathcal{A}}\left|\Psi_I^{m_s=-1/2}\Psi_J^{m_s=+1/2}\right\rangle - \hat{\mathcal{A}}\left|\Psi_I^{m_s=+1/2}\Psi_J^{m_s=-1/2}\right\rangle\right), \tag{3.3}$$

and similarly for the ^{1}AC wave function.

3.1.2 Nonorthogonal Configuration Interaction for Ensembles of Molecules

In this approach, we describe the diabatic states of an ensemble of molecules in terms of NOCI wave functions for which spin adapted ASPs of molecular wave functions, which can be in principle of any type, are combined to construct the *many*-electron basis functions, and then followed by a NOCI calculation. We take an initial state $\left|\Phi_i\right\rangle$ of an ensemble of neighbouring molecules as $\left|IJKL\ldots\right\rangle$, where $I, J, K,$ and L indicate the ground state wave function of the molecules in the ensemble. An intermediate, local excited singlet state $\left|\Phi_{m_J}\right\rangle$ could be $\left|IJ^{\mathrm{S}}KL\ldots\right\rangle$, where J^{S} represents an excited spin singlet state localised on molecule J and the other molecules are in their ground state. In the case of SF, we are interested in the delocalisation of the singlet excited state, involving other local excited singlet state like $\left|\Phi_{m_K}\right\rangle = \left|IJK^{\mathrm{S}}L\ldots\right\rangle$, where K^{S} represents an excited singlet state localised on molecule K, and in the transition rate from the (delocalised) singlet excited state to a 'final' state $\left|\Phi_f\right\rangle = \left|IJ^{\mathrm{T}}K^{\mathrm{T}}L\ldots\right\rangle$, where J^{T} and K^{T} are excited triplet states on neighbouring molecules J and K, which are coupled into an overall spin singlet. The study of the delocalisation of the excited singlet state involves computation of $\left\langle\Phi_{m_J}\left|\hat{\mathcal{H}}_{el}\right|\Phi_{m_K}\right\rangle$ and the study of the transition rate between $\left|\Phi_{m_J}\right\rangle$ and $\left|\Phi_f\right\rangle$ involves the computation of $\left\langle\Phi_{m_J}\left|\hat{\mathcal{H}}_{el}\right|\Phi_f\right\rangle$, where $\hat{\mathcal{H}}_{el}$ is the electronic Hamiltonian. The computation of these matrix elements is non-trivial because the orbitals of the molecular wave functions in $\left|\Phi_{m_J}\right\rangle$, $\left|\Phi_{m_K}\right\rangle$, and $\left|\Phi_f\right\rangle$ are optimised orbitals

for each molecular electronic state, which are different from one and another, and therefore, they are mutually not orthogonal. An interesting question that can be addressed with this approach is whether charge transfer basis functions such as $\left|IJ^{+}K^{-}L\ldots\right\rangle$ play a role in the SF process, either as virtual states or as intermediate states. Electronic relaxation effects are very important in the excitation, delocalisation, and fission processes. Besides, the orbitals that are optimal for I, for I^{S}, for I^{T}, for I^{+}, and for I^{-} are all quite different. It is therefore preferable both from the computational and from the conceptual viewpoints, to express each molecular state, and therewith each of these diabatic states, in its own optimised orbital set.

In our approach, we took an ensemble of two molecules A and B, and we used the *many*-electron basis functions of $\left|AB\right\rangle$, $\left|A^{\mathrm{S}}B\right\rangle$, $\left|AB^{\mathrm{S}}\right\rangle$, $\left|A^{\mathrm{T}}B^{\mathrm{T}}\right\rangle$, $\left|A^{+}B^{-}\right\rangle$, and $\left|A^{-}B^{+}\right\rangle$ types to construct the diabatic states. These *many*-electron basis functions describe the ground states of all molecules, singlet excitation on one of the molecules, triplet excitation on two neighbouring molecules, and inter-molecular charge transfer between the two molecules. The final NOCI wave function can be written as linear combination of these *many*-electron basis functions such that,

$$\Psi_{NOCI}=\sum_{n}C_{n}\Phi_{n}\,, \tag{3.4}$$

where the coefficients C_n are determined using the variational principle for which the evaluation of the electronic Hamiltonian and overlap matrix elements, $\left\langle\Phi_{n}\left|\hat{\mathcal{H}}_{el}\right|\Phi_{m}\right\rangle$ and $\left\langle\Phi_{n}\middle|\Phi_{m}\right\rangle$, are required. Each molecular wave function used to describe the *many*-electron basis functions uses its own optimised orbitals. The use of optimised orbitals for each molecular wave function and the formation of the *many*-electron basis functions as spin adapted ASPs of molecular wave functions make the *many*-electron basis functions mutually not orthogonal.

3.2 Computational Details

The crystal structure of DHDMPY is unknown, and therefore, to determine a plausible crystal structure, periodic DFT calculations starting from the known crystal structure of a

related compound, namely 2,5-dimethyl-1,4-benzoquinone,[17] were performed using the CRYSTAL14 code.[18] The PBE functional[19,20] and the 6-21G basis set were employed. In addition, the Grimme dispersion correction[21] was included for the optimization of atom positions and cell parameters.

The excitation energies of DHDMPY were calculated using two different active spaces, *i.e*. CASSCF(2,2) and CASSCF(6,5). Dynamical electron correlation was included up to the second order perturbation theory (CASPT2) following the CASSCF(6,5) calculation. All CASSCF and CASPT2 calculations were performed using the ANO-L basis set contracted to C,N,O[3s2p1d]/H[2s].[22] All of these calculations were performed using the MOLCAS 7.4 code.[23]

Due to technical reasons, the CASSCF(2,2) wave functions of the ground state, the lowest excited singlet and triplet states, as well as the restricted open-shell HF wave functions of the cation and anion were computed using the GAMESS-UK code.[24] These wave functions were subsequently used to construct the *many*-electron basis functions. The ensemble of molecules consists of two molecules A and B whose wave functions can be combined to form six different ASP wave functions, which are the *many*-electron basis functions. They are listed as follows: one *many*-electron basis function describing the ground state on both molecules $\Psi_{S_0S_0} = \hat{\mathcal{A}}\left|AB\right\rangle$, two *many*-electron basis functions describing the localised singlet excitation on one of the molecules $\Psi_{S_0S_1} = \hat{\mathcal{A}}\left|AB^S\right\rangle$ and $\Psi_{S_1S_0} = \hat{\mathcal{A}}\left|A^SB\right\rangle$, one *many*-electron basis function describing two triplet states that are coupled into a total spin singlet $\Psi_{^1TT} = \hat{\mathcal{A}}\left|A^TB^T\right\rangle$, and two *many*-electron basis functions describing the charge-transfer states $\Psi_{CT1} = \hat{\mathcal{A}}\left|A^+B^-\right\rangle$ and $\Psi_{CT2} = \hat{\mathcal{A}}\left|A^-B^+\right\rangle$. These *many*-electron basis functions were used to construct the diabatic $S[1]$ and $S[2]$ states and the ^{1}TT state. The electronic Hamiltonian and overlap matrix elements between these nonorthogonal *many*-electron basis functions were calculated using the GNOME (General program for NonOrthogonal Matrix Elements) code that had been developed earlier in our group.[25]

The diabatic $S[1]$ and $S[2]$ states were obtained from a 2x2 NOCI calculation in the basis of two *many*-electron basis functions, $\Psi_{S_0S_1}$ and $\Psi_{S_1S_0}$, each having one molecule in its lowest excited singlet state. The diabatic ^{1}TT state is the ^{1}TT basis function, $\Psi_{^1TT}$. To investigate the effect of charge-transfer states on these diabatic states, the two *many*-electron

basis functions describing the charge-transfer states, Ψ_{CT1} and Ψ_{CT2}, were added to the NOCI calculation for the diabatic $S[1]$ and $S[2]$ states (giving a 4x4 NOCI) and to the NOCI calculation for the diabatic ^{1}TT state (giving a 3x3 NOCI).

To investigate the importance of each *many*-electron basis function in the diabatic $S[1]$, $S[2]$, and ^{1}TT states, the weights (W_i) of the *many*-electron basis functions *i* were calculated using the Gallup and Norbeck scheme,[26] $W_i = |c_i|^2 / (S^{-1})_{ii}$, where c_i is the CI coefficient of the *many*-electron basis function *i*, and $(S^{-1})_{ii}$ is the *ii*th element of the inverse of the overlap matrix.

The effective electronic couplings between the diabatic $S[1]$ and $S[2]$ states and the ^{1}TT state were calculated using the following formula[12]

$$t_{ij} \approx \frac{H_{ij} - H^{av} S_{ij}}{1 - S_{ij}^2}, \tag{3.5}$$

where $H_{ij} = \langle \Psi(S[1,2]) | \hat{\mathcal{H}}_{el} | \Psi(^1\text{TT}) \rangle$, $S_{ij} = \langle \Psi(S[1,2]) | \Psi(^1\text{TT}) \rangle$, and $H^{av} = \frac{1}{2}\left(\langle \Psi(S[1,2]) | \hat{\mathcal{H}}_{el} | \Psi(S[1,2]) \rangle + \langle \Psi(^1\text{TT}) | \hat{\mathcal{H}}_{el} | \Psi(^1\text{TT}) \rangle \right)$.

3.3 Results and Discussion

The periodic DFT calculations of DHDMPY showed a P_{-1} symmetry with the absence of imaginary frequencies and provided the final cell parameters: *a* = 3.578 Å, *b* = 8.757 Å, *c* = 9.413 Å, α = 96.55°, β = 96.77°, γ = 109.11°, and ρ = 1.703 g/cm^3. Since to the best of our knowledge the molecule has not been successfully synthesised yet, and therefore, there are no experimental data to compare with. Figure 3.2 shows the resulting computed crystal structure. There are two different stacks in the crystal structure, to be denoted stack A and stack B. The band structure (not shown) shows dispersion mainly in the stack directions. Therefore, we considered two intra-stack pairs of neighbouring molecules (in stack A and in stack B, respectively) and also an A-B inter-stack pair for the evaluation of electronic couplings. The intra-stack pairs show π-like stacking (slip-stack) of two molecules, while the inter-stack pair

shows an arrangement of two neighbouring molecules, one is taken from stack A and the other one is taken from stack B. One difference between stack A and stack B is the N-N distance between two molecules, *i.e*. 3.854 Å and 3.638 Å, respectively (see Figure 3.2).

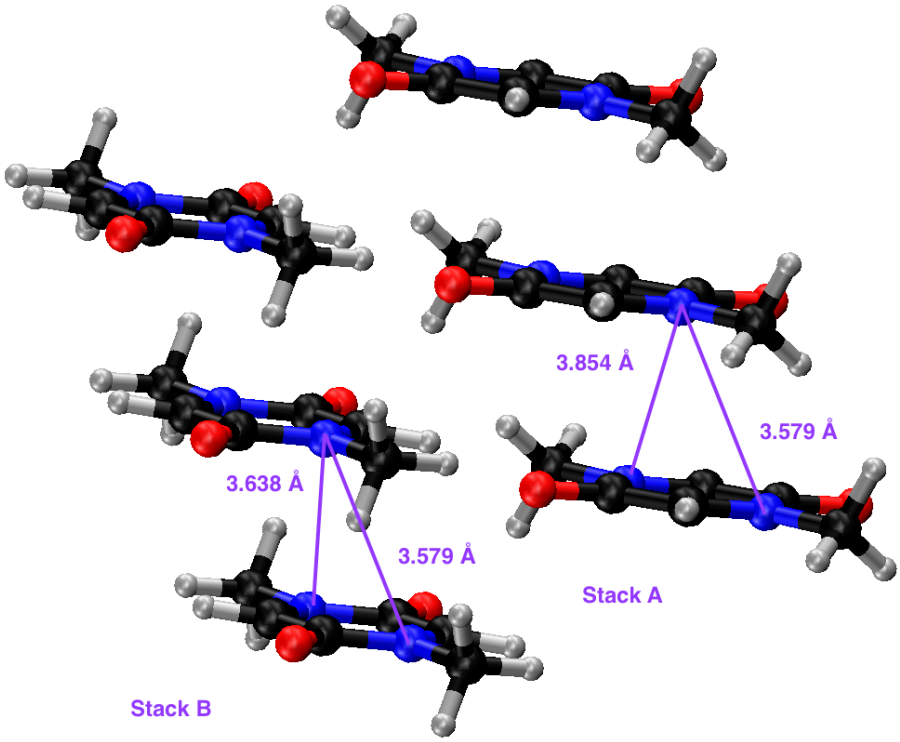

Figure 3.2 The computed crystal structure of DHDMPY (C, N, O, and H atoms are represented in black, in blue, in red, and in grey, respectively).

An interesting property of this molecule is the multireference character of its ground state. A CASSCF(2,2) calculation gives natural orbital occupation numbers of 1.76 and 0.24 for the π-type HOMO and the π*-type LUMO, respectively. Therefore, single reference methods are not suitable even to describe its ground state. The lowest excited singlet and triplet states of DHDMPY have mainly a single excitation from HOMO to LUMO, and therefore have π→π* character (see Figure 3.3).

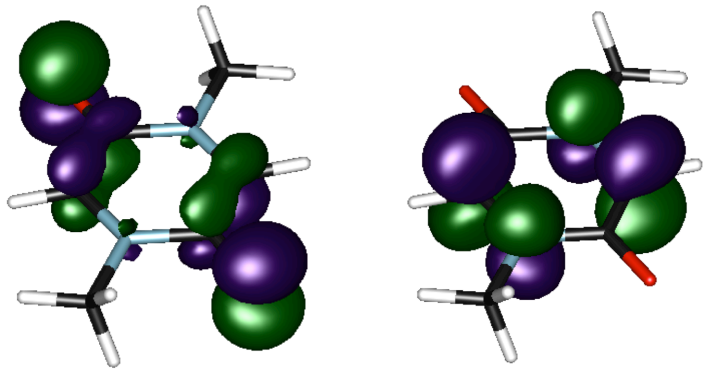

Figure 3.3 Singly occupied molecular orbitals in the S_1 state of DHDMPY.

The vertical excitation energies of the lowest excited singlet and triplet states computed with CASSCF(2,2) and CASPT2/CASSCF(6,5) are listed in Table 3.1. The S_1 excitation energy computed using CASPT2/CASSCF(6,5) is higher than that reported by Akdag *et al*.,[14] in which a larger active space had been used [CASSCF(22,14)], in contrast with the T_1 excitation energy. The inclusion of dynamical electron correlation by perturbation theory up to the second order (CASPT2) improves the excitation energies considerably. The vertical excitation energy of the lowest excited singlet state computed with CASSCF(2,2) is 1.0 eV higher than those computed with a larger active space. Since an important objective of this study is to prove the principle of the approach, and we are interested in estimating the order of magnitude of the electronic coupling, we used the CASSCF(2,2) wave functions to construct the *many*-electron basis functions for the diabatic $S[1]$ and $S[2]$ states and the ^{1}TT state, albeit their relative energies are rather poor.

Table 3.1 CASSCF(2,2) and CASPT2/CASSCF(6,5) vertical excitation energies (eV) of DHDMPY calculated at their geometry in stack A.

State	CASSCF(2,2)	CASSCF(6,5)	CASPT2(6,5)	CASPT2(22,14)[14]
S_1	3.86	2.71	2.42	2.21
T_1	0.84	0.77	1.06	1.21

As described previously, the combination of different molecular wave functions by taking their spin adapted ASPs, gives six *many*-electron basis functions that were used to construct the diabatic $S[1]$ and $S[2]$ states and the ^1TT state. The relative energies of these *many*-electron basis functions for the pairs taken from stack A and stack B, and the inter-stack pair are listed in Table 3.2. The *many*-electron basis functions $\Psi_{S_0S_1}$ and $\Psi_{S_1S_0}$ describe the localised singlet excitation on one of the molecules and were used as the basis to construct the diabatic $S[1]$ and $S[2]$ states. The relative energies of these *many*-electron basis functions are close to the excitation energy of the lowest excited singlet state of the molecule. The *many*-electron basis function $\Psi_{^1TT}$ represents by itself the diabatic ^1TT state. The relative energy of this basis function is about twice the excitation energy of the lowest excited triplet state of the molecule. The two *many*-electron basis functions Ψ_{CT1} and Ψ_{CT2} describe the charge transfer states in which an electron is transferred from one molecule to another. In all cases, the relative energies of these charge-transfer basis functions are 4.5 eV or more above the ground state energy. In principle, these charge-transfer basis functions may play a role in the SF process either as virtual states or as intermediate states, but due to their high energy they cannot act as intermediate states in this case.

Table 3.2 The relative energies (eV) of the *many*-electron basis functions for the pairs taken from stack A and stack B, and the inter-stack pair.

Many-electron basis functions	Stack A	Stack B	Inter-stack
$\Psi_{S_0S_1} = \hat{\mathcal{A}}\left\vert AB^S\right\rangle$	3.81	3.90	3.88
$\Psi_{S_1S_0} = \hat{\mathcal{A}}\left\vert A^SB\right\rangle$	3.81	3.90	3.99
$\Psi_{^1TT} = \hat{\mathcal{A}}\left\vert A^TB^T\right\rangle$	1.61	1.48	1.74
$\Psi_{CT1} = \hat{\mathcal{A}}\left\vert A^+B^-\right\rangle$	4.49	4.52	4.92
$\Psi_{CT2} = \hat{\mathcal{A}}\left\vert A^-B^+\right\rangle$	4.49	4.52	5.46

Relative energies with respect to the $\Psi_{S_0S_0} = \hat{\mathcal{A}}\left\vert AB\right\rangle$ total energy, *i.e.* -981.112938 Hartree, -981.111975 Hartree, and -981.135813 Hartree for the pairs taken from stack A and stack B, and the inter-stack pair, respectively.

A 2x2 NOCI calculation in the basis of two *many*-electron basis functions $\Psi_{S_0S_1}$ and $\Psi_{S_1S_0}$ gives the diabatic $S[1]$ and $S[2]$ states. The relative energies of these diabatic states are split by about 0.2 eV in the case of the pairs taken from stack A and stack B. The singlet excitation is delocalised (by symmetry) over the two molecules, as shown by the weights of the *many*-electron basis functions (see Table 3.3). In contrast, for the inter-stack pair, the diabatic $S[1]$ and $S[2]$ states can be interpreted as being a localised singlet excitation on one of the molecules (see the weights in Table 3.3) and negligible energy splitting is obtained. The ^{1}TT state has a triplet excited state localised on each molecule, and in this model it is equal to the *many*-electron basis function $\Psi_{^1TT}$.

Table 3.3 The relative energies (E_{rel}, eV) and weights (W) of the *many*-electron basis functions in the different diabatic states.

	Diabatic states	E_{rel}	$W_{\Psi_{S_0S_1}}$	$W_{\Psi_{S_1S_0}}$	W_{CT}
Stack A		3.72	0.50	0.50	
Stack B	$\Psi(S[1])$	3.74	0.50	0.50	
Inter-stack		3.88	0.02	0.98	
Stack A		3.90	0.50	0.50	
Stack B	$\Psi(S[2])$	4.06	0.50	0.50	
Inter-stack		3.99	0.98	0.02	
Stack A		3.64	0.45	0.45	0.09
Stack B	$\Psi'(S[1])$	3.66	0.46	0.46	0.08
Inter-stack		3.87	0.03	0.96	0.01
Stack A		3.90	0.50	0.50	0.00
Stack B	$\Psi'(S[2])$	4.04	0.48	0.48	0.03
Inter-stack		3.99	0.97	0.03	0.00

Annotation: In the unprimed wave functions the charge-transfer basis functions are not included in the NOCI calculations, while in the primed wave functions the charge-transfer basis functions are included. W_{CT} indicates the total weights of the charge-transfer basis functions Ψ_{CT1} and Ψ_{CT2}.

To investigate the role of charge transfer states, a 4x4 NOCI calculation in the basis of the *many*-electron basis functions $\Psi_{S_0S_1}$ and $\Psi_{S_1S_0}$ together with the two charge-transfer basis functions Ψ_{CT1} and Ψ_{CT2} was performed. The relative energies and weights of these *many*-electron basis functions are shown in Table 3.3. The charge-transfer basis functions (weakly) interact with the diabatic $S[1]$ and $S[2]$ states, leading to a small energy lowering and to non-zero weights of the charge-transfer basis functions (see the total weights of the charge-transfer basis functions, W_{CT}). On the contrary, the inclusion of the charge-transfer basis functions in the ^{1}TT state does not affect the relative energy of this state and the ^{1}TT state remains practically the pure ^{1}TT basis function. It is therefore not shown in Table 3.3.

The computed electronic couplings between the diabatic $\Psi(S[1])$, $\Psi(S[2])$, $\Psi(^1TT)$, $\Psi'(S[1])$, $\Psi'(S[2])$, and $\Psi'(^1TT)$ states are listed in Table 3.4. For the pairs taken from stack A or stack B the largest couplings are obtained between the diabatic $S[1]$ and ^{1}TT states for which the singlet excitation in $S[1]$ is delocalised over two molecules and its energy is lower than that of the diabatic $S[2]$. The inclusion of the charge-transfer basis functions in the diabatic $S[1]$ state increases the computed electronic couplings from 4.0 (1.9) meV to 16.5 (17.4) meV for the pairs taken from stack A (stack B). Increased computed electronic couplings are also obtained if the charge-transfer basis functions are included only in the diabatic ^{1}TT state, even though the weights of the charge-transfer basis functions are only minor. However, the inclusion of the charge-transfer basis functions only in the diabatic $S[1]$ state slightly overestimates the couplings. The most reasonable estimate of the computed electronic couplings is when the charge-transfer basis functions are allowed to interact with both the diabatic $S[1]$ and ^{1}TT states (the computed electronic couplings between the $\Psi'(S[1])$ and $\Psi'(^1TT)$ states, Table 3.4). The magnitude of the computed electronic couplings in both stack A and stack B is sufficiently large so that SF can occur efficiently.[1] The computed electronic couplings of the inter-stack pair are nearly close to zero. These results are not surprising since the band structure shows dispersion mainly along the stack direction of the crystal structure.

Table 3.4 The computed electronic couplings (meV) between the diabatic $S[1]$ and $S[2]$ wave functions and the ^{1}TT wave function.

	S[1] and S[2] states → ^{1}TT states ↓	$\Psi(S[1])$	$\Psi(S[2])$	$\Psi'(S[1])$	$\Psi'(S[2])$
Stack A	$\Psi(^1TT)$	4.0	0.0	16.5	0.0
Stack B		1.9	0.0	17.4	0.0
Inter-stack		0.4	0.1	0.2	0.3
Stack A	$\Psi'(^1TT)$	6.9	0.0	11.8	0.0
Stack B		5.5	0.0	12.2	0.0
Inter-stack		3.3	0.0	0.1	0.2

Annotation: In the unprimed wave functions the charge-transfer basis functions are not included in the NOCI calculations, while in the primed wave functions the charge-transfer basis functions are included.

3.3.1 Geometry Dependence on the Computed Electronic Couplings

Another interesting point that can be addressed in this study is the geometry dependence on the computed electronic couplings. To investigate this effect, we first performed DFT and TD-DFT calculations using the PBE functional[19,20] and the 6-21G basis set, as we did for the optimisation of the plausible crystal structure. The TD-DFT calculations were used to compute the excitation energies and also to optimise the geometry of the S_1 state, whereas the DFT calculations were used for the S_0 and T_1 geometry optimisations. All calculations were performed in vacuum. The results, presented in Table 3.5, show slight differences between the relaxed S_0 geometries obtained in the molecular crystal and in vacuum, *i.e*. the elongation of the N_2-C_7 bond by 0.04 Å and the decreasing of the bond angle C_5-C_7-N_2 by 3.11°. The excitations that characterise the S_1 and T_1 states also depend on these geometrical changes. In the relaxed S_1 geometry, the N_2-C_7 bond is shortened by 0.05 Å and the bond angle C_5-C_7-N_2 is increased by 5.46°, indicating the breathing of the six-membered ring. These results are consistent with a larger energy difference between excitation energies obtained in the S_0 relaxed geometry and in the S_1 relaxed geometry by about 0.46 eV (see Table 3.6). On the

contrary, the T_1 relaxed geometry is similar to that of the S_0 state, a fact that must be kept in mind when discussing the exploration of the PESs.

Table 3.5 Geometrical properties of DHDMPY obtained at the PBE/6-21G level of theory in different relaxed geometries. Bond distances (r) in Å and bond angles ($\angle$) in degrees.

Coordinates	S_0[a]	S_0	S_1	T_1
$r(C_{10}\text{-}N_2)$	1.490	1.485	1.478	1.475
$r(N_2\text{-}C_7)$	1.420	1.459	1.413	1.453
$r(C_7\text{-}O_3)$	1.299	1.266	1.302	1.270
$r(N_2\text{-}C_6)$	1.360	1.361	1.393	1.385
$r(C_6\text{-}C_8)$	1.416	1.428	1.417	1.428
$\angle(C_7\text{-}N_2\text{-}C_6)$	123.62	124.92	120.64	120.76
$\angle(C_5\text{-}C_7\text{-}N_2)$	114.51	111.40	116.86	115.84
$\angle(C_8\text{-}C_6\text{-}N_2)$	121.86	123.68	122.50	123.70

[a]Molecular crystal.

Table 3.6 Excitation energies (eV) of DHDMPY obtained at the TD-DFT/6-21G level of theory in different relaxed geometries. All energies are computed with respect to the ground state energy in the ground state relaxed geometry.

	Relaxed geometries		
	S_0	S_1	T_1
S_0	0.00	0.22	0.07
S_1	2.28	1.82	1.90
T_1	1.09	0.91	0.83

The S_0, S_1, and T_1 relaxed geometries were then used to replace both molecules in the stack A arrangement producing: (i) both molecules in the S_0 relaxed geometries, (ii) one in the S_0 relaxed geometry and the other one in the S_1 relaxed geometry, and (iii) both molecules in the T_1 relaxed geometries. In this way, we obtained three different stationary points, to be denoted the S_0, S_1, and ^{1}TT points, for which the exploration of the PESs were performed. To do so, nine geometries between the calculated stationary points (S_0, S_1, and ^{1}TT points) were

estimated by the linear interpolation of internal coordinates and their transition energies were computed employing the state average CASSCF(4,4)/ANO-L C,N[3s2p1d]/H[2s] procedure (see Figure 3.4). The S_1 PES shows a relatively flat surface with stabilisation energy of about 0.28 eV from the Franck-Condon point to the S_1 point and its energy slightly increases at the ^{1}TT point, in accordance with the slightly higher excitation energy of the S_1 state obtained in the T_1 relaxed geometry (see Table 3.6). On the contrary, the ^{1}TT PES is slightly steeper that that of the S_1 PES at the Franck-Condon point and its energy increases at the S_1 point then decreases drastically, reaching its minimum at the ^{1}TT point, and bringing the ^{1}TT PES much closer to the S_0 PES. This result is consistent with the closeness of the geometrical parameters between the S_0 and T_1 relaxed geometries.

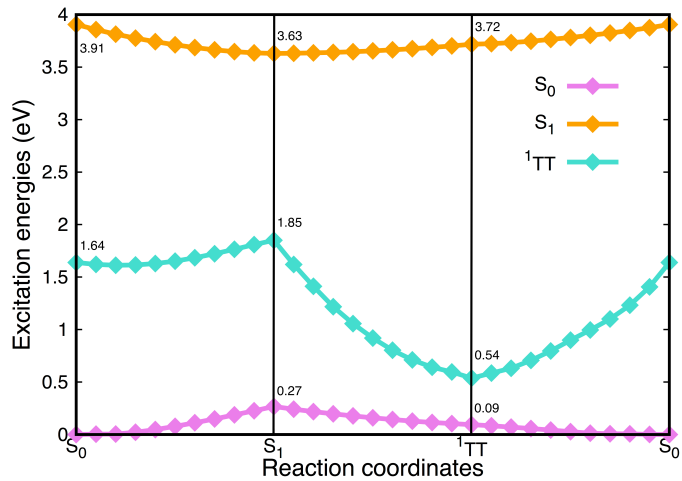

Figure 3.4 State average CASSCF(4,4)/ANO-L C,N[3s2p1d]/H[2s] potential energy surfaces of DHDMPY.

For each stationary point, we computed the electronic couplings between the diabatic $S[1]$ and $S[2]$ wave functions and the ^{1}TT wave function. From the results, presented in Table 3.7, we also observed the same trend on the computed electronic couplings with respect to the inclusion of charge transfer basis functions only in the diabatic $S[1]$ and $S[2]$ states, *i.e.* an overestimation of the computed electronic couplings. Therefore, from now on we consider the values of the computed electronic couplings with the inclusion of charge transfer basis functions in both singlet diabatic states, $S[1]$ and $S[2]$, and in the ^{1}TT state. The results

show that the computed electronic couplings between the diabatic $S[1]$ and ^1TT states with the inclusion of the charge transfer basis functions at the S_0 point—the computed electronic couplings between the $\Psi'(S[1])$ and $\Psi'(^1TT)$ states—are in the same order of magnitude with the ones computed at the geometry of the stack A obtained from the crystal structure (see Table 3.4 for comparison), in accordance with the small difference between the S_0 geometry at the molecular crystal and the S_0 relaxed geometry computed in vacuum. On one hand, at the ^1TT point, the computed electronic couplings between the $\Psi'(S[1])$ and $\Psi'(^1TT)$ states reduce to nearly half of those obtained at the S_0 point in which the energy difference of the ^1TT state with respect to the S_0 state reduces to 0.54 eV (see Figure 3.4), and it is therefore increasing the energy gap between the S_1 and ^1TT states. On the other hand, at the S_1 point, both the diabatic $S[1]$ and $S[2]$ states (weakly) interact with the ^1TT state (non-zero values of the computed electronic couplings between the $\Psi'(S[1])$ and $\Psi'(S[2])$ states and the $\Psi'(^1TT)$ state, see Table 3.7).

Table 3.7 The computed electronic couplings (meV) between the diabatic $S[1]$ and $S[2]$ wave functions and the ^1TT wave function, computed in the S_0, S_1, and T_1 relaxed geometries.

	S[1] and S[2] states → / ^1TT states ↓	$\Psi(S[1])$	$\Psi(S[2])$	$\Psi'(S[1])$	$\Psi'(S[2])$
S_0	$\Psi(^1TT)$	5.3	0.0	25.1	0.0
S_1		2.6	1.9	12.3	15.4
T_1		1.9	0.0	6.7	0.0
S_0	$\Psi'(^1TT)$	9.1	0.0	17.4	0.0
S_1		4.4	3.3	8.6	9.3
T_1		2.8	0.0	4.7	0.0

Annotation: In the unprimed wave functions the charge-transfer basis functions are not included in the NOCI calculations, while in the primed wave functions the charge-transfer basis functions are included.

3.4 Conclusions

We have used a NOCI approach for calculating the electronic couplings between the lowest diabatic excited singlet states and the ^{1}TT state. The diabatic $S[1]$ and $S[2]$ states can be interpreted as the molecular singlet excitation, delocalised over two molecules. These states are indicative for the delocalisation of the singlet excitation over the stack. These diabatic states (weakly) interact with the charge-transfer basis functions. The diabatic ^{1}TT state can be interpreted as having a localised triplet excitation on each molecule. The computed electronic couplings between the diabatic $S[1]$ and $S[2]$ states and the ^{1}TT state are in the few meV range, which is sufficient for SF to occur in pairs of molecules placed in a slip-stack orientation. The inclusion of charge-transfer basis functions enhances the computed electronic couplings and they act only as virtual states in the conversion from the initially generated photoexcited state to the ^{1}TT state. The computed electronic couplings also depend on the geometry used to construct the pair of molecules, even though they are placed in the same orientation and displacement. These results are obtained for ASPs of molecular CASSCF wave functions, which are found with a minimal active space consisting of only the two frontier molecular orbitals. Moreover, the CASSCF wave functions were obtained for isolated molecules. The resulting couplings will of course change if more accurate molecular wave functions are employed. Nevertheless, the present results do indicate that this DHDMPY molecule is indeed a potential candidate as a SF chromophore. The NOCI approach for calculating the electronic coupling between the diabatic excited singlet states and the ^{1}TT state is feasible and allows for a clear chemical interpretation of the diabatic states.

3.5 References

(1) Smith, M. B.; Michl, J. Singlet fission. *Chem. Rev.* **2010**, *110*, 6891.

(2) Smith, M. B.; Michl, J. Recent advances in singlet fission. *Annu. Rev. Phys. Chem.* **2013**, *64*, 61.

(3) Kawatsu, T.; Coropceanu, V.; Ye, A.; Brédas, J.-L. Quantum-chemical approach to electronic coupling: Application to charge separation and charge recombination pathways in a model molecular donor-acceptor system for organic solar cells. *J. Phys. Chem. C* **2008**, *112*, 3429.

(4) Pavanello, M.; Van Voorhis, T.; Visscher, L.; Neugebauer, J. An accurate and linear-scalling method for calculating charge-transfer excitation energies and diabatic couplings. *J. Chem. Phys.* **2013**, *138*, 054101.

(5) You, Z.-Q.; Hsu, C.-P. Theory and calculation for the electronic coupling in excitation energy transfer. *Int. J. Quantum Chem.* **2014**, *114*, 102.

(6) Hsu, C.-P. The electronic couplings in electron transfer and excitation energy transfer. *Acc. Chem. Res.* **2009**, *42*, 509.

(7) Alguire, E. C.; Subotnik, J. E.; Damrauer, N. H. Exploring non-condon effects in a covalent tetracene dimer: How important are vibrations in determining the electronic coupling for singlet fission? *J. Phys. Chem. A* **2015**, *119*, 299.

(8) Buchanan, E. A.; Havlas, Z.; Michl, J. Singlet fission: Optimization of chromophore dimer geometry, In *Adv. Quantum Chem.*; Zoe Kruze: 2017; Vol. 75, p 175.

(9) Havlas, Z.; Michl, J. Guidance for mutual disposition of chromophores for singlet fission. *Isr. J. Chem.* **2016**, *56*, 96.

(10) Morrison, A. F.; You, Z.-Q.; Herbert, J. M. Ab initio implementation of the Frenkel-Davydov exciton model: A naturally parallelizable approach to computing collective excitations in crystals and aggregates. *J. Chem. Theory Comput.* **2014**, *10*, 5366.

(11) Morrison, A. F.; Herbert, J. M. Evidence for singlet fission driven by vibronic coherence in crystalline tetracene. *J. Phys. Chem. Lett.* **2017**, *8*, 1442.

(12) Havenith, R. W. A.; De Gier, H. D.; Broer, R. Explorative computational study of the singlet fission process. *Mol. Phys.* **2012**, *110*, 2445.

(13) Broer, R.; Van Oosten, A. B.; Nieuwpoort, W. C. Nonorthogonal CI description of localized excitations in ionic transition metal compounds. *Rev. Solid State Sci.* **1991**, *5*, 79.

(14) Akdag, A.; Havlas, Z.; Michl, J. Search for a small chromophore with efficient singlet fission: Biradicaloid heterocycles. *J. Am. Chem. Soc.* **2012**, *134*, 14624.

(15) Walker, B. J.; Musser, A. J.; Beljonne, D.; Friend, R. H. Singlet exciton fission in solution. *Nat. Chem.* **2013**, *5*, 1019.

(16) Kasha, M. Characterization of electronic transitions in complex molecules. *Discuss. Faraday Soc.* **1950**, *9*, 14.

(17) Rabinovich, D.; Schmidt, G. M. J. Topochemistry. V. The crystal structure of 2,5-dimethyl-1,4-benzoquinone. *J. Chem. Soc.* **1964**, 2030.

(18) Dovesi, R.; Orlando, R.; Erba, A.; Zicovich-Wilson, C. M.; Civalleri, B.; Casassa, S.; Maschio, L.; Ferrabone, M.; De La Pierre, M.; D'Arco, P.; Noël, Y.; Causà, M.; Rérat, M.; Kirtman, B. CRYSTAL14: A program for the ab initio investigation of crystalline solids. *Int. J. Quantum Chem.* **2014**, *114*, 1287.

(19) Perdew, J. P.; Wang, Y. Accurate and simple analytic representation of the electron-gas correlation energy. *Phys. Rev. B* **1992**, *45*, 13244.

(20) Perdew, J. P.; Burke, K.; Ernzerhof, M. Generalized gradient approximation made simple. *Phys. Rev. Lett.* **1996**, *77*, 3865.

(21) Grimme, S. Semiempirical GGA-type density functional constructed with a long-range dispersion correction. *J. Comput. Chem.* **2006**, *27*, 1787.

(22) Widmark, P.-O.; Malmqvist, P.-Å.; Roos, B. O. Density matrix averaged atomic natural orbital (ANO) basis sets for correlated molecular wave functions. *Theor. Chim. Acta* **1990**, *77*, 291.

(23) Aquilante, F.; De Vico, L.; Ferré, N.; Ghigo, G.; Malmqvist, P. Å.; Neogrády, P.; Pedersen, T. B.; Pitonak, M.; Reiher, M.; Roos, B. O.; Serrano-Andrés, L.; Urban, M.; Veryazov, V.; Lindh, R. MOLCAS 7: The Next Generation. *J. Comput. Chem.* **2010**, *31*, 224.

(24) Guest, M. F.; Bush, I. J.; Van Dam, H. J. J.; Sherwood, P.; Thomas, J. M. H.; Van Lenthe, J. H.; Havenith, R. W. A.; Kendrick, J. The GAMESS-UK electronic structure package: algorithms, developments, and applications. *Mol. Phys.* **2005**, *103*, 719.

(25) Broer, R.; Nieuwpoort, W. C. Broken orbital symmetry and the description of valence hole states in the tetrahedral [CrO4]2- anion. *Theor. Chim. Acta* **1988**, *73*, 405.

(26) Gallup, G. A.; Norbeck, J. M. Population analyses of valence-bond wavefunctions and BeH_2. *Chem. Phys. Lett.* **1973**, *21*, 495.

Chapter 4 An Attempt to Simulate Singlet Fission in the bis(inner salt) of 2,5-dihydroxy-1,4-dimethyl-pyrazinium

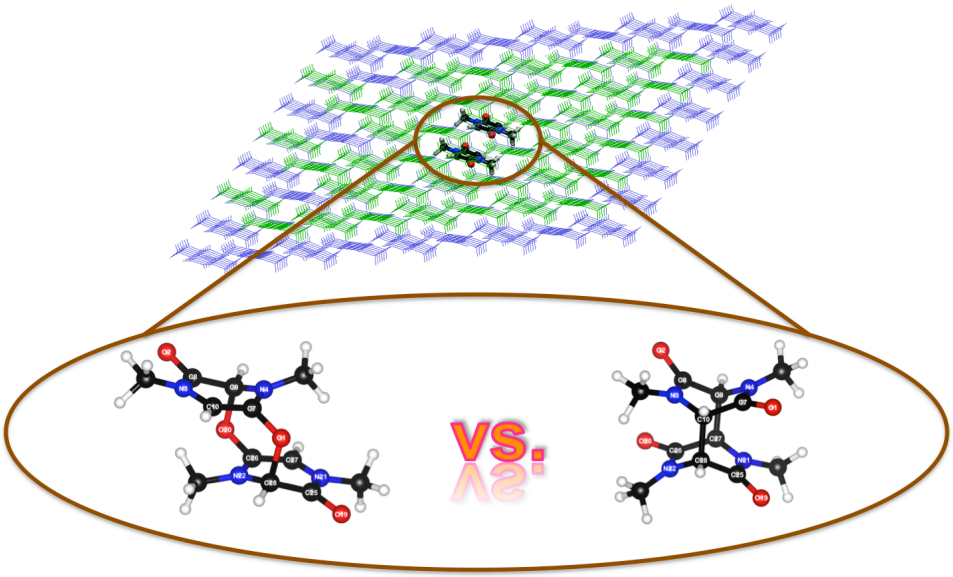

The simulation of the excited state dynamics of bis(inner salt) of 2,5-dihydroxy-1,4-dimethyl-pyrazinium using a direct semiclassical dynamics approach is presented. This molecule is a potential singlet fission chromophore because based on the quantum chemical calculations it satisfies the basic energetic conditions of $\Delta E(S_1) \approx 2\Delta E(T_1)$ *and* $\Delta E(T_2) > 2\Delta E(T_1)$. *It has also been shown that the computed electronic couplings of the pairs of two molecules placed in slip-stack orientation, as obtained from its plausible crystal structure, are in few meV ranges (about 12.0 meV), which are sufficiently large for singlet fission to occur. The excited state dynamics simulation was aimed at assessing the fission dynamics in its plausible crystal structure. Our preliminary results show that this molecule is in practice not useful as a singlet fission chromophore without a structural modification, in spite of the fact that it satisfies the basic energetic conditions of singlet fission chromophore. The reason is that it most likely dimerises even in the ground state, as is also predicted by quantum chemical calculations.*

4.1 Introduction

Accurate quantum chemical calculations performed by Akdag *et al.*[1] suggested that the bis(inner salt) of 2,5-dihydroxy-1,4-dimethyl-pyrazinium (DHDMPY) molecule (see Figure 3.1) satisfies the basic energetic requirements to undergo singlet fission (SF), $\Delta E(S_1) \approx 2\Delta E(T_1)$ and $\Delta E(T_2) > 2\Delta E(T_1)$. In addition, a rigorous nonorthogonal configuration interaction (NOCI) approach confirmed that the electronic couplings between the initially singlet diabatic state and the ^{1}TT state are sufficiently large (about 12.0 meV) for SF to occur in two different pairs of two DHDMPY molecules placed in the slip-stack orientation (see Chapter 3).[2] However, its fission dynamics and time scales required further investigation, and in addition, other possibly competing processes may also hinder the population of the ^{1}TT state.

Modelling explicitly the excited state dynamics of DHDMPY would be the key to rationalise its fission dynamics. In general, the theoretical modelling of the excited state dynamics can be done either by full quantum dynamics or by mixed quantum-classical (semiclassical) dynamics simulations. In the full quantum dynamics simulations, both electron and nuclear degrees of freedom are treated at the quantum mechanics (QM) level, while in the semiclassical dynamics simulations the quantum mechanical treatment is limited to electron only. The quantum dynamics approach based on the quantum master equation, for example, the Redfield theory, has been developed to study the fission dynamics in pentacene dimers.[3-5] Besides, the multiconfigurational time dependent Hartree approach has also been employed to study the coherent versus thermally activated SF in pentacene derivatives and in rubrene.[6] The semiclassical dynamics such as nuclear trajectories with surface hopping (SH) approach,[7] has the advantage of being able to explore the full nuclear phase space and to extend the integration time to several picoseconds, and it has been applied to study the fission dynamics in several polyacenes.[8-10]

The exploration of the DHDMPY dynamics is presented in this chapter. Our plan was to apply the direct semiclassical dynamics approach based on the SH model by computing on-the-fly the electronic energies and wave functions of two different pairs for which sufficiently large computed electronic couplings are obtained (stack A and stack B, as obtained from the study described in Chapter 3) by means of the semiempirical floating occupation molecular orbital–configuration interaction (FOMO–CI) method.[7,11] The crystal environment of the pairs was described at the molecular mechanics (MM) level, and its effect was taken into account by the QM/MM variant of the FOMO–CI method.

4.2 Computational Details

The plausible crystal structure of DHDMPY was obtained from the study described in Chapter 3.[2] In this structure, there are two DHDMPY molecules per unit cell forming slip-stacks of two kinds, denoted stack A and stack B. First, the optimisation of the plausible crystal structure at the MM level was performed, then the optimised crystal structure obtained at the MM level was used as the initial geometry for the MM thermal equilibration, and finally the thermally equilibrated crystal structure was used as the initial geometry for the

QM/MM calculations. Before performing the QM/MM calculations, careful parameterisations of the semiempirical Hamiltonian models and force field were performed.

Following the results obtained from Chapter 3, two different pairs of molecules, *i.e.* a pair taken from stack A and another one taken from stack B, were chosen to be treated at the QM level because they showed by far the largest electronic couplings.[2] For the two QM molecules, the semiempirical FOMO–CI method,[11,12] employing the optimised AM1 parameters was applied, while the OPLSAA force field[13-15] was used for treating the MM subsystem. The QM/MM coupling was represented by the electrostatic embedding plus OPLS Lennard-Jones potentials.[11,12] All the semiempirical and the QM/MM calculations were performed using a modified version of the MOPAC2002 package,[11,12,16] interfaced with the TINKER Molecular Mechanics package version 6.3,[17] when appropriate.

4.3 Optimisation of the Semiempirical Hamiltonian Model

To determine the semiempirical Hamiltonian model for the electronic calculations of the QM subsystem, the vertical and adiabatic excitation energies, ΔE_{vert} and ΔE_{adia}, of the DHDMPY molecule for the two lowest excited singlet (S_1 and S_2) and triplet (T_1 and T_2) states were computed by employing the semiempirical FOMO–CI method[11,12] with different Gaussian widths w for the floating occupation numbers (w = 0.1, 0.15, and 0.2 Hartree). Different semiempirical Hamiltonian models (AM1, MNDO, PM3, and PM5) combined with three different active spaces, *i.e.* CAS(10,7), CAS(10,6) and CAS(2,2), were used to compute these excitation energies. In addition to the small active space, CAS(2,2), much larger active spaces were tried because the orbital energies of the HOMO-1, HOMO-2, HOMO-3, and HOMO-4 are nearly degenerate. As a consequence, all of them (or none) must be included in the active space. In the FOMO–CI method, all the excitations amongst the active orbitals are considered and only the active orbitals have fractional occupation numbers. Also, an active space as small as possible, which includes the most important orbitals involved in the physical

or chemical processes, is commonly used because the effects of electron correlation are taken into account primarily *via* the parameterisation of the semiempirical Hamiltonian model.

The results, computed using the Gaussian width *w* of 0.1 Hartree (see Table 4.1), show that the excitation energies of the excited singlet states are overestimated, in contrast with the underestimation of the triplet energies. Increasing the size of the active space in the FOMO–CI calculations does not improve the computed excitation energies.

Table 4.1 Computed vertical and adiabatic excitation energies, ΔE_{vert} and ΔE_{adia}, (eV) of the two lowest excited singlet (S_1 and S_2) and triplet (T_1 and T_2) states.

Methods	Active spaces	ΔE_{vert} (S_1)	ΔE_{adia} (S_1)	ΔE_{vert} (S_2)	ΔE_{vert} (T_1)	ΔE_{adia} (T_1)	ΔE_{vert} (T_2)
CASPT2/ ANO-L VTZP[1]	CAS(22,14)	2.21	2.11	3.62	1.21	1.07	3.72
FOMO–CI/AM1	CAS(10,7)	2.77	2.42	3.53	0.37	0.35	2.85
	CAS(10,6)	3.05	2.35	3.74	0.33	0.32	4.39
	CAS(2,2)	3.20	2.45	4.16	0.32	0.30	-
FOMO–CI/PM3	CAS(10,7)	2.39	1.78	3.06	0.36	0.36	2.77
	CAS(10,6)	2.74	1.81	3.36	0.30	0.29	3.76
	CAS(2,2)	2.94	1.91	3.80	0.27	0.26	-
FOMO–CI/PM5	CAS(10,7)	2.57	2.03	2.83	0.70	0.61	2.25
	CAS(10,6)	2.84	1.99	2.89	0.70	0.65	4.14
	CAS(2,2)	2.98	2.05	4.43	0.68	0.64	-
FOMO–CI/MNDO	CAS(10,7)	2.90	2.17	3.32	0.16	0.15	3.02
	CAS(10,6)	3.22	2.23	3.62	0.15	0.14	4.49
	CAS(2,2)	3.39	2.32	3.99	0.12	0.12	-

To choose the semiempirical Hamiltonian model in which its parameters will be further optimised, we also analysed the geometrical parameters of DHDMPY obtained at the FOMO–CI level and compared them with the results obtained from the CASPT2 calculations,[1] see Table 4.2. The results show that the geometrical parameters obtained using AM1 Hamiltonian are close to the ones obtained at the CASPT2 level, but the computed excitation energies are overestimated. Therefore, AM1 parameters must be optimised in order to reproduce the

excitation energies as obtained from the CASPT2 calculations. Then, we optimised the semiempirical AM1 parameters using an active space of CAS(2,2) and Gaussian width *w* of 0.1 Hartree for the FOMO–CI calculations. This particular active space was chosen because the calculations for a pair of two molecules using large active spaces would result in active spaces of CAS(20,14) and CAS(20,12) in the QM/MM calculations, which are in practice too expensive.

Table 4.2 Comparison of the geometrical properties in the S_0, S_1, and T_1 relaxed geometries, obtained at the FOMO–CI level. Bond distances (*r*) are in Angstrom (Å), bond and dihedral angles (∠) are in degrees (°). For atom labels see Figure 3.1.

Coordinates	AM1	PM3	PM5	MNDO	CASPT2[1]
$r(N_1\text{-}C_9)$	1.44, 1.44, 1.44	1.48, 1.48, 1.48	1.48, 1.48, 1.48	1.48, 1.48, 1.48	1.47, 1.47, 1.47
$r(N_1\text{-}C_8)$	1.42, 1.53, 1.42	1.45, 1.48, 1.46	1.43, 1.49, 1.44	1.44, 1.58, 1.44	1.42, 1.42, 1.41
$r(N_1\text{-}C_5)$	1.36, 1.31, 1.36	1.37, 1.44, 1.38	1.36, 1.43, 1.37	1.38, 1.32, 1.38	1.35, 1.38, 1.38
$r(C_8\text{-}O_4)$	1.25, 1.24, 1.24	1.23, 1.21, 1.22	1.23, 1.21, 1.22	1.23, 1.22, 1.23	1.25, 1.25, 1.24
$r(C_8\text{-}C_6)$	1.45, 1.39, 1.46	1.44, 1.50, 1.45	1.43, 1.49, 1.45	1.46, 1.38, 1.47	1.43, 1.44, 1.44
$\angle(C_6\text{-}N_2\text{-}C_7)$	120.5, 119.6, 119.8	120.8, 115.6, 120.2	122.2, 117.7, 121.2	120.4, 119.8, 119.8	124.8, 120.3, 120.6
$\angle(C_8\text{-}C_6\text{-}N_2)$	122.9, 124.9, 122.7	122.1, 118.8, 121.9	122.7, 121.3, 122.3	122.8, 125.2, 122.6	123.0, 123.4, 122.7
$\angle(N_2\text{-}C_7\text{-}C_5)$	116.6, 117.6, 117.5	117.1, 112.8, 117.9	115.1, 112.7, 116.5	116.8, 117.8, 117.5	112.2, 116.3, 116.7
$\angle(C_{10}\text{-}N_2\text{-}C_7\text{-}C_5)$	180.0, 180.0, 180.0	180.0, 159.8, 180.0	180.0, 154.9, 180.0	180.0, 180.0, 180.0	180.0, 180.0, 180.0

The procedure of the optimisation of the semiempirical parameters can be summarised as follows: (i) determining a set of target values $X_i^{(T)}$, *i.e*. the vertical and adiabatic excitation energies, ΔE_{vert} and ΔE_{adia}, taken from the CASPT2 calculations,[1] which will be reproduced by the semiempirical FOMO–CI calculations; (ii) choosing the semiempirical Hamiltonian model, *i.e*. AM1 Hamiltonian, the active spaces, *i.e*. CAS(2,2), and the Gaussian width *w*, *i.e*. 0.1 Hartree, for the FOMO–CI calculations; (iii) setting up the starting semiempirical parameters, usually from the standard ones; (iv) calculating all semiempirical quantities $X_i^{(S)}$ corresponding to the target values $X_i^{(T)}$, yielding the results that depend on a given set of parameters P; (v) minimising the function $f(P) = \sum_i \left(\frac{X_i^{(T)} - X_i^{(S)}(P)}{X_i^{(T)}} \right)^2 W_i$, where P is a set of semiempirical parameters, $X_i^{(T)}$ are the target quantities, $X_i^{(S)}$ are the corresponding semiempirical values obtained from the FOMO–CI calculations, and W_i are the positive weights, which are determined by the user as the input for the minimisation of the aforementioned function. The minimisation was performed by employing the simplex algorithm coupled with a simulated annealing procedure. The last two steps, *i.e*. step (iv) and step (v), were repeated until the convergence is reached.[18-20] The target values $X_i^{(T)}$, semiempirical results $X_i^{(S)}$, %error, and positive weights W_i of this optimisation procedure are collected in Table 4.3. The description of the semiempirical parameters and the comparison between the standard AM1 parameters and the optimised ones are presented in Table 4.4 and Table 4.5, respectively. Based on the computed vertical excitation energies, ΔE_{vert}, obtained using the optimised AM1 parameters (see Table 4.3), the SF process in this DHDMPY molecules is slightly endoergic by about 0.36 eV, in agreement with the CASPT2 calculations that also show the endoergicity by about 0.27 eV. On the contrary, considering the computed adiabatic excitation energies, ΔE_{adia}, obtained from both the optimised AM1 parameters and the CASPT2 calculations, the SF process in this molecule occurs almost isoenergetically.

Table 4.3 Target values $X_i^{(T)}$, semiempirical results $X_i^{(S)}$, %error and positive weights W_i.

	$X_i^{(T)}$	$X_i^{(S)}$	%error	W_i
ΔE_{vert} (S_1)	2.2070	1.9538	-11.4719	2.00
ΔE_{adia} (S_1)	2.1140	1.8856	-10.8005	2.00
ΔE_{vert} (S_2)	3.6250	3.8907	7.3317	4.00
ΔE_{vert} (T_1)	1.2070	1.1574	-4.1080	2.00
ΔE_{adia} (T_1)	1.0710	0.9068	-15.3224	2.00
ΔE_{vert} (S_1) $_{S1min}$	1.9720	1.8215	-7.6315	2.00
ΔE_{vert} (S_2) $_{S1min}$	3.1460	3.6776	16.8989	4.00
ΔE_{vert} (T_1) $_{S1min}$	0.9520	1.0445	9.7255	2.00
ΔE_{vert} (S_1) $_{S2min}$	1.7690	1.8542	4.8183	2.00
ΔE_{vert} (S_2) $_{S2min}$	2.6690	2.9040	8.8061	4.00
ΔE_{vert} (T_1) $_{S2min}$	0.6930	0.7855	13.3610	2.00
ΔE_{vert} (S_1) $_{T1min}$	1.9660	1.9446	-1.0883	2.00
ΔE_{vert} (S_2) $_{T1min}$	3.0950	3.0913	-0.1178	4.00
ΔE_{vert} (T_1) $_{T1min}$	0.9850	0.8538	-13.3105	2.00

Table 4.4 Description of the semiempirical parameters.

Parameters	Description
U_{SS}, U_{PP}	*s* and *p* atomic orbital one-centre one-electron integrals
β_S, β_P	*s* and *p* atomic orbital two-centre one-electron integrals
ζ_S, ζ_P	*s* and *p* Slater atomic orbital exponent
α	Core-core repulsion term
G_{SS}, G_{SP}, G_{PP},	*s-s*, *s-p*, *p-p*, and *p-p'* atomic orbital one-centre two-electron repulsion
G_{P2}	integrals
H_{SP}	*s-p* atomic orbital one-centre two-electron exchange integral
FN_{nN}	Gaussian multiplier core-core repulsion
FN_{nN}	Gaussian exponent multiplier core-core repulsion
FN_{nN}	Gaussian centre core-core repulsion

Table 4.5 Comparison between the standard AM1 parameters and the optimised ones.

	Units	N_{std}	N_{opt}	O_{std}	O_{opt}	C_{std}	C_{opt}	H_{std}	H_{opt}
U_{SS}	eV	-71.8600	-68.0328	-97.8300	-135.3323	-52.0286	-46.9293	-11.3964	-11.8485
U_{PP}	eV	-57.1675	-58.3069	-78.2623	-77.3235	-39.6142	-39.0909	-	-
β_S	eV	-20.2991	-20.2908	-29.2727	-28.1479	-15.7157	-15.4624	-6.1737	-5.0317
β_P	eV	-18.2386	-17.2930	-29.2727	-27.6100	-7.7192	-8.0269	-	-
ζ_S	$bohr^{-1}$	2.3154	2.1306	3.1080	3.3211	1.8086	1.6238	1.1880	1.2064
ζ_P	$bohr^{-1}$	2.1579	2.1229	2.5240	2.3112	1.6851	1.6853	-	-
α	$Å^{-1}$	2.9472	3.3669	4.4553	4.8502	2.6482	2.8120	2.8823	2.8133
G_{SS}	eV	13.5900	14.5231	15.4200	16.4628	12.2300	12.9725	12.8480	13.3465
G_{SP}	eV	12.6600	14.1972	14.4800	13.0599	11.4700	12.2299	-	-
G_{PP}	eV	12.9800	10.3161	14.5200	11.5552	11.0800	5.2125	-	-
G_{P2}	eV	11.5900	11.5474	12.9800	13.1207	9.8400	9.5883	-	-
H_{SP}	eV	3.1400	3.3931	3.9400	4.5385	2.4300	2.4064	-	-
FN_{11}	-	0.0252	0.0277	0.2809	0.2998	0.0113	0.0116	0.1227	0.1342
FN_{21}	$Å^{-2}$	5.0000	4.4709	5.0000	5.1189	5.0000	4.5670	5.0000	5.2939
FN_{31}	Å	1.5000	1.5999	0.8479	0.7695	1.6000	1.5461	1.2000	1.2925
FN_{12}	-	0.0289	0.0313	0.0814	0.0844	0.0459	0.0508	0.0050	0.0052
FN_{22}	$Å^{-2}$	5.0000	4.3123	7.0000	6.3531	5.0000	5.4009	5.0000	5.1198
FN_{32}	Å	2.1000	1.5081	1.4450	1.1350	1.8500	1.8626	1.8000	2.1809
FN_{13}	-	-0.0058	-0.0059	-	-	-0.0200	-0.0174	-0.0183	-0.0145
FN_{23}	$Å^{-2}$	2.0000	2.2128	-	-	5.0000	5.3060	2.0000	1.6877
FN_{33}	Å	2.4000	2.5715	-	-	2.0500	2.2807	2.1000	2.1839
FN_{14}	-	-	-	-	-	-0.0012	-0.0013	-	-
FN_{24}	$Å^{-2}$	-	-	-	-	5.0000	5.5786	-	-
FN_{34}	Å	-	-	-	-	2.6500	2.7348	-	-

4.4 Molecular Dynamics Equilibration

A primary thermal equilibration of the DHDMPY crystal structure using the OPLSAA force field was performed for 10 ns employing the canonical (NVT) ensemble with a constant temperature of 300 K, imposing the periodic boundary conditions. The atomic charge parameters in the description of the OPLSAA force field are fitted from a density functional theory (DFT) calculation employing the B3LYP functional[21-23] and TZVP basis set[24] with the

charges from electrostatic potentials using a grid based (CHELPG) method.[25] This scheme uses a fitting procedure of the atomic charges in order to reproduce the molecular electrostatic potential at a number of selected points around the molecule. The atom type and its description in the OPLSAA force field for each atom in the DHDMPY molecule are presented in Table 4.6.

Table 4.6 The atom type and its description in the OPLSAA force field of each atom in the DHDMPY molecule. For atom labels see Figure 3.1.

Atom	Atom type	Atom class	Description
N_1, N_2	181	24	Amide –CO–**N**R_2
O_3, O_4	223	4	Ketone C=**O**
C_5, C_6	90	48	Aromatic **C**
C_7, C_8	173	3	Benzophenone **C**=O
C_9, C_{10}	185	13	Amide –NR–**C**H_3
H_{11}, H_{12}	91	49	Aromatic **H**–C
H_{13}, H_{15}, H_{18}	85	46	Alkane **H**–C
H_{14}, H_{16}, H_{17}	85	46	Alkane **H**–C

To ascertain that the crystal structure of DHDMPY has reached its thermal equilibrium structure, statistical analyses of the potential, kinetic, and total energies were performed. Average values and standard deviations of the potential, kinetic, and total energies from the last 5, 2, and 1 nanoseconds of this thermal equilibration are presented in Table 4.7. The average values of the kinetic energies and the corresponding standard deviations can be compared with the calculated equipartition of 32.19 kcal/mol and its standard deviation of 4.38 kcal/mol. The equipartition and its standard deviation were calculated as: $E_{kin} = \frac{3}{2} N k_B T$ and $\sigma_{kin} = \left(\frac{3}{2} N\right)^{1/2} k_B T$, where N is the total number of atoms (36 atoms), k_B is Boltzmann's constant, and T is a constant temperature (300 K). In all time intervals, the average values and standard deviations are in accordance with the theoretical values. The last frame of this equilibration was then used to start the QM/MM ground state trajectory for a cluster of MM molecules surrounding the two QM ones.

Table 4.7 Average values and standard deviations of the potential (E_{pot}), kinetic (E_{kin}), and total (E_{tot}) energies (kcal/mol).

Time interval (ns)	E_{pot} (std. dev.)	E_{kin} (std. dev.)	E_{tot} (std. dev.)
From 5 to 10	-61.82 (4.32)	31.28 (4.32)	-30.54 (6.11)
From 8 to 10	-61.82 (4.32)	31.28 (4.32)	-30.54 (6.10)
From 9 to 10	-61.82 (4.32)	31.27 (4.32)	-30.55 (6.10)

4.5 QM/MM Ground State Trajectory

The last frame of the periodic molecular dynamics equilibration of the crystal structure of DHDMPY was extracted and was used as the initial geometry to perform the QM/MM ground state trajectory. To mimic the DHDMPY crystal structure, a simulation box was constructed by replicating the thermally equilibrated crystal structure in such a way that the two QM molecules are placed in the middle of the simulation box (see Figure 4.1). The resulting simulation box consists of 504 molecules, of which 294 molecules are kept frozen, while 208 MM molecules plus 2 QM molecules are freely moving during the dynamics simulations. The outer layer molecules were kept frozen in order to mimic the substantial rigidity of the crystal structure (molecules represented in blue line model, see Figure 4.1). Two different pairs of QM molecules, a pair taken from stack A and another one taken from stack B (see Figure 3.2), were chosen.

The QM/MM ground state equilibration was performed for each pair of QM molecules taken from stack A and stack B. This equilibration was performed employing the Bussi-Parrinello thermostat[26] for 50 ps with a time step of 0.1 femtosecond (fs) and a temperature of 300 K. The optimised AM1 parameters with an active space of 4 electrons in 4 orbitals, which is equal to the CAS(2,2) we selected for the single molecule, and Gaussian width *w* of 0.1 Hartree for the floating occupation numbers in the FOMO–CI method were employed to treat the QM subsystem. The OPLSAA force field was used to treat the MM subsystem, as already described in the previous section.

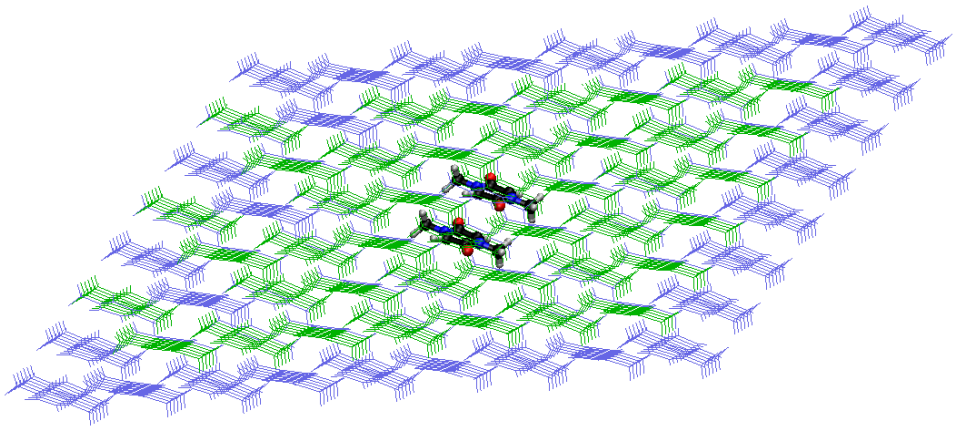

Figure 4.1 Representation of the QM and MM subsystems of the DHDMPY crystal structure. The space-filling model represents QM molecules (C, N, O, and H atoms are represented in black, in blue, in red, and in grey, respectively). The green and blue line models represent the MM molecules that are allowed to move freely and that are kept frozen, respectively, during the dynamics simulations.

We found that during the QM/MM ground state equilibration, the two QM molecules tend to react and to form a dimer structure after the simulation times of about 300 fs and 500 fs for the pairs taken from stack A and stack B, respectively. This finding gave us a hint that this molecule most probably will react with its neighbours and form a dimer (or even oligomer) in the ground state. Therefore, we extracted the dimerised structure obtained from this QM/MM ground state equilibration and performed the single point energy calculations in order to investigate the dimerisation mechanism of this molecule.

4.6 Dimerisation Mechanism

To investigate the dimerisation mechanism of DHDMPY, we ran DFT calculations to optimise the geometries of the dimerised structure extracted from the QM/MM ground state equilibration for both stack A and stack B, which will be labelled as “dimer A” and “dimer B” from now on (see Figure 4.2). The calculations were performed in gas phase employing the

PBE exchange-correlation functional[27,28] and the 6-21G basis set, the same level of theory employed for the periodic calculations of the DHDMPY crystal. To compute the energies of both dimer A and dimer B, we used a larger basis set instead, *i.e.* the Dunning correlation-consistent (cc-pVTZ) basis set.[29] Also, we ran DFT calculations to compute the energies of both stack A and stack B, which will be labelled as "initial pair A" and "initial pair B", which are taken from its plausible crystal structure (see Chapter 3). The calculations were performed in gas phase employing the PBE functional[21-23] and the cc-pVTZ basis set.[29]

In dimer A, the two DHDMPY molecules formed two C-O bonds in which the O atom of the carbonyl group from one molecules attacked the (partially) radicalic C atom of the other molecule. In dimer B, on the other hand, the C atoms with radical centres made C-C bonds with their counterparts in the other molecule, forming a two fused 8-membered rings (see Figure 4.2). The results, presented in Table 4.8, show that dimer A remains the alternate single and double bond character of the etheric C atoms, while all the C-C bonds in dimer B are lengthened because they acquire a pure single bond character. Moreover, the two molecules, which were initially planar molecules, are not longer planar due to the steric effects.

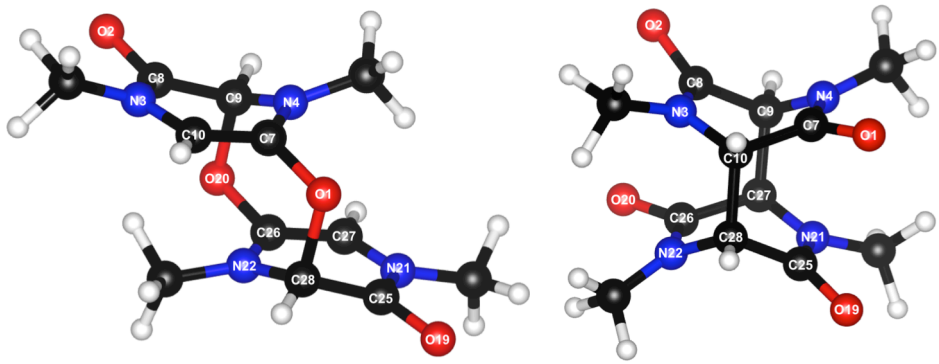

Figure 4.2 Possible chemical structures of dimer A (left) and dimer B (right).

The binding energies of the dimerisation reaction were computed as the energy difference between the dimer and the initial pair. These energies were calculated at the PBE/cc-pVTZ level of theory. Furthermore, the multiconfigurational method was also employed to compute the energies of the initial pair geometries and of the optimised dimer geometries of DHDMPY obtained at the PBE/6-21G level, namely CASPT2//PBE approach,[30] for which the obtained

energies were used to calculate the binding energies. The ANO-L basis set contracted to C,N,O [4s3p2d]/H [3s2p] was used.[31] The use of the CASPT2 method allows us to appropriately assess both the static and dynamical electron correlations, thereby treating correctly the nature of the biradicaloid molecule, which shows partially an open-shell and a closed-shell character. In fact, this procedure also offers a validation of the DFT method. The π-HOMO and π*-LUMO of each molecule are included in the active space, producing an active space CAS(4,4).

Table 4.8 Geometrical properties of the optimised dimer A and dimer B (*italic*), computed at the PBE/6-21G level of theory. Bond lengths (*r*) and distances (*d*) are in Å, and dihedral angles (∠) are in degrees.

Coordinates		Coordinates	
$r(N_{21}\text{-}C_{27})$	1.41 (*1.47*)	$r(N_3\text{-}C_{10})$	1.41 (*1.47*)
$r(C_{27}\text{-}C_{26})$	1.36 (*1.55*)	$r(C_{10}\text{-}C_7)$	1.36 (*1.555*)
$r(C_{26}\text{-}O_{20})$	1.37 (*1.25*)	$r(C_7\text{-}O_1)$	1.37 (*1.25*)
$r(C_{26}\text{-}N_{22})$	1.44 (*1.38*)	$r(C_7\text{-}N_4)$	1.44 (*1.38*)
$r(N_{22}\text{-}C_{28})$	1.39 (*1.47*)	$r(N_4\text{-}C_9)$	1.39 (*1.47*)
$r(C_{28}\text{-}C_{25})$	1.52 (*1.55*)	$r(C_9\text{-}C_8)$	1.52 (*1.55*)
$r(C_{25}\text{-}O_{19})$	1.26 (*1.25*)	$r(C_8\text{-}O_2)$	1.26 (*1.25*)
$r(C_{25}\text{-}N_{21})$	1.40 (*1.38*)	$r(C_8\text{-}N_3)$	1.40 (*1.38*)
$d(O_{20}\text{---}C_9)$	1.72	$d(O_1\text{---}C_{28})$	1.72
$d(C_{27}\text{---}C_9)$	(*1.62*)	$d(C_{10}\text{---}C_{28})$	(*1.62*)
$d(C_{26}\text{---}C_9)$	2.51	$d(C_7\text{---}C_{28})$	2.51
$\angle(N_{22}\text{-}C_{28}\text{-}C_{25}\text{-}N_{21})$	27.8 (44.9)	$\angle(N_4\text{-}C_9\text{-}C8\text{-}N3)$	153.2 (135.1)

The results, presented in Table 4.9, show that the dimer B is much more stable than dimer A. A possible reason is that in dimer A two of the carbon atoms bound to nitrogen and to one etheric bridging oxygen are considerably pyramidalised, in spite of the double bond they share with the next carbon in the ring. Other significant changes in the geometry of dimer A are the increased of the C-O bond length of the carbonyl group and the C-C bond length of one of the ethylene groups by about 0.1 Å (see Table 4.8). The computed binding energy of dimer A, which has a positive large value, indicates that most probably this dimer is not as

stable as the semiempirical QM/MM would suggest. On the contrary, the computed binding energy of dimer B obtained from both levels of theory implies that the dimerisation forming two fused 8-membered rings is thermodynamically allowed.

Table 4.9 Computed binding energies (E_{bind}, eV) of the dimer A and B, calculated at the semiempirical FOMO–CI/AM1, PBE/cc-pVTZ and CASPT2/ANO-L C,N,O [4s3p2d]/H [3s2p] levels of theory.

Structures	E_{bind} (eV)		
	FOMO–CI/AM1	PBE	CASPT2
dimer A	-2.2096	0.4686	0.6854
dimer B	-3.7406	-2.2132	-2.3363

4.7 Summary and Conclusions

This chapter discusses the explicit modelling of the excited state dynamics of DHDMPY, which is aimed to further investigate its fission dynamics. The method employed is the direct semiclassical dynamics approach, *i.e.* surface hopping described in Chapter 2. This efficient method has the advantage that one can explore the full nuclear phase space and that the dynamics can run for many picoseconds. The electronic energies and wave functions were computed on-the-fly for two different pairs of molecules that show, based on the results obtained in Chapter 3, sufficiently large computed electronic couplings.

The hybrid QM/MM approach was applied to take into account the interaction between the QM subsystem which consists of pairs of two molecules for which their photodynamics were further investigated and the crystal environment, which was described by a MM force field. The crystal structure of DHDMPY, as obtained from the results of Chapter 3, has two DHDMPY molecules per unit cell, each forming a slip-stack, denoted stack A and stack B. First, this crystal structure was reoptimised at the MM level, then this optimised structure was used as the initial geometry for the MM thermal equilibration, and finally the resulting thermally equilibrated crystal structure was used as the initial geometry for the QM/MM calculations. To set up the QM/MM calculations, a careful parameterisation of the semiempirical QM Hamiltonian models and force field was performed.

Using the outcomes of Chapter 3, two different pairs of molecules, one taken from stack A and another one from stack B, were chosen to be treated at the QM level because these pairs showed by far the largest electronic couplings. The electronic energies and wave functions of the two QM molecules were computed on-the-fly during the dynamics simulations using the semiempirical FOMO–CI method,[11,12] employing the optimised AM1 parameters. The OPLSAA force field was used to treat the MM subsystem, and the QM/MM coupling was represented by electrostatic embedding plus OPLS Lennard-Jones potentials.[32]

In summary, we started this work to investigate the fission dynamics of DHDMPY, but we found that this molecule dimerises in the ground state according to the semiempirical QM/MM treatment. This would also explain the difficulties experienced by our experimental colleagues, when they tried to synthesise this molecule.[33,34] Hence, it would be impossible to use this DHDMPY molecule as a SF chromophore without some important structural modifications. We propose a two fused 8-membered rings structure as a possible dimer. However, we must take into account that the semiempirical Hamiltonian was not optimised to treat dimerisation reaction, so it must be tested versus higher quality calculations. The most accurate results we obtained indicate that the dimerisation reaction is exoergic. A complete assessment of the relevance of such reaction would require the determination of the activation energy. This is a difficult task because probably one cannot relay on DFT to determine the transition state geometry of this kind of biradicaloid molecule. Moreover, in case we found large activation energy before carrying out the nonadiabatic simulations, we should modify again the semiempirical Hamiltonian to rule out the dimerisation reactions. Since we had already started the simulations of SF for another chromophore, as described in Chapter 5, there was no time to investigate further this biradicaloid system.

4.8 Appendix: Optimised geometries of DHDMPY

The optimised geometries of pair A, pair B, dimer A, and dimer B of DHDMPY, computed at the PBE/6-21G level of theory, are presented. Atomic coordinates are in Å.

Pair A:				**Pair B:**			
N	2.531608	-0.086651	-0.009634	N	0.496015	-1.711768	0.372166
N	0.585114	1.612008	-0.882623	N	2.533425	0.096736	0.652991
N	-0.581332	-1.610157	0.881540	N	-2.529751	-0.098695	-0.651748
N	-2.527827	0.088502	0.008552	N	-0.492340	1.709808	-0.370923
O	1.291112	3.268019	0.643421	O	-0.590354	-0.833786	2.288686
O	1.825610	-1.742663	-1.535678	O	3.619795	-0.781245	-1.263528
O	-1.821829	1.744514	1.534595	O	-3.616119	0.779286	1.264772
O	-1.287330	-3.266169	-0.644503	O	0.594030	0.831827	-2.287442
C	3.619649	-1.002828	0.434297	C	-0.615774	-2.687403	0.179090
C	1.444794	2.077794	0.146747	C	3.645215	1.072371	0.846068
C	-0.502927	2.528184	-1.326554	C	0.402128	-0.794019	1.463689
C	1.671928	-0.552438	-1.039004	C	2.627314	-0.821013	-0.438532
C	2.428612	1.145176	0.557688	C	1.543323	-1.732985	-0.499865
C	0.688110	0.380180	-1.449945	C	1.486119	0.117953	1.525023
C	0.506709	-2.526333	1.325471	C	-3.641539	-1.074330	-0.844824
C	-1.668146	0.554288	1.037921	C	0.619449	2.685443	-0.177846
C	-3.615867	1.004678	-0.435379	C	-2.623637	0.819054	0.439775
C	-1.441013	-2.075944	-0.147829	C	-0.398453	0.792059	-1.462446
C	-0.684329	-0.378329	1.448862	C	-1.482443	-0.119913	-1.523779
C	-2.424830	-1.143326	-0.558770	C	-1.539647	1.731026	0.501109
H	3.191486	1.407097	1.303644	H	1.531899	-2.536189	-1.250294
H	4.185838	-0.479028	1.225805	H	1.497542	0.921157	2.275452
H	-0.074764	0.118259	-2.195901	H	-0.624391	-2.987701	-0.883173
H	-1.069116	2.004384	-2.118062	H	3.653833	1.372669	1.908330
H	3.192585	-1.953981	0.798108	H	-0.481190	-3.580751	0.828889
H	-0.075863	3.479338	-1.690365	H	3.510631	1.965720	0.196269
H	4.245569	-1.213718	-0.454427	H	-1.558414	-2.194995	0.460413
H	-1.128847	2.739075	-0.437830	H	4.587854	0.579963	0.564744
H	0.078545	-0.116409	2.194819	H	-1.493867	-0.923116	-2.274209
H	1.072897	-2.002533	2.116979	H	-1.528224	2.534229	1.251538
H	-3.187704	-1.405246	-1.304726	H	-3.650157	-1.374629	-1.907087

H	-4.182056	0.480878	-1.226887	H	0.628068	2.985742	0.884416
H	0.079643	-3.477487	1.689283	H	-3.506956	-1.967678	-0.195025
H	-3.188803	1.955832	-0.799190	H	0.484865	3.578791	-0.827645
H	1.132628	-2.737224	0.436748	H	-4.584179	-0.581923	-0.563501
H	-4.241787	1.215569	0.453344	H	1.562089	2.193036	-0.459170
Dimer A:				**Dimer B:**			
O	5.163334	-5.012961	2.113403	O	0.098873	-1.321576	1.987762
O	3.083709	-4.691661	7.156007	O	-0.186628	0.348004	-2.978287
N	4.441443	-6.086984	4.151614	N	0.016114	0.940549	-0.727168
N	3.172299	-3.812710	4.986879	N	0.733882	-1.678717	-0.232366
C	4.637217	-7.443942	3.592332	C	-0.860160	2.118378	-0.878225
C	2.204468	-2.752215	5.346321	C	0.590311	-3.143127	-0.119026
C	4.382577	-4.969840	3.244190	C	0.465274	-0.885869	0.870208
C	3.545163	-4.726197	5.987917	C	0.275421	0.145096	-1.830090
C	4.525666	-5.785502	5.510843	C	0.644994	0.622601	0.559748
C	3.739892	-3.857018	3.699157	C	1.191907	-1.055333	-1.479097
H	4.484795	-6.661937	6.165891	H	0.104030	1.156236	1.354325
H	3.723516	-2.937818	3.114736	H	1.063384	-1.777095	-2.298427
H	5.285798	-7.351384	2.707149	H	-1.204346	2.096215	-1.925091
H	1.283199	-2.854356	4.748825	H	-0.129873	-3.521430	-0.865359
H	5.113409	-8.087395	4.346639	H	-1.721120	2.052384	-0.190343
H	2.646389	-1.754072	5.178973	H	0.214139	-3.323399	0.901208
H	3.667115	-7.881916	3.292958	H	-0.307851	3.055872	-0.689838
H	1.986359	-2.900411	6.415426	H	1.561077	-3.652629	-0.251122
O	8.140818	-5.442518	0.864000	O	3.584630	-0.341968	2.116638
O	6.061221	-5.121300	5.906625	O	3.299156	1.327452	-2.849396
N	8.052326	-6.321447	3.033144	N	2.664010	1.684636	-0.629314
N	6.783081	-4.047228	3.868434	N	3.381781	-0.934630	-0.134442
C	9.020156	-7.381934	2.673678	C	2.807652	3.149041	-0.742660
C	6.587245	-2.690288	4.427739	C	4.258120	-2.112410	0.016624

C	7.679432	-5.407957	2.032116	C	3.122516	-0.139126	0.968455
C	6.841993	-5.164384	4.775838	C	2.932685	0.891766	-1.731858
C	7.484728	-6.277173	4.320864	C	2.206006	1.061276	0.617441
C	6.698910	-4.348687	2.509206	C	2.752928	-0.616694	-1.421379
H	7.501140	-7.196376	4.905278	H	2.334523	1.783067	1.436746
H	6.739723	-3.472246	1.854165	H	3.293901	-1.150355	-2.215931
H	9.238257	-7.233720	1.604574	H	3.183843	3.329289	-1.762892
H	6.111145	-2.046814	3.673392	H	3.705866	-3.049932	-0.171780
H	9.941429	-7.279803	3.271169	H	1.836908	3.658586	-0.610573
H	7.557316	-2.252328	4.727235	H	4.602289	-2.090231	1.063494
H	8.578238	-8.380082	2.841010	H	3.527848	3.527316	0.003676
H	5.938564	-2.782864	5.312846	H	5.119090	-2.046366	-0.671242

4.9 References

(1) Akdag, A.; Havlas, Z.; Michl, J. Search for a small chromophore with efficient singlet fission: Biradicaloid heterocycles. *J. Am. Chem. Soc.* **2012**, *134*, 14624.

(2) Wibowo, M.; Broer, R.; Havenith, R. W. A. A rigorous nonorthogonal configuration interaction approach for the calculation of electronic couplings between diabatic states applied to singlet fission. *Comput. Theor. Chem.* **2017**, *1116*, 190.

(3) Berkelbach, T. C.; Hybertsen, M. S.; Reichman, D. R. Microscopic theory of singlet exciton fission. II. Application to pentacene dimers and the role of superexchange. *J. Chem. Phys.* **2013**, *138*, 114103.

(4) Berkelbach, T. C.; Hybertsen, M. S.; Reichman, D. R. Microscopic theory of singlet exciton fission. I. General formulation. *J. Chem. Phys.* **2013**, *138*, 114102.

(5) Berkelbach, T. C.; Hybertsen, M. S.; Reichman, D. R. Microscopic theory of singlet exciton fission. III. Crystalline pentacene. *J. Chem. Phys.* **2014**, *141*, 074705.

(6) Tamura, H.; Huix-Rotllant, M.; Burghardt, I.; Olivier, Y.; Beljonne, D. First-principles quantum dynamics of singlet fission: Coherent versus thermally activated mechanisms governed by molecular phi stacking. *Phys. Rev. Lett.* **2015**, *115*, 107401.

(7) Persico, M.; Granucci, G. An overview of nonadiabatic dynamics simulations methods, with focus on the direct approach versus the fitting of potential energy surfaces. *Theor. Chem. Acc.* **2014**, *133*, 1.

(8) Akimov, A. V.; Prezhdo, O. V. Nonadiabatic dynamics of charge transfer and singlet fission at the pentacene/C60 interface. *J. Am. Chem. Soc.* **2014**, *136*, 1599.

(9) Mou, W.; Hattori, S.; Rajak, P.; Shimojo, F.; Nakano, A. Nanoscopic mechanisms of singlet fission in amorphous molecular solid. *Appl. Phys. Lett.* **2013**, *102*, 173301.

(10) Wang, L.; Olivier, Y.; Prezhdo, O. V.; Beljonne, D. Maximizing singlet fission by intermolecular packing. *J. Phys. Chem. Lett.* **2014**, *5*, 3345.

(11) Granucci, G.; Persico, M.; Toniolo, A. Direct semiclassical simulation of photochemical processes with semiempirical wave functions. *J. Chem. Phys.* **2001**, *114*, 10608.

(12) Granucci, G.; Toniolo, A. Molecular gradients for semiempirical CI wavefunctions with floating occupation molecular orbitals. *Chem. Phys. Lett.* **2000**, *325*, 79.

(13) Jorgensen, W. L.; Maxwell, D. S.; Tirado-Rives, J. Development and testing of the OPLS All-Atom force field on conformational energetics and properties of organic liquids. *J. Am. Chem. Soc.* **1996**, *118*, 11225.

(14) Jorgensen, W. L.; McDonald, N. A. Development of an all-atom force field for heterocycles. Properties of liquid pyridine and diazenes. *J. Mol. Struc.-THEOCHEM* **1996**, *424*, 145.

(15) McDonald, N. A.; Jorgensen, W. L. Development of an all-atom force field for heterocycles. Properties of liquid pyrrole, furan, diazoles, and oxazoles. *J. Phys. Chem. B* **1998**, *102*, 8049.

(16) Stewart, J. J. P. MOPAC 2002; Fujitsu Limited: Tokyo, Japan, 2002.

(17) Ponder, J. W.; Richards, F. M. An efficient Newton-like method for molecular mechanics energy minimization of large molecules. *J. Comput. Chem.* **1987**, *8*, 1016.

(18) Cusati, T. Computational simulation of the excited states dynamics of azobenze in solution. University of Pisa, 2009.

(19) Cusati, T.; Granucci, G.; Martínez-Núñez, E.; Martini, F.; Persico, M.; Vázquez, S. Semiempirical Hamiltonian for simulation of azobenzene photochemistry. *J. Phys. Chem. A* **2012**, *116*, 98.

(20) Favero, L.; Granucci, G.; Persico, M. Surface hopping investigation of benzophenone excited state dynamics. *Phys. Chem. Chem. Phys.* **2016**.

(21) Becke, A. D. Density-functional thermochemistry. III. The role of exact exchange. *J. Chem. Phys.* **1993**, *98*, 5648.

(22) Lee, C.; Yang, W.; Parr, R. G. Development of the Colle-Salvetti correlation-energy formula into a functional of the electron density. *Phys. Rev. B* **1988**, *37*, 785.

(23) Stephens, P. J.; Devlin, F. J.; Chabalowski, C. F.; Frisch, M. J. Ab initio calculation of vibrational absorption and circular dichroism spectra using density functional force fields. *J. Phys. Chem.* **1994**, *98*, 11623.

(24) Schäfer, A.; Huber, C.; Ahlrichs, R. Fully optimized contracted Gaussian basis sets of triple zeta valence quality for atoms Li to Kr. *J. Chem. Phys.* **1994**, *100*, 5829.

(25) Breneman, C. M.; Wiberg, K. B. Determining atom-centered monopoles from molecular electrostatic potentials. The need for high sampling density in formamide conformational analysis. *J. Comput. Chem.* **1990**, *11*, 361.

(26) Bussi, G.; Parrinello, M. Accurate sampling using Langevin dynamics. *Physical Review E* **2007**, *75*, 056707.

(27) Perdew, J. P.; Burke, K.; Ernzerhof, M. Generalized gradient approximation made simple. *Phys. Rev. Lett.* **1996**, *77*, 3865.

(28) Perdew, J. P.; Wang, Y. Accurate and simple analytic representation of the electron-gas correlation energy. *Phys. Rev. B* **1992**, *45*, 13244.

(29) Kendall, R. A.; Dunning, T. H., Jr.; Harrison, R. J. Electron affinities of the first-row atoms revisited. Systematic basis sets and wave functions. *J. Chem. Phys.* **1992**, *96*, 6796.

(30) Andersson, K.; Malmqvist, P.-Å.; Roos, B. O.; Sadlej, A. J.; Wolinski, K. Second-order perturbation theory with a CASSCF reference function. *J. Phys. Chem.* **1990**, *94*, 5483.

(31) Widmark, P.-O.; Malmqvist, P.-Å.; Roos, B. O. Density matrix averaged atomic natural orbital (ANO) basis sets for correlated molecular wave functions. *Theor. Chim. Acta* **1990**, *77*, 291.

(32) Granucci, G.; Persico, M.; Toniolo, A. Semiclassical methods for excited state dynamics. Dipartimento di Chimica e Chimica Industriale Università di Pisa.

(33) Nedungadi, S. Starting materials for the synthesis of biradicaloid heterocycles as small chromophores for singlet fission. Master Thesis, University of Colorado, Boulder, 2016.

(34) Michl, J., Biradicaloid structure presented in JACS 2012 by Akdag, et al. 2017, (personal communication).

Chapter 5 Nonadiabatic Dynamics Simulations of Singlet Fission in 2,5-bis(fluorene-9-ylidene)-2,5-dihydro-thiophene Crystals

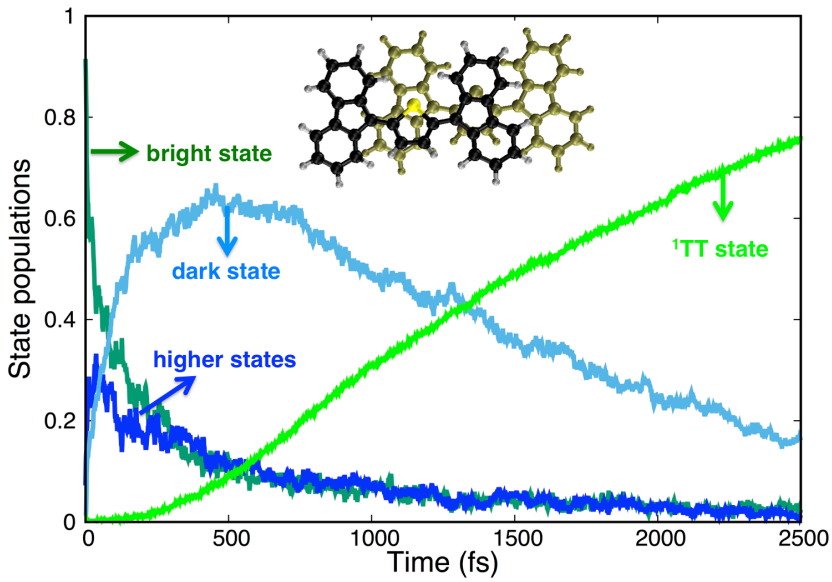

Part of the work presented in this chapter has been published as M. Wibowo, M. Persico, and G. Granucci, *Phys. Chem. Chem. Phys.*, **2019**, *21*, 692-701, DOI: 10.1039/c8cp05474f.

Simulations of the singlet fission dynamics in a pair of 2,5-bis(fluorene-9-ylidene)-2,5-dihydrothiophene molecules embedded in their crystal environment is presented. The ability of this molecule to undergo singlet fission has been proven by using it, in crystalline form, as the electron donor in the photovoltaic devices and by detecting the magnetic field dependence of the photocurrent.[1] However, its fission dynamics, its time scale, and other possible competing processes are hitherto unknown. The work presented here is aimed to shed lights on the photodynamics of this molecule, by means of trajectory surface hopping simulations. The simulations were performed by computing on-the-fly the electronic energies and wave functions employing the semiempirical floating occupation molecular orbital–configuration interaction method.[2,3] Our results show that the initially photogenerated excitonic bright state decays to the lower dark state, and this state in turn decays to the lowest singlet excited state with a lifetime of about 1 picosecond. At the end of the simulation time (2.5 picosecond) about 75% of the total state population is found in the lowest singlet excited state, which can be identified as the ^{1}TT state most of the time, and practically no decay to the ground state has taken place. The singlet fission quantum yield is predicted to be close to the theoretical maximum of 200%.

5.1 Introduction

In the singlet fission (SF) process, which requires (at least) two interacting chromophores A and B, the initially photogenerated excited singlet state can be localised on one chromophore, $S_1(A)+S_0(B)$ or $S_0(A)+S_1(B)$, or be instead the result of exciton coupling between the two chromophores in their S_1 states.[4] The ^{1}TT state, on the other hand, can be seen as a localised triplet excited state on each chromophore coupled into a total singlet spin. To get a large SF quantum yield, the transition from the initially photogenerated excited singlet state to the ^{1}TT state has to be faster than internal conversion (IC) and intersystem

crossing (ISC). Additionally, the ^{1}TT state should not be depopulated by IC to the ground state nor by ISC to a close-lying triplet state such as $T_n(A)+S_0(B)$ or $S_0(A)+T_n(B)$.[5,6]

Recently, non-polycyclic aromatic molecules based on the thienoquinoidal structure have been synthesised. Their ability to undergo SF has been proven by using them, in crystalline form, as the electron donor in organic photovoltaic devices and by detecting the magnetic field dependence of the photocurrent.[1] In addition, in the same work the energies of the excited singlet and triplet states were determined by measuring their absorption spectra and by performing DFT/TD-DFT calculations. These molecules satisfy the basic energetic condition of $\Delta E(S_1) \geq 2\Delta E(T_1)$ for SF chromophores. However, the SF mechanism, its time scale, and the possible competing processes are thus far unknown. The study presented in this chapter sheds light on the photodynamics of the simplest of such molecules, namely 2,5-bis(fluorene-9-ylidene)-2,5-dihydrothiophene (ThBF, see Figure 5.1), by means of trajectory surface hopping (SH) simulations.[2,3,7,8]

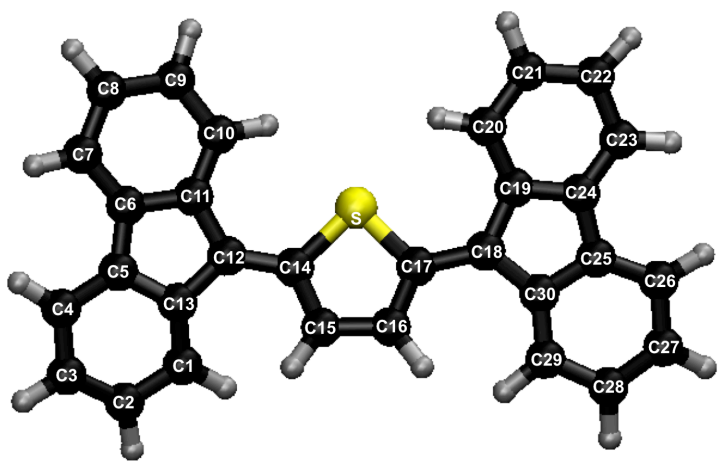

Figure 5.1 Chemical structure of ThBF.

Time-resolved spectroscopy techniques such as transient absorption, up-converted fluorescence, time-resolved two-photon photoemission, and 2-D electronic spectroscopy have been applied to other chromophores in order to investigate their fission dynamics, to reveal their time scales, and to determine some important parameters controlling their efficiencies.[9-14] The theoretical modelling of SF dynamics often complements the experimental findings and

allows exploring the SF mechanism, which may not be univocally inferred from the experimental results. In the present case, the computational simulation comes first and can be a useful basis to plan transient spectroscopy experiments.

Both full quantum mechanics (QM) and mixed quantum-classical theoretical methods have been applied to the study of SF. Important insight was gained by Berkelbach *et al*. by applying the Redfield theory to fully QM model systems with an electron-phonon coupling scheme.[15-17] Their results suggest the importance of charge transfer states in the SF dynamics of pentacene. Tamura *et al*. employed the multiconfigurational time-dependent Hartree QM approach to investigate the SF mechanism in a pentacene derivative and in rubrene.[18] They showed how the crystal structure of the pentacene derivative favours a coherent and ultrafast population transfer to the ^{1}TT state, while thermally activated symmetry-breaking intermolecular vibrations are needed to guarantee a non-vanishing electronic coupling between the initial and final states in rubrene. Mixed quantum-classical theoretical methods such as nuclear trajectories with SH,[3] have the advantage of allowing to explore the full nuclear phase space and to extend the integration time to several picoseconds. In particular, while small amplitude internal motions can be efficiently treated by fully quantum models with harmonic potentials,[15-17] it would be more difficult to set up such models for the relative motions of the molecules in a molecular crystal like the model used in this study (see the discussion about geometrical changes that bring about transitions to the ^{1}TT state in Section 5.4).

The SH simulations were already performed to study the SF dynamics in several polyacenes.[19,20] In the present study, we applied the direct approach to trajectory SH simulations in which the electronic energies and wave functions of the pair of molecules undergoing the photodynamics were computed on-the-fly by means of the semiempirical floating occupation molecular orbital–configuration interaction (FOMO–CI) method.[2,3] The crystal environment was described using molecular mechanics (MM) (force field) and its effect was taken into account by employing the QM/MM variant of the FOMO–CI method.[7] All the semiempirical calculations and the QM/MM simulations were performed using a modified version of MOPAC2002,[21] interfaced with the TINKER Molecular Mechanics package version 6.3,[22] when appropriate.

5.2 Molecular Calculations and Semiempirical Method

In order to characterise the singlet and triplet excited states of a ThBF molecule, we first ran DFT and TD-DFT calculations with the B3LYP functional[23-25] and the 6-31G+(d) basis set. The TD-DFT method was used to calculate the vertical excitation energies (ΔE_{vert}) of both states, and also to optimise the geometry of the S_1 state. For the T_1 optimisation we used DFT rather than TD-DFT, because the closeness of the T_1 and S_0 energies makes the latter method not reliable at such geometries.

ThBF is mainly a closed-shell molecule with an extended conjugated π system, the core of which is made of three π bonds, one belonging to the dihydrothiophene moiety and two connecting it to the fluorene groups. This view is supported by the bond lengths (see Table 5.1) and by the nature of the HOMO and LUMO, shown in Figure 5.2.

Table 5.1 Geometrical properties of ThBF (bond lengths are in Å and dihedral angles are in degrees). For atom labels see Figure 5.1.

States	Methods	$r(C_{12}C_{14})$	$r(C_{14}C_{15})$	$r(C_{15}C_{16})$	$\angle C_{13}C_{12}C_{14}C_{15}$
S_0[a]	X-ray diffraction[1]	1.38	1.43	1.33	2.1
S_0	DFT B3LYP/6-31+(d)	1.38	1.44	1.36	10.4
S_1	TD-DFT B3LYP/6-31+(d)	1.43	1.41	1.40	23.5
T_1	DFT B3LYP/6-31+(d)	1.44	1.39	1.41	33.7
S_0	FOMO–CI, PM3	1.35	1.46	1.35	2.2
S_0	FOMO–CI, reparam. PM3	1.38	1.48	1.37	1.1
S_1	FOMO–CI, reparam. PM3	1.38	1.48	1.37	0.1
T_1	FOMO–CI, reparam. PM3	1.44	1.44	1.40	16.7

[a]Molecular crystal.

At the equilibrium S_0 geometry computed at the FOMO–CI level using a reparameterised PM3 Hamiltonian, the point group of ThBF is C_s symmetry with a symmetry plane that divides the molecule in half and contains the sulphur atom. The HOMO and LUMO belong to a′ and a″ irreducible representations, respectively, therefore the $S_0 \rightarrow S_1$ transition dipole is

perpendicular to the symmetry plane. By forcing the molecule in a planar C_{2v} conformation, which is approximately the situation in the crystal, the transition dipole lies in the molecular plane.

The excitations that characterise the T_1 and S_1 states mainly concern this triene system in which the HOMO and LUMO π orbitals are well localised (see Figure 5.2). Looking at the nodal character of the LUMO, it is clear why the bond length alternation is reversed in going from the ground state to the excited ones. Actually this feature is much more pronounced in the T_1 state than in the S_1 state, so the bonds linking the dihydrothiophene and fluorene moieties have an increasing single bond character in the order $S_0 < S_1 < T_1$. Therefore, the twisting of these bonds (dihedral angles $C_{13}C_{12}C_{14}C_{15}$ and $C_{16}C_{17}C_{18}C_{30}$), driven by the repulsion of the pairs of H atoms bound to C_1/C_{15} and C_{16}/C_{29}, also increases in the same order. Consistently with the larger geometrical changes from the Franck-Condon point to the excited PES minimum, the difference between the vertical transition energy (ΔE_{vert}) and the adiabatic transition energy (ΔE_{adia}) is much larger in the T_1 state than in the S_1 state (see Table 5.2).

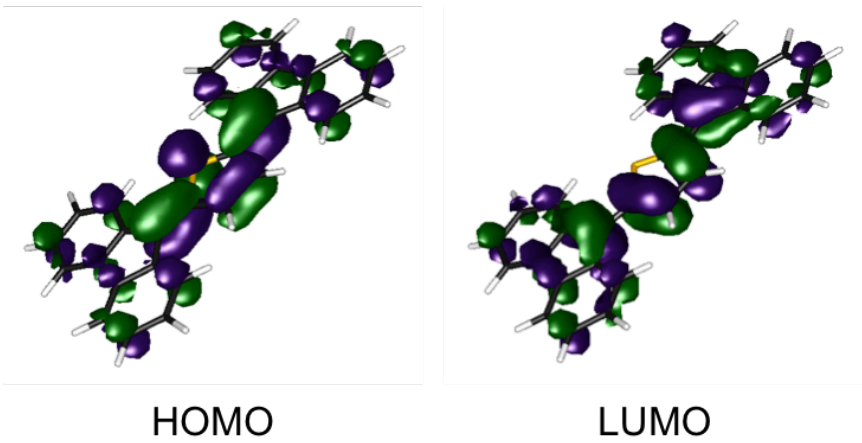

Figure 5.2 The HOMO and LUMO of ThBF, computed at the FOMO–CI level.

Table 5.2 Transition energies (eV) of ThBF.

Method	ΔE_{vert} (S_1)	ΔE_{adia} (S_1)	ΔE_{vert} (T_1)	ΔE_{adia} (T_1)
Absorption spectrum[1]	2.30	~2.2		
TD-DFT B3LYP/6-311G+(d)[a]	2.22			
ΔSCF B3LYP/6-311G+(d)[a]			0.90	
TD-DFT B3LYP/6-31G+(d)	2.31	2.09	0.97	
ΔSCF B3LYP/6-31G+(d)			1.20	0.77
FOMO–CI, PM3	2.96	2.86	1.84	1.08
FOMO–CI, reparam. PM3	2.17	2.16	0.91	0.54

[a]The ONIOM procedure was applied to simulate the effect of the crystal embedding.[1]

To choose the semiempirical Hamiltonian and other details of the FOMO–CI calculations, we compared the FOMO–CI description of the S_0, S_1, and T_1 states of ThBF with the experimental and DFT/TD-DFT results, focusing on the ΔE_{vert} and ΔE_{adia} transition energies. We tried the MNDO, AM1, PM3 and PM5 Hamiltonians with three different active spaces, *i.e.* CAS(6,5), CAS(6,4) and CAS(2,2). Moreover, we also varied the Gaussian widths w, which determine the floating occupation numbers (w = 0.1, 0.15, and 0.2 Hartree).[2] In all cases the description of the electronic structure was qualitatively correct, but the transition energies turned out too large (see for instance the PM3 entry in Table 5.2). Therefore, we proceeded to optimise the semiempirical parameters for the most promising combinations of the semiempirical Hamiltonian, the Gaussian width w, and the active space, using a well-tested procedure.[26,27] The best results were obtained with the PM3 Hamiltonian, the Gaussian width w of 0.1 Hartree, and an active space of CAS(2,2). The detail of the optimisation of PM3 parameters is presented in Section 5.2.1. The excitation energies are well reproduced, within the uncertainty of the available data. The torsion angles are underestimated, as can be seen in Table 5.1, and only the T_1 state presents a non-negligible twisting. However, this feature seems to be scarcely important in the simulations we performed, because in the crystal structure all molecules are practically planar, due to the strong stacking interactions.

5.2.1 Optimisation of the PM3 Parameters

The optimisation procedure of the semiempirical Hamiltonian model can be found in Section 4.3. The orbital energies of the HOMO-1 and HOMO-2 are nearly degenerate because they belong to the fluorene moieties (see Figure 5.3). As a consequence, both orbitals (or neither) have to be included in the active space, resulting in CAS(6,4) (or CAS(2,2)). The optimisation of the PM3 parameters was done for both active spaces, CAS(6,4) and CAS(2,2). The optimisation was converged to minimum values with the average percentage error of 3.00 and 1.98 for CAS(6,4) and CAS(2,2), respectively. The target values $X_i^{(T)}$ and semiempirical results $X_i^{(S)}$ of the transition energies (eV), ΔE_{vert} and ΔE_{adia}, obtained with the optimised PM3 parameters for the FOMO–CI calculations using CAS(2,2) and the Gaussian width w of 0.1 Hartree, %error, and the weights used for the optimisation are presented in Table 5.3. The comparison between the standard and optimised PM3 parameters is shown in Table 5.4.

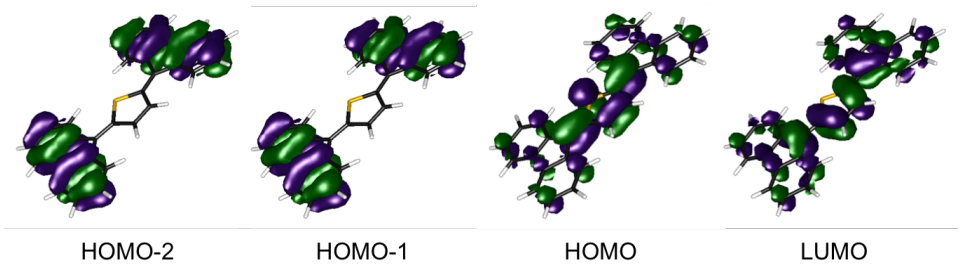

Figure 5.3 HOMO-2, HOMO-1, HOMO, and LUMO of ThBF, computed at the FOMO–CI level.

Table 5.3 The target values $X_i^{(T)}$, semiempirical results $X_i^{(S)}$, %error, and positive weights W_i for the optimisation of the PM3 parameters.

	$X_i^{(T)}$	$X_i^{(S)}$	%error	W_i
ΔE_{vert} (S_1)	2.2000	2.1723	-1.2555	3.00
ΔE_{vert} (T_1)	0.9000	0.9092	1.0269	2.00
ΔE_{adia} (S_1)	2.1000	2.1640	3.0485	2.50

Table 5.4 Comparison between the standard and optimised PM3 parameters for each S, C, and H atoms.

	Units	S_{std}	S_{opt}	C_{std}	C_{opt}	H_{std}	H_{opt}
U_{SS}	eV	-49.895371	-49.652227	-47.270320	-47.008592	-13.073321	-13.076403
U_{PP}	eV	-44.392583	-42.999534	-36.266918	-36.563642	-	-
β_S	eV	-8.827465	-8.753605	-11.910015	-11.899754	-5.626512	-5.590259
β_P	eV	-8.091415	-7.842710	-9.802755	-9.731624	-	-
ζ_S	$bohr^{-1}$	1.891185	1.882268	1.565085	1.549094	0.967807	0.969963
ζ_P	$bohr^{-1}$	1.658972	1.657581	1.842345	1.885028	-	-
α	$Å^{-1}$	2.269706	2.280149	2.707807	2.720603	3.356386	3.424330
G_{SS}	eV	8.964667	9.101272	11.200708	10.943581	14.794208	14.859227
G_{SP}	eV	6.785936	6.884667	10.265027	10.258203	-	-
G_{PP}	eV	9.968164	10.061875	10.796292	9.084341	-	-
G_{P2}	eV	7.970247	8.071794	9.042566	8.814852	-	-
H_{SP}	eV	4.041836	4.041174	2.290980	2.298389	-	-
FN11	-	-0.399191	-0.396684	0.050107	0.049424	1.128750	1.103372
FN21	$Å^{-1}$	6.000669	6.072489	6.003165	6.022090	5.096282	5.123068
FN31	Å	0.962123	0.963353	1.642214	1.653716	1.537465	1.527356
FN12	-	-0.054899	-0.054615	0.050733	0.051003	-1.060329	-1.061164
FN22	$Å^{-1}$	6.001845	6.113818	6.002979	6.116574	6.003788	5.998236
FN32	Å	1.579944	1.587803	0.892488	0.906359	1.570189	1.566024

5.3 Ground State Crystal Structure and Dynamics

To thermalize the ThBF crystal, we first optimised the crystal structure of ThBF by using the OPLSAA force field,[28] starting from the X-ray data of Kawata *et al*.[1] The atomic charge parameters were obtained from a DFT calculation employing the B3LYP functional[23-25] and the 6-311+G(d,p) basis set, by fitting the electrostatic potentials using the CHELPG scheme with the additional constraint to reproduce the overall molecular dipole moment.[29] The crystal

structure contains four molecules per unit cell, which belong to four equivalent slipped stacks with orientations only differing in the slope of the molecular planes and/or by a rotation of 180° (see Figure 5.4 and Figure 5.5). This optimised crystal structure was then taken as the starting point to thermalize the ThBF crystal by performing a molecular dynamics (MD) simulation employing the canonical (NVT) ensemble with a constant temperature of 300 K for 10 nanoseconds. Periodic boundary conditions were imposed during this thermal equilibration.

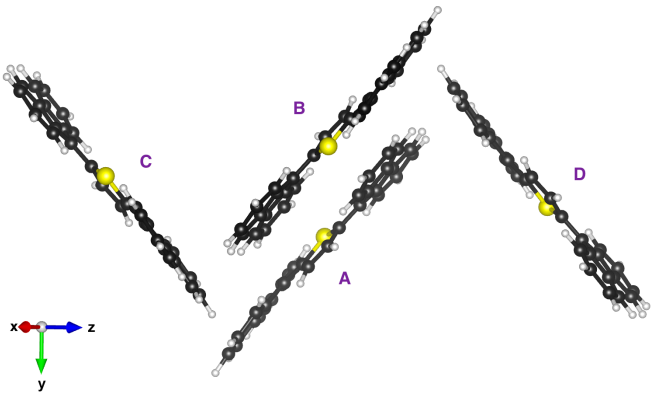

Figure 5.4 Unit cell of the ThBF crystal, obtained from the optimisation using the OPLSAA force field.

The last frame of the periodic MD simulation was then used to start a QM/MM thermal trajectory for a cluster containing 490 molecules, arranged in a 7x7 array of 49 slipped stacks of 10 molecules each (see Figure 5.5 upper panel). Two molecules (number 5 and 6) of the central stack were represented at the QM level and the others at the MM level. 162 MM molecules at the boundary of the cluster were kept frozen in order to keep the substantial rigidity of the crystal structure, while 326 MM molecules plus 2 QM molecules are freely moving during the dynamics simulations.

In the slip-stack arrangement, the two molecules are approximately planar with their planes 3.6 Å apart and a slip of 3.5 Å, such that a fluorene group of one molecule overlaps with the dihydrothiophene group of the other molecule. This is in particular the relationship between the two QM molecules, as represented in Figure 5.5 lower panel. The two QM

molecules were treated by the FOMO–CI method as described in the previous section, using an active space of CAS(4,4) which is equivalent to the CAS(2,2) we selected for a single molecule. The MM molecules were treated using the OPLSAA force field as mentioned earlier. The electrostatic embedding was applied to represent the interactions between the QM and MM subsystems.[7]

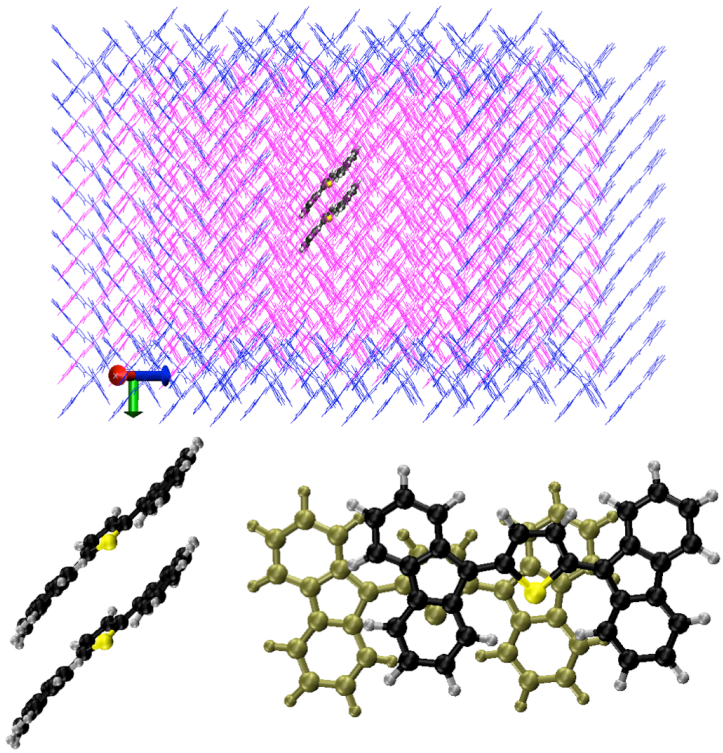

Figure 5.5 Upper panel: The representation of the QM and MM subsystems of the ThBF crystal structure. The space-filling model represents a pair of molecules in the QM subsystem (C, S, and H atoms are in black, in yellow, and in grey, respectively), while the line model in magenta and blue represents molecules in the MM subsystem which move freely and are kept frozen, respectively, during the dynamics simulations. Lower panel: The mutual position and orientation of the two QM molecules in a slip-stack arrangement, shown from two different points of view (in the right hand side, the farther molecule is depicted in a different colour for a better clarity).

The QM/MM ground state equilibration was performed employing the Bussi-Parrinello thermostat[30] for 14 picosecond (ps) with a time step of 0.1 femtosecond (fs)[31] and a constant temperature of 300 K. To monitor the progress of this equilibration, we computed the total energy of the QM/MM cluster and the transition energies from the ground state to the eight lowest excited singlet states of the two QM molecules, presented in Figure 5.6. In discussing the excited singlet and triplet states of the molecular pair we shall adopt the notation S[n] and T[n], meaning the n-th adiabatic singlet and triplet states in energy ordering, in order to distinguish them from the single molecule ones (S_0, S_1, S_2, T_1, T_2, *etc*.).

As can be deduced from the single molecule excitation energies, the S[1] state, with an average excitation energy of 1.7 eV, most of the time is essentially the ^{1}TT state. The S[2] and S[3] states are mainly the linear combinations of the S_1 state localised on each of the two QM molecules, $S_1(A)S_0(B)$ and $S_0(A)S_1(B)$. Since the two molecules are oriented essentially in the same way, the lower state, S[2], is the dark combination and the higher one, S[3], is the bright state.[4] The average of their energies is about 2.1 eV, with an exciton splitting of 0.25 eV. The S[4] and higher singlet states are of mainly charge transfer nature. The energy profiles presented in Figure 5.6 lower panel confirm that the basic energetic condition of SF is satisfied, in the sense that the process is slightly exoergic even starting from the lower excitonic state, *i.e*. the dark state S[2]. However, we note that the S[2] and S[3] transition energies undergo very small oscillations, with an amplitude of the order of 0.05 eV, whereas the energy of other states is much more sensitive to the small geometry changes occurring during the thermal ground state trajectory. In particular, the S[1] transition energy fluctuates by about ±0.5 eV. This is consistent with the larger energetically and geometrical differences found in the single molecule between the minimum and the Franck-Condon point of the T_1 state with respect to the S_1 state (see Section 5.2). In fact, one can see that from time to time the energy fluctuations bring the S[1] state at the same level where normally one finds the S[2] state, or, more seldom, even the S[3] state. This is a hint that the ^{1}TT and excitonic states from time to time switch in energy, a fact that must kept in mind when discussing the excited state dynamics simulations.

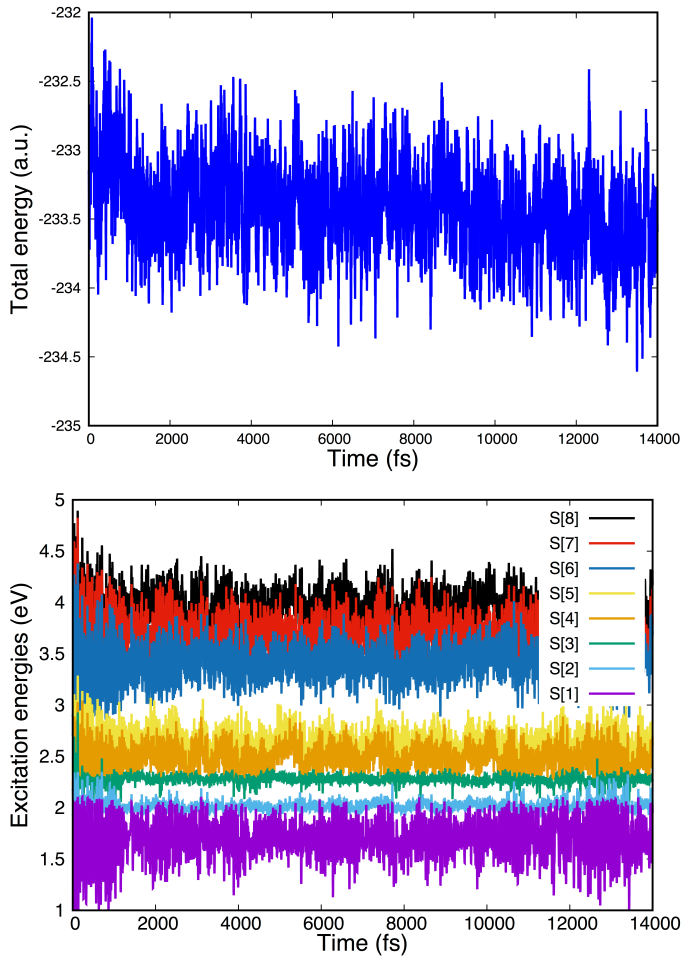

Figure 5.6 Upper panel: The total energy of the QM/MM cluster obtained during the QM/MM ground state equilibration, as a function of time. Lower panel: Excitation energies of the eight excited singlet states obtained during the QM/MM ground state equilibration, as a function of time.

We also computed the S[0]→S[n] transition dipole moments, from which we obtained the absorption spectrum in the form of an energy histogram, by averaging over the whole QM/MM thermal trajectory (see Figure 5.7). The maximum of the main band is at 2.28 eV, in good agreement with the experimental spectrum,[1] and the oscillator strength per molecule is $f \simeq 1.0$ ($f = 1.17$ for the vertical excitation of a single molecule computed at the TD-DFT/B3LYP level). The band is however too narrow and tall, due to the common problem of

neglecting the zero point vibrations in classical simulations, but probably also to a somewhat underestimated slope of the excited state PES around the Franck-Condon point by the FOMO–CI calculations. In fact, the dominant contribution is due to the bright state, *i.e.* S[3], which shares with the S_1 state of the single molecule a small difference between the ground and excited states equilibrium geometries. A small contribution to the main band is also due to the S[4] state. The S[1] and S[2] states show very weak absorptions between 1.95 and 2.10 eV: since the transition to the ^{1}TT state is forbidden unless some mixing with other states occurs,[32] the real responsible for this weak band is the dark state, which most of the time is the S[2] state and more seldom is the S[1] state. For a similar reason, the S[2] state also contributes very weakly to the main band: this occurs when the ^{1}TT state is temporarily higher in energy than both excitonic states, and the S[2] state is then the bright state. These observations confirm the switching of states already discussed with regard to the computed excitation energies presented in Figure 5.6. The absorption spectra by averaging over different time intervals during the thermal equilibration of the QM/MM ThBF cluster, which allow us to monitor the progress of this equilibration, are presented in Figure 5.8.

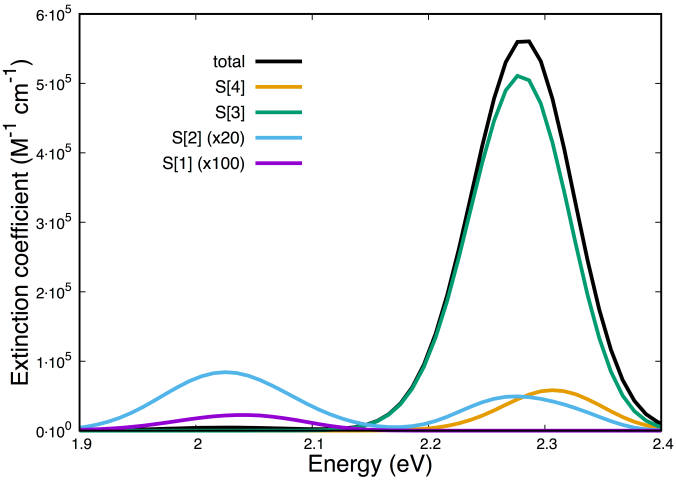

Figure 5.7 The computed electronic absorption spectrum obtained as the average from 0 to 14 picosecond of the QM/MM ground state equilibration.

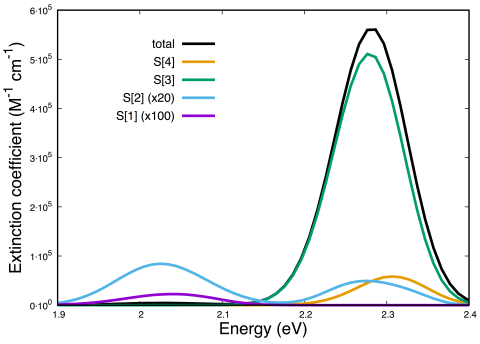

a) time interval 0–14 ps

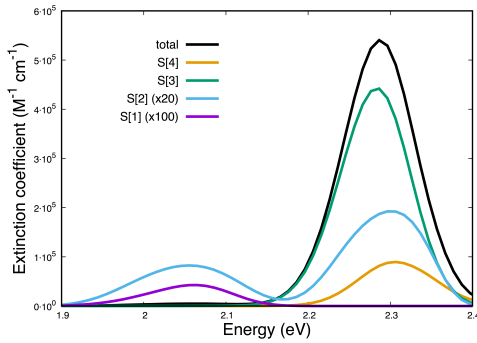

b) time interval 0–2 ps

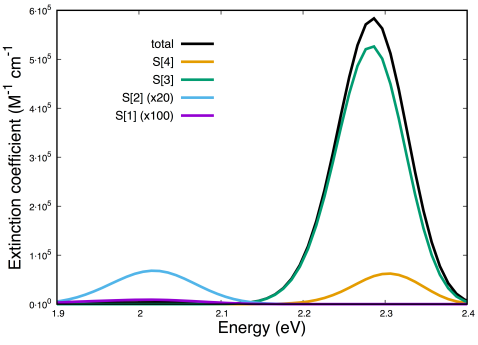

c) time interval 2–5 ps

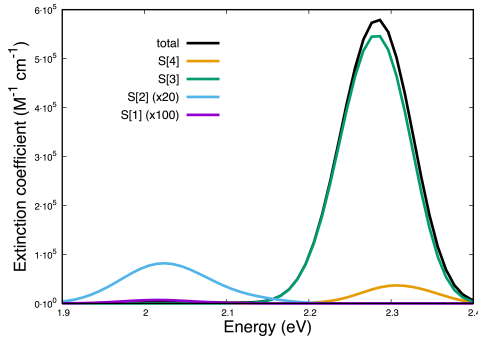

d) time interval 5–8 ps

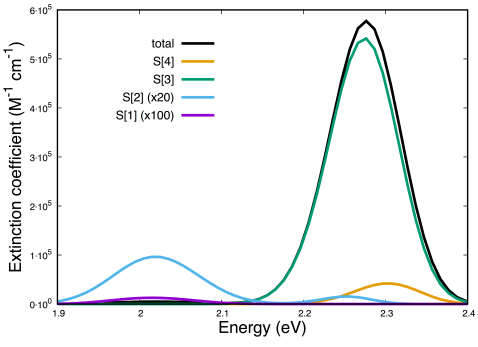

e) time interval 8–11 ps

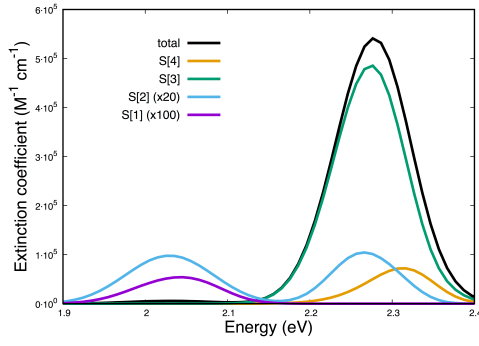

f) time interval 11–14 ps

Figure 5.8 Computed absorption spectra obtained by averaging over different time intervals during the thermal equilibration of the QM/MM ThBF cluster.

5.4 Excited State Dynamics Simulations

The time dependence of the total energy and excitation energies (Figure 5.6), and of the absorption spectra (Figure 5.8) shows that after 2 ps the QM/MM cluster is sufficiently equilibrated, *i.e.* the perturbation due to the small difference between the full MM and the QM/MM treatments has died off. Therefore, the sampling of the initial conditions for the excited state trajectories was done by taking at random a set of phase points belonging to the QM/MM ground state equilibration trajectory, with the exclusion of the first 2 ps. For each phase point, a number of trajectories (0, 1, or more) were launched by vertical transitions to the excited states lying within 1.6 to 2.8 eV from the ground state energy. The probability of starting a trajectory in state S[n] is taken proportional to the square of the S[0]→S[n] transition dipole moment.[3] As a result, 484 trajectories were launched, of which 6 started in S[2], 443 in S[3], 34 in S[4], and 1 in S[5], consistently with the dominant role of S[3] (the bright state) in the absorption band.

The excited state dynamics was modelled by SH[2,3] with overlap based decoherence corrections.[8] A time step of 0.2 fs was used to integrate the classical trajectories up to the final time of 2.5 ps. The parameters for the decoherence corrections were $\sigma = 1.0$ Hartree for the Gaussian width and $S_{min} = 0.005$ for the minimum overlap. The integration of the TDSE for the electrons was performed by an algorithm that guarantees stable results even in the case of very weak interactions, that is, of narrowly avoided crossings.[2,31]

Table 5.5 shows the averaged transition rates between pairs of states, *i.e.* the number of hops per picosecond, divided by the number of trajectories, along the whole simulation. It should be kept in mind that many hops are due to energy switches between two states, for instance, the bright and charge transfer states that are usually the S[3] and S[4] states. In most cases, due to weak interactions between the two states, the system goes diabatically through the avoided crossing, that is, a transition between the adiabatic states occurs by leaving the nature of the electronic state unchanged. Since the energy changes that cause such switches usually last for a short span of time (see Figure 5.6 lower panel), we have some very large m→n and n→m rates with smaller net rates. This is the case for the S[4]→S[3], S[3]→S[2], and S[2]→S[1] transitions.

Table 5.5 Hopping rates (ps^{-1}).

State m	State n	Rate m→n[a]	Rate n→m[a]	Net rate[b]
S[1]	S[0]	0.000	0.001	-0.001
S[2]	S[0]	0.042	0.018	0.024
S[3]	S[0]	0.007	0.007	0.000
S[4]	S[0]	0.002	0.009	-0.007
S[5]	S[0]	0.000	0.002	-0.002
S[6]	S[0]	0.005	0.002	0.003
S[7]	S[0]	0.002	0.002	0.000
S[8]	S[0]	0.001	0.002	-0.001
S[2]	S[1]	3.540	3.192	0.348
S[3]	S[1]	0.016	0.031	-0.015
S[4]	S[1]	0.002	0.012	-0.010
S[5]	S[1]	0.001	0.009	-0.008
S[6]	S[1]	0.000	0.006	-0.006
S[7]	S[1]	0.000	0.002	-0.002
S[8]	S[1]	0.000	0.002	-0.002
S[3]	S[2]	3.326	2.165	1.161
S[4]	S[2]	0.796	1.208	-0.412
S[5]	S[2]	0.105	0.340	-0.235
S[6]	S[2]	0.074	0.123	-0.049
S[7]	S[2]	0.042	0.055	-0.013
S[8]	S[2]	0.013	0.031	-0.018
S[4]	S[3]	5.127	4.357	0.770
S[5]	S[3]	0.086	0.062	0.024
S[6]	S[3]	0.050	0.048	0.002
S[7]	S[3]	0.026	0.039	-0.013
S[8]	S[3]	0.014	0.014	0.000
S[5]	S[4]	1.545	1.242	0.303
S[6]	S[4]	0.083	0.047	0.036
S[7]	S[4]	0.025	0.033	-0.008
S[8]	S[4]	0.011	0.018	-0.007

S[6]	S[5]	0.135	0.067	0.068
S[7]	S[5]	0.019	0.007	0.012
S[8]	S[5]	0.002	0.002	0.000
S[7]	S[6]	0.119	0.070	0.049
S[8]	S[6]	0.012	0.007	0.005
S[8]	S[7]	0.068	0.043	0.025

[a]Average rate over the whole simulation in ps^{-1} = $\frac{\#\,hops}{\#\,trajectories \cdot time}$.

[b]Net rate = difference between the m→n and the n→m rates.

The adiabatic state populations as functions of time are presented in Figure 5.9. The population P_n is computed as the fraction of trajectories running on the adiabatic PES number n, that is, those trajectories for which S[n] is the "current state" (n = 0 … 8). The bright state S[3], which is initially the most populated, decays rapidly within 100–200 fs, transferring populations to the S[4] state, which is very close in energy, and to a lesser extent to the higher states S[5]-S[8], as well as to the lower lying S[2] state, *i.e.* the dark state (see Figure 5.10 for a better clarity). The upper group of states (S[4] and the higher ones) keep exchanging population with the S[3] state, so in the long run they decay approximately at the same rate. Moreover, these states acquire population from the S[2] state and transfer it to the S[3] state, so they effectively slow down the S[3]→S[2] decay. Of course this effect is negligible at the beginning of the simulation, when the population of the S[2] state is very low, and becomes important after ~200 fs: as a result, the decay of the S[3] and upper states is initially very fast, but gets slower after a few hundred femtosecond. The S[2] state in turn decays to the S[1] state, which can be identified as the ^{1}TT state most of the time, and also, quite marginally, to the S[0] state. The decay of the S[2] state is slower than that of the S[3] state, so its population accumulates, reaches a maximum at about 500 fs, and then decreases smoothly.

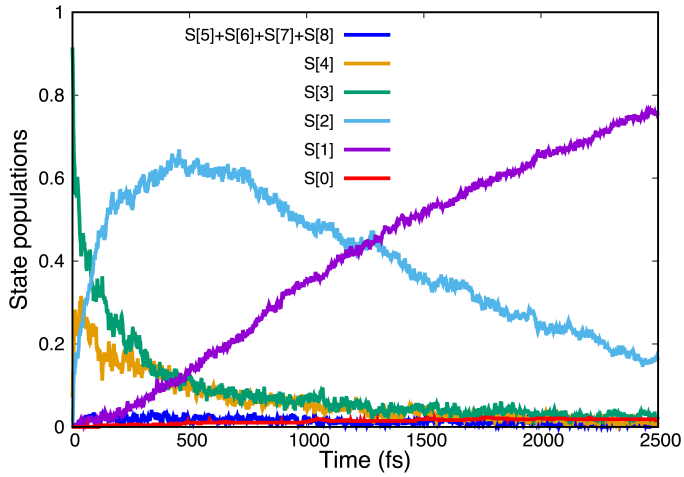

Figure 5.9 The adiabatic state populations in a total simulation time (2.5 picosecond).

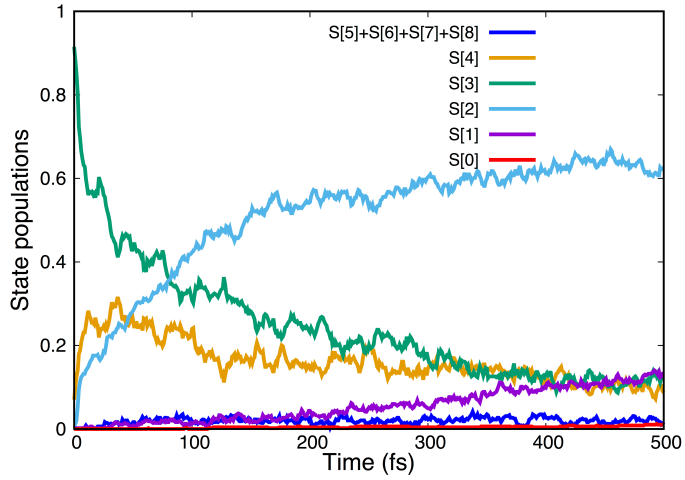

Figure 5.10 The adiabatic state populations in the first 500 femtosecond.

Since we are dealing with adiabatic states, that are linear combinations of the diabatic ones, *i.e.* $S_0(A)S_0(B)$, $S_1(A)S_0(B)$, $S_0(A)S_1(B)$, ^{1}TT, A^-B^+, and A^+B^-, our simulations do not provide direct evidence of the importance of the electronic couplings in the diabatic representation. Therefore, we resorted to a diabatisation procedure based on orbital localisation, devised ad hoc for the FOMO–CI method.[33] In Table 5.6 we report the electronic Hamiltonian matrix elements computed in the diabatic basis for an arrangement of two ThBF

molecules in their planar S_0 equilibrium geometry with an overall C_2 symmetry. We see that the direct couplings $\left\langle S_1(A)S_0(B)\left|\hat{\mathcal{H}}_{el}\right|{}^1TT\right\rangle$ and $\left\langle S_0(A)S_1(B)\left|\hat{\mathcal{H}}_{el}\right|{}^1TT\right\rangle$ are extremely small, whereas much larger matrix elements couple both the ^{1}TT and localised singlet states with the charge transfer states. The interaction mediated by the charge transfer states[6] can be evaluated to about 0.9 meV, and is therefore the main cause of transitions from the localised singlets (or rather their combination, the dark state) to the ^{1}TT state. However, because of the different energy gaps, the S[4] and higher states, which are essentially of charge transfer nature, are easily populated starting from the S[2] and S[3] states, but they do not exchange population with the S[1] state, *i.e.* the ^{1}TT state.

Table 5.6 The electronic Hamiltonian matrix elements in the basis of 6 low-lying diabatic states for a pair of two ThBF molecules, computed with the semiempirical FOMO–CI method. The pair is made of two ThBF planar molecules at the S_0 equilibrium geometry, with a distance between the two molecular planes of 3.6 Å and a slip of 3.5 Å, similar to the situation of a pair of ThBF molecules in the QM subsystem. Matrix elements are in meV.

	$S_0(A)S_0(B)$	^{1}TT	$S_1(A)S_0(B)$	$S_0(A)S_1(B)$	A^-B^+	A^+B^-
$S_0(A)S_0(B)$	0.00	0.22	30.46	-30.46	39.88	-39.88
^{1}TT	0.22	1780.29	0.02	-0.02	-29.41	29.41
$S_1(A)S_0(B)$	30.46	0.02	2148.98	155.06	-18.17	-2.04
$S_0(A)S_1(B)$	-30.46	-0.02	155.06	2148.98	2.04	-18.17
A^-B^+	39.88	-29.41	-18.17	-2.04	2424.00	0.01
A^+B^-	-39.88	29.41	-2.04	-18.17	0.01	2424.00

The adiabatic energy difference at S[2]→S[1] hopping events is small, *i.e.* 27 meV in the average, because of the weak interaction between the dark and ^{1}TT states. Note that SH performs well in the presence of weakly avoided crossings or conical intersections with small couplings, whereby the transition events are well localised in time and space,[34,35] so quantum effects are unlikely to be important in this case. The quasi-degeneracy between the S[1] and S[2] states is reached thanks to a substantial energy lowering of the upper state in going from the initial geometry (Franck-Condon region) to the hopping ones. Taking as a reference the

ground state S[0], the lowering of the S[2] state is about -0.6 eV (see Table 5.7). As already commented, in the single molecule of ThBF the difference between the adiabatic and vertical transition energy, $\Delta E_{adia} - \Delta E_{vert}$, for the first singlet excited state is quite small, so the geometrical changes that cause such energy lowering must involve the relative position and orientation of the two molecules. In fact, Table 5.7 shows almost no change in the four internal coordinates already chosen to characterise the equilibrium geometries of the single molecular states (Table 5.1), while the distances between atoms of molecule A and the corresponding atoms of molecule B decrease noticeably in going from the Franck-Condon region to the hopping geometries. More in detail, the distance between the two dihydrothiophene cores decreases by 0.16 Å (averaging over the five heavy atoms), two of the fluorene groups get closer by about 0.2 Å, while the other two do not move appreciably. The energetic effects are due in part to the increase of the exciton coupling, as shown by the bright to dark states energy splitting, ΔE S[3]-S[2], which averages to 0.28 eV at the initial geometries and to 0.54 eV at the hopping ones. An important contribution must also come from the change in the monomer-to-monomer interaction energy, which is affected by the difference in the charge distribution caused by excitation. In fact, the electronic density of the LUMO is more spread than that of the HOMO, and shifted away from the S atom, so that the S_1 state of the monomer develops a large dipole moment (3.7 Debye at FOMO–CI level, to be compared with 0.3 Debye of the ground state).

Table 5.7 Comparison of the state energies and geometrical parameters at the initial time (t = 0) and at the S[2]→S[1] hopping events, averaged over all trajectories.

Energies[a] or coordinates[b]	At $t = 0$ (X_0)	At S[2]→S[1] hops (X_h)	Difference $(X_h - X_0)$
ΔE S[1]-S[0]	1.5828	1.3064	-0.2764
ΔE S[2]-S[0]	1.9589	1.3335	-0.6254
ΔE S[2]-S[1]	0.3761	0.0271	-0.3490
ΔE S[3]-S[0]	2.2417	1.8691	-0.3726
ΔE S[3]-S[2]	0.2828	0.5355	0.2527
$\angle C_{13}C_{12}C_{14}C_{15}$	8.8430	9.5528	0.7098
$r(C_{12}C_{14})$	1.3818	1.3841	0.0023
$r(C_{14}C_{15})$	1.4862	1.4838	-0.0025

$r(C_{15}C_{16})$	1.3667	1.3723	0.0056
S	5.6920	5.5042	-0.1879
C_{14}	5.5513	5.3294	-0.2219
C_{15}	5.4607	5.2585	-0.2022
C_{16}	5.4447	5.3397	-0.1050
C_{17}	5.5534	5.4806	-0.0728
C_{12}	5.5116	5.2020	-0.3096
C_7	5.4823	5.3020	-0.1804
C_4	5.4898	5.3766	-0.1131
C_9	5.4867	5.1739	-0.3128
C_2	5.4555	5.2956	-0.1598
C_{18}	5.5319	5.4807	-0.0512
C_{23}	5.5988	5.5113	-0.0875
C_{26}	5.4364	5.4487	0.0124
C_{21}	5.6505	5.5678	-0.0826
C_{28}	5.3366	5.3813	0.0447

[a]Energy differences between the specified electronic states are in eV.

[b]Dihedral angles are in degrees, bond lengths and distances are in Å. For distances between an atom in molecule A and the corresponding atom in molecule B, only the former is specified. For atom labels see Figure 5.1.

In order to extract the excited state lifetimes from the simulation data, the adiabatic state populations were fitted by a simple consecutive decay model,

$$S[3], S[4] \ldots S[8] \rightarrow S[2] \rightarrow S[1], S[0]. \tag{5.1}$$

Since the decay of the S[3] and higher states follows two different regimes in the short and long time range, we modelled the sum of their populations with a biexponential function,

$$P_{3-8}(t) = P_{3-8}(0)\left[W\, e^{-t/\tau_3} + (1-W)\, e^{-t/\tau_3'}\right], \tag{5.2}$$

where $P_{3-8}(0)$ is the total initial state populations from the S[3] to S[8] states, W is a constant, τ_3 and τ_3' are the short- and long-life times of the S[3] and higher states, respectively. By assuming a fixed decay rate $1/\tau_2$ for the S[2] state, its population is then

$$P_2(t) = X\, e^{-t/\tau_3} + X'\, e^{-t/\tau_3'} + Y\, e^{-t/\tau_2}, \tag{5.3}$$

with

$$X = P_{3\text{–}8}(0)\, W\, \frac{\tau_2}{\tau_3 - \tau_2}, \quad X' = P_{3\text{–}8}(0)(1-W)\frac{\tau_2}{\tau_3' - \tau_2}, \quad Y = P_2(0) - X - X', \tag{5.4}$$

where $P_2(0)$ and τ_2 are the initial state population and the lifetime of the S[2] state, respectively. Of course, the sum of the populations of the two lowest states is

$$P_0(t) + P_1(t) = 1 - P_{3\text{–}8}(t) - P_2(t). \tag{5.5}$$

The initial populations are known, *i.e.* $P_{3\text{–}8}(0)$ = 0.988 and $P_2(0)$ = 0.012. The τ_3, τ_3', and W parameters were determined by fitting $P_{3\text{–}8}(t)$, and the lifetime of the S[2] state, τ_2, was determined by subsequently fitting $P_2(t)$. This procedure yielded τ_3 = 0.11 ps, τ_3' = 1.05 ps, τ_2 = 1.32 ps, and W = 0.645. Time-resolved spectroscopy experiments should be able to confirm these data.

The fitting of the adiabatic state populations obtained by this simple decay model is shown in Figure 5.11.

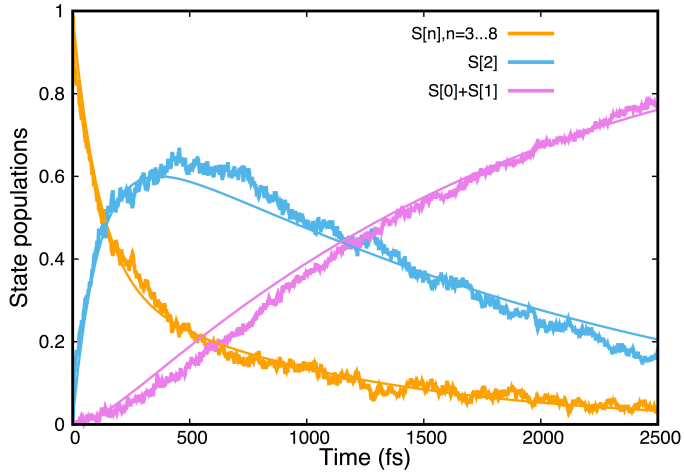

Figure 5.11 The fitting of the adiabatic state populations obtained by a simple decay model.

One of the main goals of this study was to determine the SF quantum yield, which is apparently very high since the S[1] state is by far the most populated one at the end of the simulation. However, as already observed, one cannot take for granted that the S[1] state is univocally identified as the ^{1}TT state. Therefore, we extracted the ^{1}TT population from the

simulation data in a different way. We first identify the ^{1}TT state among the nine adiabatic singlet states considered in the simulation, as the one that is closest to be a double excitation. In practice, given the four diagonal elements $\rho_{n,ii}$ of the density matrix of state n restricted to the active space, we computed the index

$$V_n = \sum_{i=1}^{4} \left(\rho_{n,ii} - 1\right)^2 , \tag{5.6}$$

and we identified the ^{1}TT state as the state S[n] with the smallest value of V_n. Then, we evaluated the ^{1}TT population by computing the fraction of trajectories $F_{^1\mathrm{TT}}$ in which n is the current state.

Figure 5.12 compares the populations of the adiabatic state S[1] with that of the ^{1}TT state, computed as the fraction of trajectories where the current state can be identified as the ^{1}TT state. We can see that $F_{^1\mathrm{TT}}$ and P_1 practically coincide, especially towards the end of the simulation. In fact, once the system settles in the deep minimum of the S[1] PES and the vibrational energy excess of the excited molecules starts to be dissipated by coupling with other modes, the probability that the ^{1}TT and dark states switch in energy fades away. So, the SF quantum yield can be evaluated as twice the asymptotic S[1] population (two triplet states for every dimer that reaches the S[1] state). We can assume that in the S[2] decay the branching ratio between the S[0] and S[1] states is the ratio of their final populations at the end of the simulation time (t = 2.5 ps): P_0/P_1 = 0.022. So, the computed SF quantum yield is 1.96, close to the theoretical maximum.

This high quantum yield seems to contrast with the low power conversion efficiencies measured in the photodevices using ThBF as the electron donor (at best, about 1%), but other factors may explain such failure.[1] A feature highlighted in this work, namely the low adiabatic transition energy of the T_1 state of ThBF (see Table 5.2), is probably an important drawback. The value of ΔE_{adia} (T_1) sets an upper limit to the energy available to produce a charge separation: 0.77 eV according to ΔSCF DFT, or 0.54 eV according to FOMO–CI. However, the process is more probably "vertical", that is, it takes place at a fixed geometry corresponding to the minimum of the T_1 PES. Then, the energy difference with respect to the ground state further reduces to 0.27 eV, according to FOMO–CI. We conclude that, within this class of compounds, it is probably worth trying molecules with higher T_1 and S_1 energies.

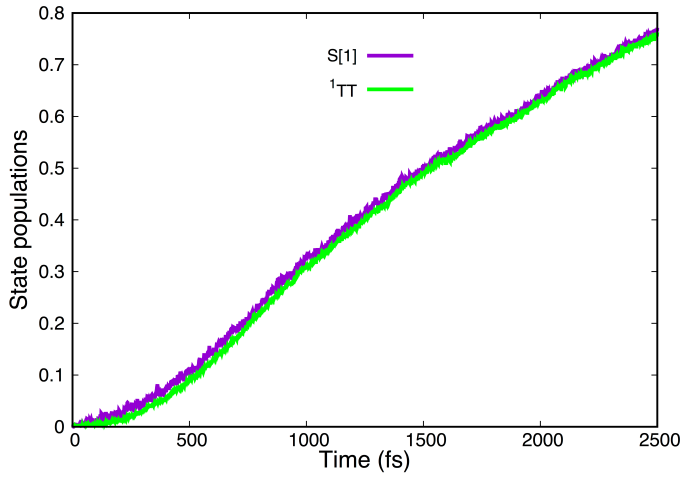

Figure 5.12 Population of the adiabatic state S[1] compared with that of the ^{1}TT state.

A limitation of our model, namely the fact that only two molecules are treated at the QM level, in principle might lead to an overestimation of the SF quantum yield. In fact, taking into account the delocalisation over more than two molecules, the lowest excitonic state would be lower in energy than the dimer dark state. Would such state be lower or of comparable energy with the ^{1}TT state, the quantum yield might considerably decrease. However, as already discussed when comparing the ^{1}TT and S[1] populations, at long times the system settles in the minima of the PESs and the ^{1}TT minimum is sufficiently low as to exclude an energy switch even with very delocalised excitonic states. In fact, according to the ΔE_{adia} values of Table 5.2 the ^{1}TT equilibrium energy is 1.1–1.5 eV. Concerning the lowest excitonic state, the theoretical limit for the energy lowering with respect to the monomer of a very delocalised state is twice the lowering observed in the dimer, *i.e.* about 0.25 eV, which puts such state at 1.9–2.0 eV, well above the ^{1}TT state (here we assume delocalisation over many molecules along a single stack and we take into account first-neighbour interactions only). Of course, delocalisation over more than two molecules can also change the couplings and therefore the transition rates.

The small energy gap between the T_1 and S_0 states at the T_1 equilibrium geometry has potentially another negative consequence. In fact, the same energy gap separates the ^{1}TT state from the two lowest triplet states in the dimer. Such triplets are almost degenerate, being

essentially two equivalent excitations localised on each monomer, $T_1(A)S_0(B)$ and $S_0(A)T_1(B)$, or linear combinations thereof. Their energy proximity to the ^{1}TT state may facilitate the ISC transitions: ^{1}TT→T[1] or ^{1}TT→T[2], so shortening the lifetime of the ^{1}TT state. To investigate this possibility, we ran a simulation taking into account the spin-orbit coupling (SOC), hereafter indicated as the "SOC simulation", to distinguish it from the "singlet-only simulation" discussed till now. It included, in addition to the five most important singlet states (S[0] to S[4]), also five triplet states (T[1] to T[5]) and one quintet state (Q[1]). The third triplet T[3] and quintet Q[1] states are the higher spin combinations of the double triplet excitation, almost degenerate with the ^{1}TT state.

The sampling of initial conditions was more limited than in the singlet-only simulation, resulting in 66 trajectories. The SOC was treated in a semiempirical way as described in the previous work.[27,36] One parameter ξ for each heavy atom enters the one electron effective spin-orbit Hamiltonian adopted in our calculations.[36] For the carbon atoms we chose ξ_C = 28.6 cm^{-1}, that fits the splitting of the ^{3}P ground state of the C atom. Actually, the value of ξ_C turned out to be almost irrelevant in determining the SOC between the states of ThBF we are interested in, the largest contribution being due to the S atom. To fix the ξ_S value for S atom, we determined the SOCs between the first three electronic states at CASSCF(6,6) level with the ANO basis set[37] contracted to S,C[3s2p1d]/H[2s1p], at the DFT equilibrium geometry of the S_0 state. The SOC between the S_0 and T_1 states, expressed as norm of the coupling vector for the three triplet components, was 2.7 cm^{-1}, and between the S_1 and T_1 states was 0.9 cm^{-1}. These rather small values are due to scarce involvement of the S atom in the HOMO and LUMO. At the FOMO–CI level, using ξ_S = 275 cm^{-1}, we get 2.8 cm^{-1} for the S_0-T_1 SOC, and zero for the S_1-T_1 SOC. The latter result embodies El-Sayed's rule,[38] which is exactly obeyed when the A″ S_1 and T_1 states are represented by a CAS(2,2) configuration interaction. Non-zero values can be obtained at asymmetric geometries, where the HOMO→LUMO excitation mixes with the closed-shell configurations.

The results of the SOC simulation are shown in Figure 5.13. Very few ISC transitions to the triplet states occur in the first 2.5 ps and only T[3], thanks to its quasi-degeneracy with the ^{1}TT state, gets a small population: 2.0 x 10^{-3} in the average over the time interval 1.5–2.5 ps. The population of the quintet state also remains very low, *i.e.* 0.5 x 10^{-3}, by averaging over the same interval. A bold extrapolation leads to the prediction that a considerable population

exchange between the ^{1}TT, ^{3}TT, and ^{5}TT states would occur in a time scale of 100-1000 ps. In any case, these results indicate that the ^{1}TT state does not decay to the lower energy states, at least during many picoseconds.

Qualitatively, the SOC simulation confirms the same nonadiabatic dynamics as the singlet-only one, but shows a faster decay of the S[3] and S[4] states, so the peak of the S[2] population occurs earlier and the increase of the S[1] population is steeper. By fitting the populations with the same model as before, Eq. (5.1) – (5.5), we get $\tau_3 = 0.11$ ps, $\tau_3' = 1.83$ ps, $\tau_2 = 0.93$ ps, and $W = 0.934$. So, we see that the main difference with respect to the singlet-only simulation is the almost complete suppression of the slow component in the decay of the S[3] and S[4] states.

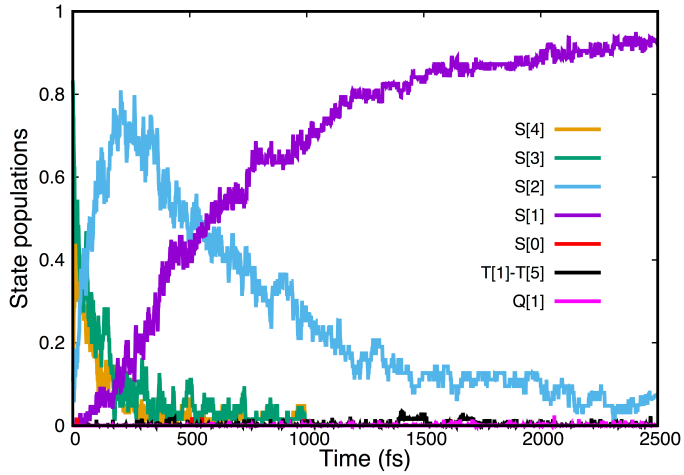

Figure 5.13 State populations obtained in a simulation taking into account the spin-orbit coupling and including triplet and quintet states. The S[3] and S[4] populations are plotted only up to 1 ps in order to improve the visibility of the triplet and quintet ones.

We remind that the SOC simulation differs from the singlet-only one in three ways: (i) the absence of the S[5]-S[8] states, (ii) the presence of triplet and quintet states and the addition of the SOC to the electronic Hamiltonian, and (iii) the reduced sampling of initial conditions. In order to ascertain which of these variables most affects the results, we show in Figure 5.14 and Figure 5.15 in the appendix the results obtained without SOC and with singlet states only (five and nine singlets, respectively). In both cases, the sampling of initial

conditions was similar to the one performed for the SOC simulation. We see that the results obtained with five states (Figure 5.14) agree with those of the SOC simulation. Conversely, using nine states (Figure 5.15) one gets results close to those of the singlet-only simulation described above. This confirms that the S[5] and higher singlet states, although scarcely populated, play a role in slowing down the decay of the S[3] and S[4] states, as already discussed in relation with the hopping rates of Table 5.5.

5.5 Conclusions

Kawata *et al*. showed that the ThBF molecule undergoes SF. No experimental data concerning the excited state dynamics nor the SF quantum yield are available, but the use of ThBF in organic photovoltaic devices resulted in very small power conversion efficiencies.[1] We have performed SH simulations of the SF in a pair of two ThBF molecules embedded in their crystal environment to characterise the excited state dynamics and to predict the SF quantum yield. The essential steps of the dynamics are the decay from the bright excitonic state of the pair of molecules to the underlying dark state and from the latter to the singlet coupled triplet states, the ^{1}TT state. The first step is initially ultrafast, with a lifetime in the order of 0.1 ps, but is subsequently slowed down by transitions to close-lying higher states, resulting in biexponential behaviour. After the first ~200 fs, the state populations evolve in the picosecond time scale. The dark state converts to the ^{1}TT state when the two molecules move closer, at geometries where the two states are almost degenerate. The interaction responsible for this transition is essentially mediated by the higher lying charge transfer states. These results can be used to plan the time-resolved spectroscopy experiments and to help their interpretation.

The SF quantum yield is predicted to be close to the theoretical upper limit of 200%. Very little decay from the dark state to the ground state occurs. Upon inclusion of SOC in the simulation, no decay of the ^{1}TT state to the lower but close lying single excitation triplet state is observed. The low efficiency of the tested photovoltaic devices was attributed by Kawata *et al*.[1] to the low T_1 energy of ThBF, and in one case also to inefficient coupling with the electron acceptor. Our calculations show that the vertical energy gap between the T_1 and S_0

states decreases considerably in going from the equilibrium geometry of S_0 to that of T_1, respectively, 0.91 eV and 0.27 eV. The latter value is most probably the energy that comes into play in charge or energy transfer transitions, the upper limit being the adiabatic transition energy (0.54 eV). These data show that the assessment of chromophores for SF should also include the optimisation of the excited state geometries and confirm that suitable thienoquinoid compounds must have higher triplet energies.

5.6 Acknowledgement

We thank Prof. Pu Yong-Jin from the Emergent Supramolecular Materials Research Team, Centre for Emergent Matter Science (CEMS), RIKEN, Japan for providing the crystal data.

5.7 Appendix: Simulation of ThBF including spin-orbit coupling

The simulation of the excited state dynamics taking into account the SOC was performed by using a more limited sampling of initial conditions, resulting in 66 trajectories, with respect to the singlet-only one described in Section 5.4, which featured a swarm of 484 trajectories. Moreover, it included five singlet states (S[0] to S[4]), whereas the singlet-only simulation had nine states (up to S[8]). Figure 5.9 and Figure 5.13 report the state populations obtained in the singlet-only and SOC simulations, respectively. Figure 5.14 and Figure 5.15 allow comparing those results with those of two singlet-only simulations using a sampling similar to that of the SOC one (a more limited sampling of initial conditions): one with five singlet states (Figure 5.14) and the other one with nine states (Figure 5.15).

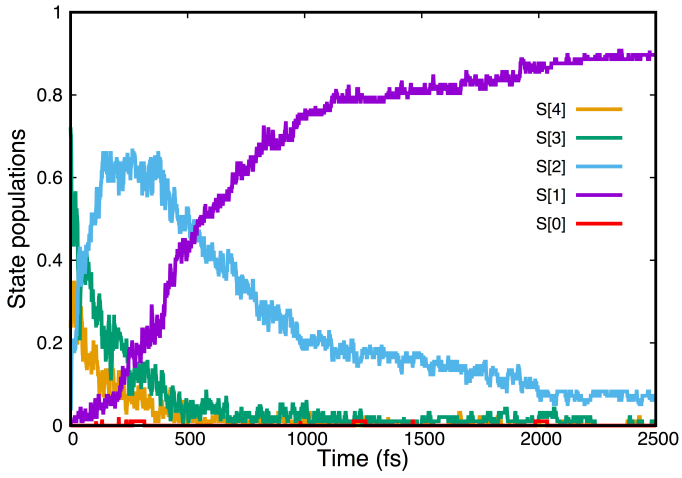

Figure 5.14 The adiabatic state populations obtained in a singlet-only simulation with five singlet states and a sampling of initial conditions similar to that of the SOC simulation.

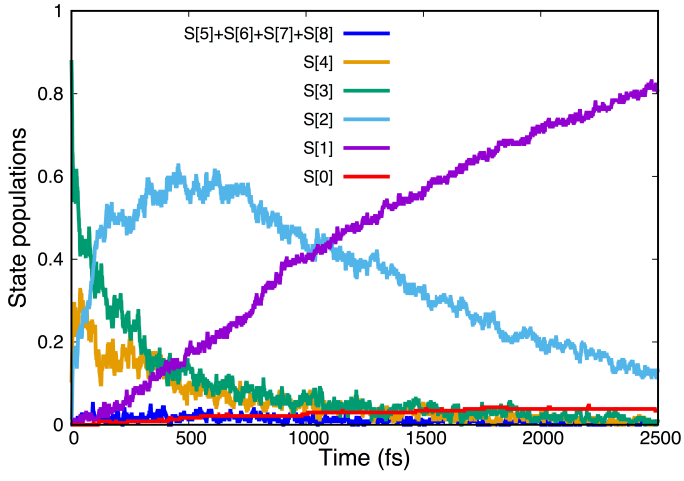

Figure 5.15 The adiabatic state populations obtained in a singlet-only simulation with nine singlet states and a sampling of initial conditions similar to that of the SOC simulation.

5.8 References

(1) Kawata, S.; Pu, Y.-J.; Saito, A.; Kurashige, Y.; Beppu, T.; Katagiri, H.; Hada, M.; Kido, J. Singlet fission of non-polycyclic aromatic molecules in organic photovoltaics. *Adv. Mater.* **2016**, *28*, 1585.

(2) Granucci, G.; Persico, M.; Toniolo, A. Direct semiclassical simulation of photochemical processes with semiempirical wave functions. *J. Chem. Phys.* **2001**, *114*, 10608.

(3) Persico, M.; Granucci, G. An overview of nonadiabatic dynamics simulations methods, with focus on the direct approach versus the fitting of potential energy surfaces. *Theor. Chem. Acc.* **2014**, *133*, 1.

(4) Persico, M.; Granucci, G. *Photochemistry: A Modern Theoretical Perspective*; Springer: Berlin, 2018.

(5) Smith, M. B.; Michl, J. Singlet fission. *Chem. Rev.* **2010**, *110*, 6891.

(6) Smith, M. B.; Michl, J. Recent advances in singlet fission. *Annu. Rev. Phys. Chem.* **2013**, *64*, 61.

(7) Persico, M.; Granucci, G.; Inglese, S.; Laino, T.; Toniolo, A. Semiclassical simulation of photochemical reactions in condensed phase. *J. Mol. Struc.-THEOCHEM* **2003**, *621*, 119.

(8) Granucci, G.; Persico, M.; Zoccante, A. Including quantum decoherence in surface hopping. *J. Chem. Phys.* **2010**, *133*, 134111.

(9) Bakulin, A. A.; Morgan, S. E.; Kehoe, T. B.; Wilson, M. W. B.; Chin, A. W.; Zigmantas, D.; Egorova, D.; Rao, A. Real-time observation of multiexcitonic states in ultrafast singlet fission using coherent 2D electronic spectroscopy. *Nat. Chem.* **2016**, *8*, 16.

(10) Chan, W.-L.; Tritsch, J. R.; Zhu, X.-Y. Harvesting singlet fission for solar energy conversion: One- versus two-electron transfer from the quantum mechanical superposition. *J. Am. Chem. Soc.* **2012**, *134*, 18295.

(11) Johnson, J. C.; Nozik, A. J.; Michl, J. The role of chromophore coupling in singlet fission. *Acc. Chem. Res.* **2013**, *46*, 1290.

(12) Kolata, K.; Breuer, T.; Witte, G.; Chatterjee, S. Molecular packing determines singlet exciton fission in organic semiconductors. *ACS Nano* **2014**, *8*, 7377.

(13) Monahan, N. R.; Sun, D.; Tamura, H.; Williams, K. W.; Xu, B.; Zhong, Y.; Kumar, B.; Nuckolls, C.; Harutyunyan, A. R.; Chen, G.; Dai, H.-L.; Beljonne, D.; Rao, Y.; Zhu, X.-Y.

Dynamics of the triplet-pair state reveals the likely coexistence of coherent and incoherent singlet fission in crystalline hexacene. *Nat. Chem.* **2017**, *9*, 341.

(14) Wilson, M. W. B.; Rao, A.; Clark, J.; Kumar, R. S. S.; Brida, D.; Cerullo, G.; Friend, R. H. Ultrafast dynamics of exciton fission in polycrystalline pentacene. *J. Am. Chem. Soc.* **2011**, *133*, 11830.

(15) Berkelbach, T. C.; Hybertsen, M. S.; Reichman, D. R. Microscopic theory of singlet exciton fission. II. Application to pentacene dimers and the role of superexchange. *J. Chem. Phys.* **2013**, *138*, 114103.

(16) Berkelbach, T. C.; Hybertsen, M. S.; Reichman, D. R. Microscopic theory of singlet exciton fission. I. General formulation. *J. Chem. Phys.* **2013**, *138*, 114102.

(17) Berkelbach, T. C.; Hybertsen, M. S.; Reichman, D. R. Microscopic theory of singlet exciton fission. III. Crystalline pentacene. *J. Chem. Phys.* **2014**, *141*, 074705.

(18) Tamura, H.; Huix-Rotllant, M.; Burghardt, I.; Olivier, Y.; Beljonne, D. First-principles quantum dynamics of singlet fission: Coherent versus thermally activated mechanisms governed by molecular phi stacking. *Phys. Rev. Lett.* **2015**, *115*, 107401.

(19) Mou, W.; Hattori, S.; Rajak, P.; Shimojo, F.; Nakano, A. Nanoscopic mechanisms of singlet fission in amorphous molecular solid. *Appl. Phys. Lett.* **2013**, *102*, 173301.

(20) Wang, L.; Olivier, Y.; Prezhdo, O. V.; Beljonne, D. Maximizing singlet fission by intermolecular packing. *J. Phys. Chem. Lett.* **2014**, *5*, 3345.

(21) Stewart, J. J. P. MOPAC 2002; Fujitsu Limited: Tokyo, Japan, 2002.

(22) Ponder, J. W.; Richards, F. M. An efficient Newton-like method for molecular mechanics energy minimization of large molecules. *J. Comput. Chem.* **1987**, *8*, 1016.

(23) Becke, A. D. Density-functional thermochemistry. III. The role of exact exchange. *J. Chem. Phys.* **1993**, *98*, 5648.

(24) Lee, C.; Yang, W.; Parr, R. G. Development of the Colle-Salvetti correlation-energy formula into a functional of the electron density. *Phys. Rev. B* **1988**, *37*, 785.

(25) Stephens, P. J.; Devlin, F. J.; Chabalowski, C. F.; Frisch, M. J. Ab initio calculation of vibrational absorption and circular dichroism spectra using density functional force fields. *J. Phys. Chem.* **1994**, *98*, 11623.

(26) Cusati, T.; Granucci, G.; Martínez-Núñez, E.; Martini, F.; Persico, M.; Vázquez, S. Semiempirical Hamiltonian for simulation of azobenzene photochemistry. *J. Phys. Chem. A* **2012**, *116*, 98.

(27) Favero, L.; Granucci, G.; Persico, M. Surface hopping investigation of benzophenone excited state dynamics. *Phys. Chem. Chem. Phys.* **2016**.

(28) Jorgensen, W. L.; Maxwell, D. S.; Tirado-Rives, J. Development and testing of the OPLS All-Atom force field on conformational energetics and properties of organic liquids. *J. Am. Chem. Soc.* **1996**, *118*, 11225.

(29) Breneman, C. M.; Wiberg, K. B. Determining atom-centered monopoles from molecular electrostatic potentials. The need for high sampling density in formamide conformational analysis. *J. Comput. Chem.* **1990**, *11*, 361.

(30) Bussi, G.; Parrinello, M. Accurate sampling using Langevin dynamics. *Physical Review E* **2007**, *75*, 056707.

(31) Plasser, F.; Granucci, G.; Pittner, J.; Barbatti, M.; Persico, M.; Lischka, H. Surface hopping dynamics using a locally diabatic formalism: Charge transfer in the ethylene dimer cation and excited state dynamics in the 2-pyridone dimer. *J. Chem. Phys.* **2012**, *137*, 22A514.

(32) Accomasso, D.; Granucci, G.; Havenith, R. W. A.; Persico, M. Testing new chromophores for singlet fission: A computational protocol applied to 2,3-diamino-1,4-benzoquinone. *Chem. Phys.* **2018**, in press.

(33) Accomasso, D.; Granucci, G.; Persico, M., in preparation.

(34) Cattaneo, P.; Persico, M. Wave packet dynamics in the presence of a conical intersection. *J. Phys. Chem. A* **1997**, *101*, 3454.

(35) Ferretti, A.; Granucci, G.; Lami, A.; Persico, M.; Villani, G. Quantum mechanical and semiclassical dynamics at a conical intersection. *J. Chem. Phys.* **1996**, *104*, 5517.

(36) Granucci, G.; Persico, M.; Spighi, G. Surface hopping trajectory simulations with spin-orbit and dynamical couplings. *J. Chem. Phys.* **2012**, *137*, 22A501.

(37) Widmark, P.-O.; Persson, B. J.; Roos, B. O. Density matrix averaged atomic natural orbital (ANO) basis sets for correlated molecular wave functions. *Theor. Chim. Acta* **1991**, *79*, 419.

(38) El-Sayed, M. A. Triplet state: Its radiative and nonradiative properties. *Acc. Chem. Res.* **1968**, *1*, 8.

Chapter 6 Outlook

A comprehensive view of this thesis is presented. This comprehensive view includes interesting aspects, which have not been developed in this thesis, to be pursued further for a future perspective of high-performance solar cell applications.

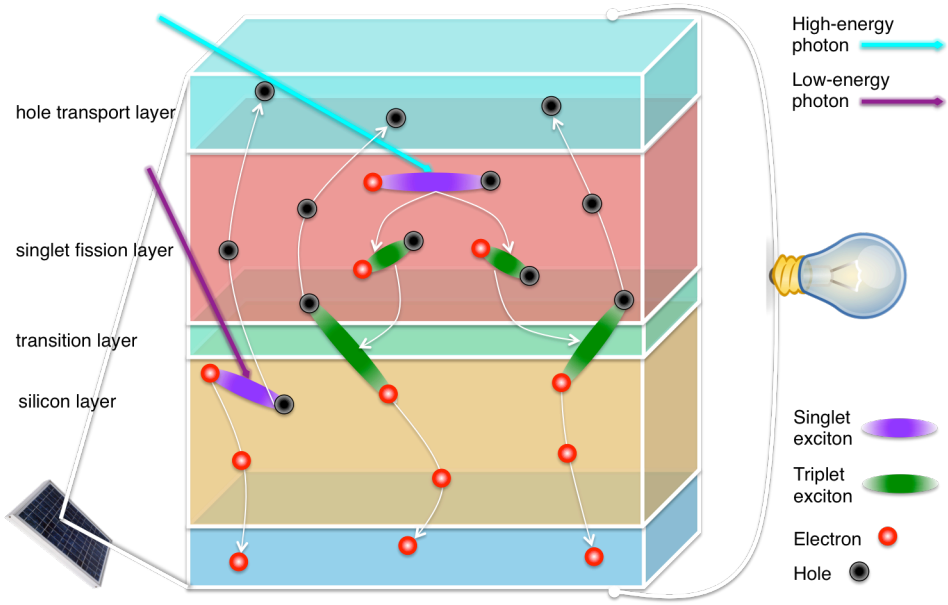

6.1 Comprehensive View

The aim of the theoretical study and computational modelling conducted in this thesis is to determine the singlet fission (SF) mechanism and the suitability of chromophores that satisfy the basic energetic requirements. On one hand, the static quantum chemical calculations of the electronic Hamiltonian matrix elements in the diabatic representation of the states involved in SF facilitate the investigation of the SF mechanism and of the role of charge transfer states. On the other hand, the nonadiabatic excited state dynamics simulations of SF rationalise the fission dynamics and enable one to explore other possible competing processes that might decrease the SF quantum yield.

The diabatic representation is very useful to characterise the states involved in SF and to resolve the fission mechanism.[1,2] However, the construction of the diabatic states is not unique, and depending on how these states are built, the computed matrix elements and subsequently the electronic couplings will of course vary considerably. Therefore, we have applied the nonorthogonal configuration interaction (NOCI) approach to construct the diabatic states directly, to compute explicitly the electronic couplings in SF (parameter that can be used to determine the spontaneous SF), and to investigate the role of charge transfer states in SF. Although the calculations were performed using a minimal active space for describing the wave functions of each molecular state and using only two neighbouring molecules in the cluster, we have shown that the evaluation of electronic couplings using the NOCI method is feasible, providing a clear chemical interpretation of the diabatic states involved in SF. A next step for the future study will be: (i) to use more accurate wave functions to describe the molecular electronic state, and (ii) to include more than two neighbouring molecules in the cluster in order to study the delocalisation effects of the molecular excited states. Besides, more general aspects of the process can also be considered, such as the role of excimer states or other factors controlling the population of the ^{1}TT state.[3] The inclusion of other processes such as fluorescence, dissociation of the singlet coupled triplet states, intersystem crossing from the initially photoexcited state or from the ^{1}TT state to lower lying triplet states, and geometry relaxation for the evaluation of overall rates will ultimately lead to the prediction of the SF efficiency.[4]

The nonadiabatic excited state dynamics simulations of SF based on the trajectory surface hopping approach, which have been presented in Chapter 5, allow us: (i) to investigate the

evolution from the initial photoexcitation process to the transfer of population to the ^{1}TT state, (ii) to predict the lifetimes of excited states and the SF quantum yield, and (iii) to explore other processes that might occur during the dynamics such as the decay of the excited singlet state to the ground state or to close-lying triplet states, so identifying possible drawbacks of the simulated SF chromophores. The hybrid QM/MM approach adopted in these dynamics simulations has also the advantage to treat large systems and to include the environmental effects. In the nonadiabatic dynamics simulations of SF performed in this study, only a pair of neighbouring chromophores placed in the slip-stack orientation undergoing the photodynamics is treated at the QM level, while the crystal environment was described using a force field. Hence, a next step that can be done is to include more than two chromophores that are treated at the QM level, so that the delocalisation effects, which will decrease the transition energies of the excited states, on the transition rates and on the pathways can be investigated. A further challenge would be to include electron acceptor molecules or semiconductor materials in the simulated model, so that we can represent the real situation of the photovoltaic devices. This will complicate the computational modelling, but a more complete understanding on the excitation and/or energy transfer processes occurring in the photovoltaic devices can potentially be achieved.

So far, the incorporation of SF in solar cells has been applied using intermolecular SF chromophores in the crystalline structures, where the orientation between two neighbouring chromophores is mostly (slip-) stack, as in the two cases studied in this thesis.[5-8] However, several intramolecular SF chromophores in covalently linked dimers and polymers have also been recently proposed, designed, and synthesised.[9-14] Moreover, the effects of the solvent polarity on the spontaneous SF have recently been studied.[10,15] In this sense, the theoretical studies and computational modelling will become important in order to understand the electronic structure and properties of these chromophores, and also to further investigate the effects of solvent polarity on the SF rates. Understanding primarily the electronic structure of these chromophores would lead to further exploration of their potentials as SF chromophores. Furthermore, the computational modelling of the fission dynamics and of the photovoltaic devices would also gain an insight on how these chromophores can be used and integrated in solar cell applications.

Investigations on the diffusion of the generated singlet coupled triplet states from SF in the simulated models of photovoltaic devices will provide a good understanding on important

parameters that control the charge dissociation of triplet excitons at the interface. A comprehensive understanding starting from the initial photoexcitation of the chromophore to the formation of the singlet coupled triplet states even until the dissociation of the ^{1}TT state needs to be further studied and continuously explored because it is of great importance for the successful application of SF in solar cells, which may lead to high-performance solar cells.

6.2 References

(1) Smith, M. B.; Michl, J. Singlet fission. *Chem. Rev.* **2010**, *110*, 6891.

(2) Smith, M. B.; Michl, J. Recent advances in singlet fission. *Annu. Rev. Phys. Chem.* **2013**, *64*, 61.

(3) Dover, C. B.; Gallaher, J. K.; Frazer, L.; Tapping, P. C.; Petty, A. J.; Crossley, M. J.; Anthony, J. E.; Kee, T. W.; Schmidt, T. W. Endothermic singlet fission is hindered by excimer formation. *Nat. Chem.* **2018**, *10*, 305.

(4) Casanova, D. Theoretical modeling of singlet fission. *Chem. Rev.* **2018**, *118*, 7164.

(5) Congreve, D. N.; Lee, J.; Thompson, N. J.; Hontz, E.; Yost, S. R.; Reusswig, P. D.; Bahlke, M. E.; Reineke, S.; Van Voorhis, T.; Baldo, M. A. External quantum efficiency above 100% in a singlet-exciton-fission-based organic photovoltaic cell. *Science* **2013**, *340*, 334.

(6) Ehrler, B.; Walker, B. J.; Bôhm, M. L.; Wilson, M. W. B.; Vaynzof, Y.; Friend, R. H.; Greenham, N. C. In situ measurement of exciton energy in hybrid singlet-fission solar cells. *Nat. Commun.* **2012**, *3:1019*.

(7) Ehrler, B.; Wilson, M. W. B.; Rao, A.; Friend, R. H.; Greenham, N. C. Singlet exciton fission-sensitized infrared quantum dot solar cells. *Nano Lett.* **2012**, *12*, 1053.

(8) Lee, J.; Jadhav, P.; Reusswig, P. D.; Yost, S. R.; Thompson, N. J.; Congreve, D. N.; Hontz, E.; Van Voorhis, T.; Baldo, M. A. Singlet exciton fission photovoltaics. *Acc. Chem. Res.* **2013**, *46*, 1300.

(9) Busby, E.; Xia, J.; Wu, Q.; Low, J. Z.; Song, R.; Miller, J. R.; Zhu, X.-Y.; Campos, L. M.; Sfeir, M. Y. A design strategy for intramolecular singlet fission mediated by charge-transfer states in donor-acceptor organic materials. *Nat. Mater.* **2015**, *14*, 426.

(10) Fuemmeler, E. G.; Sanders, S. N.; Pun, A. B.; Kumarasamy, E.; Zeng, T.; Miyata, K.; Steigerwald, M. L.; Zhu, X.-Y.; Sfeir, M. Y.; Campos, L. M.; Ananth, N. A direct mechanism

of ultrafast intramolecular singlet fission in pentacene dimers. *ACS Central Science* **2016**, *2*, 316.

(11) Lavarda, G.; Zirzlmeier, J.; Gruber, M.; Rami, P. R.; Tykwinski, R. R.; Torres, T.; Guldi, D. M. Tuning intramolecular Förster resonance energy transfer and activating intramolecular singlet fission. *Angew. Chem. Int. Ed.* **2018**, *57*, 1.

(12) Minami, T.; Ito, S.; Nakano, M. Theoretical study of singlet fission in oligorylenes. *J. Phys. Chem. Lett.* **2012**, *3*, 2719.

(13) Sanders, S. N.; Kumarasamy, E.; Pun, A. B.; Trinh, M. T.; Choi, B.; Xia, J.; Taffet, E. J.; Low, J. Z.; Miller, J. R.; Roy, X.; Zhu, X.-Y.; Steigerwald, M. L.; Sfeir, M. Y.; Campos, L. M. Quantitative intramolecular singlet fission in bipentacenes. *J. Am. Chem. Soc.* **2015**, *137*, 8965.

(14) Zeng, T.; Goel, P. Design of small intramolecular singlet fission chromophores: An azaborine candidate and general small size effects. *J. Phys. Chem. Lett.* **2016**, *7*, 1351.

(15) Montero, R.; Martínez-Martínez, V.; Longarte, A.; Epelde-Elezcano, N.; Palao, E.; Lamas, I.; Manzano, H.; Agarrabeitia, A. R.; López-Arbeloa, Í.; Ortiz, M. J.; Garcia-Moreno, I. Singlet fission mediated photophysics of BODIPY dimers. *J. Phys. Chem. Lett.* **2018**, *9*, 641.

Summary

Singlet fission is one feasible strategy for the next generation solar cells, enabling the possibility to overcome the theoretical limit efficiency of a single junction solar cell. In the singlet fission solar cell, high-energy photons are absorbed and then two low-energy excitons are generated per absorbed photon. In the singlet fission process, an optically excited singlet state of one chromophore is converted into a pair of triplet states in two neighbouring chromophores, which are transiently correlated to a singlet-spin state. The lack of microscopic understanding of the mechanisms through which singlet fission occurs has brought to the development of both experimental techniques and theoretical studies. Experiments with ultrafast lasers such as time-resolved two-photon photoelectron spectroscopy and two-dimensional electronic spectroscopy have provided more detailed information of the excited state dynamics of singlet fission chromophores, following the course of this process. However, the interpretation of these measurements is not always straightforward, and hence calls for theoretical studies and computational modelling of singlet fission dynamics. The computational modelling of singlet fission dynamics often complements the experimental findings. It opens up a channel for guiding the interpretation of experimental measurements and allows to explore the singlet fission mechanisms, rendering a more complete understanding of fission dynamics through which key determining factors controlling the singlet fission efficiency would potentially be identified.

From singlet fission to solar cell

Singlet fission, a process whereby an optically spin singlet excited state is converted into two triplet states that are coupled into a singlet state (^{1}TT), has been discussed in the literature for five decades. However, only in the last decade, the interests on fundamentals of singlet fission have emerged, driven by its promising potential to improve the efficiency of solar cells. The technological application of singlet fission in solar cells has been demonstrated in various proof-of-principle studies using polyacenes.

Polyacenes such as tetracene and pentacene are prototype singlet fission chromophores, which have been widely studied both experimentally and theoretically. In bulk pentacene, efficient fission was found to occur very rapidly, relying on very strong electronic coupling between the initially singlet excited state and the correlated triplet states. Nevertheless, such sizeable electronic coupling seems inconsistent with most recent time-resolved spectroscopic studies that pointed out the importance of vibronic couplings. Transient absorption measurements on pentacene derivatives suggested that the driving fission mechanism is a conical intersection. Yet, two-dimensional electronic spectroscopy measurements showed that high-frequency intramolecular vibrations generate a resonance between excited singlet state and correlated triplets, enhancing the population transfer to the ^{1}TT state.

The occurrence of singlet fission in other chromophores than polyacenes has remained a quite rare and exotic phenomenon. A theoretical study based on a simple model was performed to provide a guideline for the design of singlet fission chromophores and for finding mutual orientations between pairs of chromophores resulting in sufficiently large electronic coupling. This study was followed by other theoretical and experimental studies in order to search for potential chromophores, expanding the spectrum of suitable chromophores. Nonetheless, their fission dynamics remain unknown, and even their technological applications in solar cells still have a long way to go.

Equivocal explanations of experimental measurements and lack of microscopic understanding of singlet fission dynamics have called for theoretical studies and computational modelling and simulation. With regard to this need, computational modelling and simulations come first and can be a useful basis for: (i) planning the experiment, (ii) guiding the interpretation of experimental results, (iii) engineering solar cell devices, and (iv) investigating the fission dynamics and mechanisms. By utilising these tools and by working in

close collaboration with other experimental and theoretical groups, the realisation of high-performance singlet fission solar cells would more easily be achieved.

This thesis

Fundamental interest in singlet fission has driven the research presented in this thesis. The aim is to investigate the singlet fission mechanism from the static picture of the process by means of electronic structure calculations and to understand the fission dynamics with the aid of nonadiabatic dynamics simulations, enabling the prediction of the singlet fission mechanisms, the quantum yield, and the excited state lifetimes.

Two recently proposed chromophores, namely the bis(inner salt) of 2,5-dihydroxy-1,4-dimethyl-pyrazinium (DHDMPY) and 2,5-bis(fluorene-9-ylidene)-2,5-dihydrothiophene (ThBF), satisfy the basic energetic criteria of singlet fission chromophores according to quantum chemical calculations. With respect to the latter chromophore, its technological application in solar cells has also been demonstrated by using it as an electron donor in solar cell devices. However, the singlet fission mechanisms and dynamics of both chromophores are hitherto unknown.

In Chapter 3, the static picture of singlet fission in DHDMPY was obtained by computing electronic couplings between the initial singlet diabatic state and the final ^{1}TT state employing a rigorous nonorthogonal configuration interaction approach. The magnitude of electronic couplings is an important parameter for determining the rate of the conversion from a photoexcited singlet state to the ^{1}TT state. This rigorous approach allows the direct calculation of diabatic states in terms of antisymmetrised products of molecular wave functions, the inclusion of important static electron correlation and orbital relaxation effects, and a clear chemical interpretation of states involved in terms of molecular states. The results indicated that the inclusion of charge-transfer configurations enhances the computed electronic couplings, and these states act as virtual states. Also, the computed electronic couplings depend on the geometry of the molecules and the molecular wave functions used to construct the diabatic states. Nevertheless, the resulting couplings, which were obtained using

antisymmetrised products of molecular complete active space self-consistent field wave functions with a minimal active space that is composed of two frontier molecular orbitals, showed that DHDMPY is indeed a potential singlet fission chromophore.

In Chapter 4, following the results obtained from the electronic structure calculations of DHDMPY; an attempt to simulate its fission dynamics was performed. The preliminary results showed that this molecule is in practice not useful as singlet fission chromophore without a structural modification because it dimerises in the ground state according to the semiempirical QM/MM treatment. This would also explain the difficulties experienced by our experimental colleagues, when they tried to synthesise this molecule. However, the semiempirical Hamiltonian used in this dynamics simulation was not optimised to treat the dimerisation reaction, thus it has to be tested against higher quality calculations. The most accurate results we obtained suggested that the dimerisation reaction is exoergic and required the determination of the activation energy, which is a difficult task due to the partially open-shell character of this molecule and one cannot rely on the density functional theory.

Lastly, in Chapter 5, the singlet fission dynamics simulations of a pair of ThBF molecules embedded in their crystal environment were carried out, aiming to shed light on the photodynamics of this molecule. The simulations were performed by means of trajectory surface hopping approach, by computing 'on-the-fly' the electronic energies and wave functions employing the semiempirical floating occupation molecular orbital–configuration interaction method. The essential steps of the dynamics are the decay from the bright excitonic state to the underlying dark state, and from the latter to the correlated triplet states, the ^{1}TT state. The first step is initially ultrafast, but is subsequently slowed down by transitions to close-lying higher states, resulting in biexponential behaviour. The shorter lifetime of this state is about one hundred femtoseconds, but after the first ~200 femtosecond, the state populations evolve in the picosecond time scale. The dark state converts to the ^{1}TT state when the two molecules move closer, at geometries where the two states are almost degenerate. The interaction responsible for this transition is essentially mediated by higher lying charge transfer states. The singlet fission quantum yield is predicted to be close to the theoretical upper limit of 200%. Very little decay from the dark state to the ground state occurs. Upon inclusion of spin orbit coupling in the simulation, no decay of the ^{1}TT state to the lower but close lying single excitation triplet states is observed. The low efficiency of

photoenergy conversion measured in previous experiments can be attributed to the low adiabatic energy of the ThBF triplets.

Finally

As the computer and information technology is getting more powerful over time, the technical implementation of computational modelling and simulations will only improve. Besides, more sophisticated and integrative approaches along with more powerful computers allow for calculation of the fission rates and dynamics of molecular and extended systems in an accurate way. These developments, which have their roots in the work that many researchers have done over the past years, will bring much progress in the research of singlet fission and its technological application for high-performance solar cells.

Samenvatting

'Singlet fission' is een van de mogelijke strategieën voor de volgende generatie zonnecellen die het mogelijk maakt de theoretische limiet voor de efficiëntie van de 'single junction' zonnecel te doorbreken. In een singlet fission zonnecel worden hoogenergetische fotonen geabsorbeerd die vervolgens resulteren in twee excitonen per geabsorbeerd foton. In het singlet fission proces wordt een optisch aangeslagen singlet toestand van een chromofoor omgezet in triplet toestanden op twee naburige chromoforen die gecorreleerd zijn als een singlet spin toestand. Het ontbreken van een microscopisch begrip van het singlet fission mechanisme heeft tot de ontwikkeling van zowel experimentele technieken als theoretische studies geleid. Experimenten met ultrasnelle lasers aan het verloop van dit proces, zoals tijd-opgeloste twee-foton foto-elektron spectroscopie en tweedimensionale elektron spectroscopie, hebben meer gedetailleerde informatie over de dynamica van de aangeslagen toestand van de singlet fission chromoforen opgeleverd. Echter de interpretatie van deze metingen is niet altijd eenvoudig. Dit heeft geleid tot theoretische studies en computationele modellering van de singlet fission dynamica. Modellering van de dynamica van singlet fission vult vaak de experimentele bevindingen aan. Het helpt bij de interpretatie van experimentele metingen en maakt onderzoek naar het mechanisme van singlet fission mogelijk. Zodoende ontstaat een beter begrip van de dynamica en zouden belangrijke factoren die van invloed zijn op de singlet fission efficiëntie kunnen worden gevonden.

Van ‘singlet fission’ tot zonnecel

Al vijf decennia wordt er in de literatuur over singlet fission gediscussieerd. Singlet fission is een proces waar een optische spin-singlet aangeslagen toestand wordt omgezet in twee triplet toestanden die gekoppeld zijn tot een singlet toestand (^{1}TT). Gemotiveerd door een veelbelovend potentieel om de efficiëntie van zonnecellen te vergroten is er in het laatste decennium interesse ontstaan in de grondslagen van singlet fission. In diverse ‘proof-of-principle’ studies aan polyacenen is de technologische bruikbaarheid van singlet fission in zonnecellen aangetoond.

Polyacenen zoals tetraceen en pentaceen zijn prototype singlet fission chromoforen die uitgebreid zijn bestudeerd, zowel experimenteel als theoretisch. In bulk pentaceen is efficiënte singlet fission gevonden die heel snel plaatsvindt en berust op sterke elektronische koppeling tussen de initiële singlet aangeslagen toestand en de gecorreleerde triplet toestanden. Anderzijds lijken dit soort grote elektronische koppelingen inconsistent met de meest recente tijd opgeloste spectroscopische studies die het belang aanduiden van vibronische koppelingen. Uit ‘transient’ absorptie metingen aan pentaceen derivaten wordt gesuggereerd dat een conische intersectie de drijvende kracht achter het singlet fission mechanisme is. Echter twee-dimensionele elektronische spectroscopie metingen laten zien dat hoog frequente intramoleculaire vibraties een resonantie tussen de aangeslagen singlet toestand en de gecorreleerde triplets opleveren die de populatie overdracht naar de ^{1}TT toestand vergroot.

Het voorkomen van singlet fission in andere materialen dan polyacenen blijft een zeldzaam en exotisch fenomeen. Een op een eenvoudig model gebaseerde theoretische studie is uitgevoerd om als richtlijn te dienen voor het ontwerp van singlet fission chromoforen en voor het vinden van oriëntaties tussen chromofoorparen die leiden tot een voldoende grote elektronische koppeling. Deze studie werd gevolgd door andere theoretische en experimentele studies om te zoeken naar potentiële chromoforen en om daarmee het arsenaal van geschikte chromoforen te vergroten. Niettemin blijft de singlet fission dynamica vooralsnog onbekend en er is nog een lange weg te gaan voordat singlet fission toegepast kan worden in zonnecellen.

Het gemis aan een microscopisch begrip van de dynamica van singlet fission en dubbelzinnige verklaringen van experimentele metingen maken de noodzaak duidelijk voor theoretische studies en computationele modellering en simulaties. Met betrekking tot het

gemis aan begrip dient computationele modellering en simulatie eerst gedaan te worden en dat kan een bruikbare basis zijn voor: (i) de planning van experiment, (ii) de interpretatie van experimentele resultaten, (iii) de constructie van zonnecellen, (iv) het onderzoek naar singlet fission dynamica en mechanismes. Door gebruik te maken van deze tools en door nauw samen te werken met andere experimentele en theoretische groepen kan de realisatie van zeer goed presterende singlet fission zonnecellen mogelijk worden bereikt.

Dit proefschrift

De interesse in de grondslagen van singlet fission is de drijvende kracht achter het onderzoek in dit proefschrift. Het doel is het statische beeld van het mechanisme van singlet fission te onderzoeken door middel van elektronische structuur berekeningen. Begrip van de dynamica van singlet fission wordt onderzocht met behulp van niet-adiabatische dynamica simulaties. Dat maakt een voorspelling mogelijk van het singlet fission mechanisme, de kwantum opbrengst en de levensduur van aangeslagen toestanden.

Twee recent voorgestelde chromoforen, namelijk het bis(inner salt) van 2,5-dihydroxy-1,4-dimethyl-pyrazinium (DHDMPY) en 2,5-bis(fluorene-9-ylidene)-2,5-dihydrothiophene (ThBF) voldoen aan de energetische basisvoorwaarden voor singlet fission chromoforen volgens kwantum chemische berekeningen. Met betrekking tot het laatste chromofoor is de technologische toepassing in zonnecellen aangetoond door het als elektron donor te gebruiken. Echter de singlet fission mechanismen en dynamica van beide chromoforen is tot nu toe onbekend.

In hoofdstuk 3, het statische beeld van singlet fission in DHDMPY is verkregen door elektronische koppelingen tussen de diabatische singlet begintoestand en de ^{1}TT eindtoestand uit te rekenen met een niet-orthogonale configuratie interactie aanpak. De grootte van de elektronische koppelingen is een belangrijke parameter voor het bepalen van de snelheid van de conversie van een geëxciteerde singlet toestand naar de ^{1}TT toestand. Deze aanpak berust op de berekening van diabatische toestanden in termen van anti-gesymmetriseerde producten van moleculaire golffuncties. Het brengt belangrijke statische elektroncorrelatie en orbitaal

relaxatie effecten in rekening, en het biedt bovendien een duidelijke chemische interpretatie van de betrokken toestanden in termen van moleculaire toestanden. De resultaten geven aan dat het gebruik van 'charge transfer' configuraties de berekende elektronische koppelingen vergroot en dat deze toestanden als virtuele toestanden optreden. Ook hangen de berekende elektronische koppelingen af van de geometrie van de moleculen en van de gebruikte moleculaire golffuncties om de diabatische toestanden te construeren. Niettemin tonen de resulterende koppelingen, die zijn verkregen met anti-gesymmetriseerde producten van moleculaire 'complete active space self-consistent' field golffuncties en met een minimale actieve ruimte die is opgebouwd uit twee moleculaire orbitalen, aan dat DHDMPY inderdaad een mogelijke singlet fission chromofoor is.

In hoofdstuk 4, volgend op de resultaten die werden verkregen uit elektronenstructuur berekeningen aan DHDMPY wordt een poging gedaan om de singlet fission dynamica ervan te simuleren. De voorlopige resultaten lieten zien dat dit molecule in de praktijk niet bruikbaar is als singlet fission chromofoor zonder een structurele aanpassing omdat volgens de semi-empirische QM/MM studie het dimeriseert in de grondtoestand. Dit zou ook de moeilijkheden kunnen verklaren die onze experimentele collegae ervaren wanneer ze dit molecule proberen te synthetiseren. Echter, de semiempirische Hamiltonian die gebruikt werd in deze dynamica simulaties was niet geoptimaliseerd voor een dimerisatie reactie, dus moet het resultaat getest worden met berekeningen van hogere kwaliteit. De meest nauwkeurige resultaten die we verkregen suggereren dat de dimerisatiereactie exoenergetisch is en dat de bepaling van de activeringsenergie benodigd is. Dit is een moeilijke taak door het gedeeltelijk open-schil karakter van dit molecule waardoor niet kan worden vertrouwd op dichtheidsfunctionaaltheorie.

Tenslotte, in hoofdstuk 5, zijn singlet fission dynamica simulaties uitgevoerd voor een paar in hun kristal omgeving ingebedde ThBF moleculen met als doel om de fotodynamica van dit molecule te bekijken. De simulaties werden uitgevoerd met een 'trajectory surface hopping' benadering door 'on-the-fly' elektronische energieën en golffuncties te berekenen met de semiempirische 'floating occupation molecular orbital–configuration interaction' methode. De essentiële stappen van de dynamica zijn het verval van de initiële exciton toestand via een lagere optisch niet-actieve toestand naar de gecorreleerde triplet toestand: de ^{1}TT toestand. Het proces verloopt initieel heel snel maar verdere overgangen naar dichtbij aangeslagen toestanden verlopen vervolgens langzamer hetgeen resulteert in biexponentieel

gedrag. De exciton toestand heeft een levensduur van ongeveer honderd femtoseconden. Ongeveer na de eerste 200 femtoseconden veranderen de toestand populaties op picoseconden tijdschaal. De conversie van de optisch niet-actieve toestand naar de ^{1}TT toestand verloopt wanneer de twee moleculen elkaar naderen met geometrieën waarbij de twee toestanden bijna ontaard zijn. De interactie die verantwoordelijk is voor deze overgang wordt in essentie gemedieerd door hoger liggende 'charge transfer' toestanden. De voorspelde singlet fission kwantum opbrengst ligt dichtbij de bovenlimiet van 200%. Er is weinig verval van de optisch niet bereikbare toestand naar de grondtoestand. Ook wanneer we spin-baan koppeling in rekening brengen in de simulaties zien we geen verval van de ^{1}TT naar de lager liggende moleculaire triplet toestanden. Het lage rendement van foto-energieconversie gemeten in eerdere experimenten kan worden toegeschreven aan de lage adiabatische energie van de ThBF-tripletten.

Tenslotte

Zoals de computer en informatietechnologie over de tijd verbetert zal ook de technische implementatie van computationele modellering en simulaties verbeteren. Bovendien kunnen met betere en meer integrale benaderingen samen met krachtigere computers op een nauwkeurige manier de singlet fission snelheden en dynamica van moleculaire en uitgebreide systemen berekend worden. Deze ontwikkelingen, die hun oorsprong hebben in het werk dat veel onderzoekers hebben gedaan over de laatste jaren, zullen veel vooruitgang brengen in het onderzoek naar singlet fission en technologische toepassing ervan voor hoogwaardige zonnecellen.

Riassunto

La 'singlet fission' costituisce una possibile strategia per lo sviluppo di celle fotovoltaiche di nuova generazione che possano portare al superamento del limite teorico di efficienza delle celle a giunzione singola. In una cella fotovoltaica a singlet fission, i fotoni con alta energia vengono assorbiti e quindi vengono generati due eccitoni a bassa energia per fotone assorbito. Nel processo di singlet fission, un stato eccitato per via ottica viene convertito in due stati di tripletto che sono temporaneamente accoppiati in uno stato di singoletto. La mancanza di comprensione dei meccanismi microscopici attraverso i quali si verifica la singlet fission ha portato allo sviluppo sia di tecniche sperimentali che di studi teorici. Esperimenti che utilizzano 'ultrafast laser' come la 'time-resolved two-photon photoelectron spectroscopy' e la 'two-dimensional electronic spectroscopy' hanno fornito informazioni dettagliate sulla dinamica degli stati eccitati di cromofori che mostrano singlet fission, permettendo di studiare questo processo. L'interpretazione di questi studi sperimentali però non è banale ma anzi richiede l'aiuto di studi teorici e modelli computazionali per la dinamica di singlet fission. La modellazione computazionale della dinamica di singlet fission complementa spesso risultati sperimentali, guidando così l'interpretazione di detti risultati e permettendo di esplorare il meccanismo della singlet fission; questo fa sì che si possa raggiungere una comprensione più completa della singlet fission attraverso la quale fattori chiave che ne controllano l'efficienza possono essere identificati.

Dalla ‘singlet fission’ alla cella solare

La singlet fission, un processo dove un stato di spin singoletto eccitato per via ottica viene convertito in due stati di tripletto che sono accoppiati in stato di singoletto (^{1}TT), è stato discusso nella letteratura scientifica per cinque decenni. Tuttavia, è solo nell’ultimo decennio che interessi negli aspetti fondamentali della singlet fission sono emersi, spinti dalla promessa di poter riuscire a migliorare l’efficienza di celle solari. L’applicazione tecnologica della singlet fission in celle solari è stata dimostrata in vari studi di ‘proof-of-principle’ utilizzando poliaceni.

Poliaceni come il tetracene e il pentacene sono cromofori prototipi per la singlet fission e sono stati studiati sia dal punto di vista sperimentale che teorico. Nel caso del pentacene, la singlet fission occorre efficientemente e molto rapidamente, facendo leva su accoppiamenti elettronici molto forti fra gli stati di singoletto iniziali e gli stati di tripletto correlati. Tuttavia, accoppiamenti elettronici di tale grandezza sembrano essere incompatibili con recenti risultati ottenuti via ‘time-resolved spectroscopy’, i quali hanno evidenziato l'importanza degli accoppiamenti di tipo vibronico. Misurazioni di ‘transient absorption’ eseguiti su derivati del pentacene suggeriscono che il meccanismo chiave per la singlet fission coinvolga una ‘conical intersection’. Inoltre, studi di ‘two-dimensional electronic spectroscopy’ hanno mostrato che vibrazioni intramolecolari ad alta frequenza generano una risonanza fra lo stato eccitato di singoletto e gli stati correlati di tripletto, intensificando così il population transfer verso lo stato ^{1}TT.

Che la singlet fission venga osservata in molecole che non siano poliaceni è rimasto un fenomeno piuttosto raro ed esotico. Uno studio teorico basato su un modello semplice è stato condotto con lo scopo di tracciare delle line guida per il design di cromofori per la singlet fission e allo stesso tempo individuare le mutue orientazioni fra coppie di tali cromofori che danno luogo ad accoppiamenti elettronici sufficientemente grandi. Questo studio è stato seguito da altri studi teorici e sperimentali volti alla ricerca di potenziali cromofori, espandendo così lo spettro di cromofori idonei alla singlet fission. Ciònonostante, la dinamica della singlet fission di tali cromofori rimane sconosciuta e la loro applicazione tecnologica in celle solari ha ancora molta strada da fare.

Le spiegazioni ambigue delle misurazioni sperimentali e la mancanza di comprensione microscopica della dinamica della singlet fission hanno richiesto studi teorici, modelli

computazionali e simulazioni. A questo proposito, modelli computazionali e simulazioni possono formare una utile base per: (i) pianificare esperimenti, (ii) guidare l'interpretazione di risultati sperimentali, (iii) concepire l'architettura delle celle solari a singlet fission, e (iv) studiare la dinamica della singlet fission e il suo meccanismo. Utilizzando questi strumenti e lavorando in stretta collaborazione con altri gruppi sperimentali e teorici, la realizzazione di celle solari a singlet fission ad alte prestazioni può essere raggiunta.

Questa tesi

L'interesse negli aspetti fondamentali della singlet fission ha motivato la ricercar presentata in questa tesi. Lo scopo è quello di esaminare il meccanismo della singlet fission da un punto di vista statico tramite dai calcoli di struttura elettronica e di capire la dinamica di singlet fission con l'aiuto di 'nonadiabatic dynamics simulations', che permettono di predire i meccanismi di singlet fission, le rese quantiche e i lifetime degli stati eccitati.

Due cromofori suggeriti recentemente, il bis(inner salt) di 2,5-dihydroxy-1,4-dimethyl-pyrazinium (DHDMPY) e il 2,5-bis(fluorene-9-ylidene)-2,5-dihydrothiophene (ThBF), soddisfano i criteri energetici di base per la realizzazione della singlet fission sulla base di calcoli di 'quantum chemical calculations'. Sulla base di quest'ultimo cromoforo, l'applicazione tecnologica di questo cromoforo in celle solari è stata dimostrata anche usandoli come accettori di elettroni in dispositivi a celle solari. Tuttavia, il meccanismo e la dinamica di singlet fission per entrambi i cromofori sono finora sconosciuti.

Nel capitolo 3, un punto di vista statico sulla singlet fission in DHDMPY è stato ottenuto calcolando gli accoppiamenti elettronici fra lo stato diabatico iniziale di singoletto e lo stato finale ^{1}TT tramite un metodo rigoroso: l'interazione di configurazione non-ortogonale. L'entità degli accoppiamenti elettronici è un parametro importante per determinare la singlet fission spontanea, principalmente per la conversione da uno stato di singoletto fotoeccitato allo stato ^{1}TT. Questo metodo rigoroso permette il calcolo diretto di stati diabatici come prodotti antisimmetrizzati di funzioni d'onda molecolari, il trattamento di importanti effetti di correlazione elettronica statica e effetti di rilassamento degli orbitali, e una chiara

interpretazione chimica degli stati coinvolti in termini di stati molecolari. I risultati indicano che l'inclusione delle configurazioni di trasferimento di carica aumenta l'entità degli accoppiamenti elettronici ottenuti e che tali stati agiscono da stati virtuali. Inoltre, gli accoppiamenti elettronici ottenuti dipendono dalla geometria delle molecole e dalle funzioni d'onda molecolari utilizzate per costruire gli stati diabatici. Ad ogni modo, gli accoppiamenti risultanti, ottenuti utilizzando prodotti antisimmetrizzati di funzioni d'onda 'complete active space self-consistent field' molecolari con un minimalo 'active space' composto da due orbitali di frontiera, mostrano come DHDMPY sia indubbiamente un potenziale cromoforo per la singlet fission.

Nel capitolo 4, dopo aver ottenuto questi risultati dai calcoli di struttura elettronica di DHDMPY, è stato eseguito un tentativo di simulare la sua dinamica di singlet fission. Risultati preliminari mostrano come questa molecola non sia adatta in pratica alla singlet fission senza nessuna modifica strutturale poichè dimerizza nel suo stato fondamentale secondo calcoli semiempirici QM/MM. Questo spiegherebbe anche le difficoltà incontrate dai nostri collaboratori sperimentali nel sintetizzare questa molecola. Tuttavia, l'hamiltoniano semiempirico usato in questa simulazione della dinamica non era stato ottimizzato per il trattamento di reazioni di dimerizzazione e perciò dovrà essere testato tramite comparazione con calcoli di qualità più elevata. I risultati più accurati che abbiamo ottenuto suggeriscono che la reazione di dimerizzazione è esoenergetica e richiede la determinazione di una energia di attivazione; quest'ultimo è un compito difficile a causa del carattere parzialmente 'open-shell' di questa molecola per cui non si può fare affidamento sulla teoria del funzionale della densità.

Infine, nel capitolo 5, simulazioni della dinamica di singlet fission di una coppia di molecole di ThBF circondate dal loro ambiente cristallino sono state eseguite con l'intento di fare luce sulla fotodinamica di tale molecola. Le simulazioni sono state eseguite per mezzo di un approccio di 'trajectory surface hopping', calcolando 'on-the-fly' le energie elettroniche e le funzioni d'onda impiegando il metodo semiempirico 'floating occupation molecular orbital–configuration interaction'. I passaggi essenziali della dinamica sono il decadimento dal 'bright excitonic state' verso il sottostante 'dark state' e da quest'ultimo agli stati di tripletto correlati, ^{1}TT. Il primo passaggio è inizialmente ultraveloce, con un lifetime di circa cento femtosecondi; tuttavia, viene successivamente rallentato da transizioni verso 'close-lying higher states', risultando in un decadimento biesponenziale. Dopo i primi ~200

femtosecondi, le popolazioni degli stati evolvono nella scala temporale del picosecondo. Il dark state si converte nello stato ^{1}TT quando le due molecole si avvicinano, in geometrie dove questi due stati sono quasi degeneri. L'interazione responsabile per questa transizione è essenzialmente mediate da stati di trasferimento di carica più alti in energia. La resa quantica di singlet fission predetta è vicina al limite superiore teorico del 200%. Viene osservato un decadimento molto piccolo dal dark state allo stato fondamentale. A seguito dell'inclusione dell'accoppiamento spin-orbita nella simulazione, non si osserva alcun decadimento dello stato ^{1}TT verso gli stati di tripletto con energia più bassa. La bassa efficienza della conversione fotoelettrica misurata in esperimenti precedenti può essere attribuita alla bassa energia adiabatica delle triplette ThBF.

Infine

Man mano che il computer e la tecnologia informatica miglioreranno nel tempo, l'implementazione tecnica della modellazione e delle simulazioni computazionali migliorerà. Inoltre, approcci più raffinati e integrativi con computer più potenti possono calcolare i tassi di fissione e le dinamiche dei sistemi molecolari ed estesi in modo accurato. Questi sviluppi, che hanno le loro radici nel lavoro svolto da molti ricercatori nel corso degli ultimi anni, porteranno progressi avanzati alla ricerca della fissione di singoletto e alla sua applicazione tecnologica per celle solari ad alte prestazioni.

Glossary

AO	Atomic orbital
ASP	Antisymmetrised product
BOA	Born Oppenheimer approximation
CASPT2	Complete active space second order perturbation theory
CASSCF	Complete active space self-consistent field
CC	Coupled cluster
CI	Configuration interaction
CNDO	Complete neglect of differential overlap
CSF	Configuration state function
DFT	Density functional theory
DHDMPY	Bis(inner salt) of 2,5-dihydroxy-1,4-dimethyl-pyrazinium
FOMO–CI	Floating occupation molecular orbital–configuration interaction
FORS	Fully optimised reaction space
FSD	Fragment spin difference
FSSH	Fewest switches surface hopping
GGA	Generalised gradient approximation
GTO	Gaussian-type orbital
H-K	Hohenberg-Kohn
HF	Hartree-Fock
HOMO	Highest occupied molecular orbital
IC	Internal conversion
ISC	Intersystem crossing
INDO	Intermediate neglect of differential overlap
KS-DFT	Kohn-Sham density functional theory

LDA	Local density approximation
LUMO	Lowest unoccupied molecular orbital
MCSCF	Multiconfigurational self-consistent field
MCTDH	Multiconfigurational time-dependent Hartree
MM	Molecular mechanics
MO	Molecular orbital
MPPT	Møller-Plesset perturbation theory
NDDO	Neglect of diatomic differential overlap
NOCI	Nonorthogonal configuration interaction
PES	Potential energy surface
PT	Perturbation theory
QM	Quantum mechanics
RASSCF	Restricted active space self-consistent field
RSPT	Rayleigh-Schrödinger perturbation theory
SCVB	Spin-coupled valence bond
SF	Singlet fission
SH	Surface hopping
SOC	Spin-orbit coupling
STO	Slater-type orbital
TD-DFT	Time-dependent density functional theory
TDSE	Time-dependent Schrödinger equation
ThBF	2,5-bis(fluorene-9-ylidene)-2,5-dihydrothiophene
VB	Valence bond
ZDO	Zero differential overlap

Acknowledgements

Finally, I arrive in the least scientific part of the entire thesis, but it is the most exciting part to write (as well as to read, my guess). I found this small piece of writing is the only part in the entire thesis where I can express how grateful I am not only because I succeeded in completing this thesis but most of all for whom I have become at the end. I had started my PhD training back in 2015 when the leaf colours started to warm up with a great excitement and a huge ambition, but I had no ideas about how arduous the process would be. I thought sometimes I was at the top of a mountain, while at some other times I found myself in the deepest valley. Also, there was a time when I felt that this was too much to take on. Many times I thought how other people could carry on with this process. However, this process has changed and shaped me into a different person, in a positive way. It will always remind me of a great adventure of 39.5 months. Many people have been involved in different ways and in unexpected circumstances. For that, I would like to acknowledge them.

I am thankful for this great opportunity, which might not be existed without the persistency and hard work of a great team. I am deeply grateful to the coordinator, supervisory board members, and all supervisors from the consortium that have been working on the ITN-EJD-TCCM programme, starting from the preparation, application, execution, implementation even until the ending of this programme. Many things have to be taken care of and adjusted along the way, some of them turned out well but not all of them. However, at the end, we have succeeded to arrive at the finish line regardless the complicated bureaucracy and administrative tasks.

Ria, I am forever grateful for you being there and for walking together through the hardest part of this journey. Thank you for your concern, patience, caring, support, and understanding. Your critiques and unexpected (simple but not always!) questions during our

discussions always intrigue me to think over and over again, to look at the problems from different point of view, to find the reasons, and finally to understand them.

Maurizio, even with the workload as the director of the department, you still found some time to look at the results and to discuss them. Thank you for your time and critical comments on the obtained results, so that I could have paid more attention and have analysed them much deeper. Also, thank you for your guidance and kindness.

Remco, thank you for supervising all the work performed during the first part of this project. Working under your supervision allows me to learn different ways of thinking, to be more creative, and to be more multitasking, which (sometimes) is not easy to do.

Giovanni, thank you for the time you have spent on explaining the scientific and technical details of the codes. Without your help during the second part of this project, I will not be able to perform the semiclassical dynamics simulations and to understand them.

Ria, Maurizio, Remco, and Giovanni, thank you for the opportunity you have given me to be part in your scientific journey. Thank you for everything you have taught me.

I would like to acknowledge the assessment committee: Prof. Shirin Faraji, Prof. Ferdinand Grozema, Prof. Nathalie Guihéry, and Prof. Benedetta Mennucci. Thank you very much for your time and careful reading on this thesis.

To our emeritus professor, Wim Nieuwpoort, thank you very much! Thank you for your thoughtful advice and encouragement.

I would like to acknowledge Mónica Garciá-Mota and Federico Marchesin from the Simune Atomistic Simulations and David Lopez from the CIC NanoGUNE for our collaboration and insightful discussion during my short stay in San Sebastián, Spain.

I would like to acknowledge the coordinator of the Doctorate School at the Department of Chemistry and Industrial Chemistry, University of Pisa, Lorenzo Di Bari, for his support, caring, and kindness. Thank you for your warm welcome and 'PhD students get together' initiative in both formal and social events. This initiative has given us an opportunity to share our stories and good memories.

I would like to acknowledge our group leader, Shirin Faraji, for her support and motivation. Without your support, I would not have the courage to apply for the HPC-Europa3 grant. It was a great experience! Thank you, Shirin.

Even though it is not directly related with the work presented in this thesis, I would like also to acknowledge Dr. David Casanova who is willingly accepting my proposal to be my

host during the HPC-Europa3 programme. Thank you for letting me to learn a new technique while preparing my PhD thesis defence and enjoying the beautiful San Sebastián. Thank you for your support and for every fruitful discussion.

I am really thankful to Ms. Henriet and Ms. Maria Caccamo who have helped with all the bureaucracy, documentation, paperwork, and administration. Without your support, the transition from Groningen to Pisa and back to Groningen again would not be possible.

I am grateful for having other ITN-EJD-TCCM fellows who have shared this adventure together even though we were working in different projects, universities, and countries. It was a great fun that we were able to meet at least ten times (or even more) in our ten one-week mandatory activities and in other international conferences.

Anna and Luis, beside your support during these last three years, thank you for accepting to be my paranymphs. Also, I would like to thank you here (in advance) for all your assistances and help before, during and after the ceremony.

I would like to thank all members of the theoretical chemistry group at the University of Groningen and some colleagues at the Department of Chemistry and Industrial Chemistry, University of Pisa as well as some people whom I met along this journey and became friends. Marwa, thanks for cheering me up. Gerrit-Jan, Riccardo, Anna, Luis, María, Selim, Kathir, Tommy, Siva, Kiana, and Wouter thank you for sharing your ideas and time with me. Davide, your help during my stay in Pisa is really invaluable. Lorenzo, Marchin, Angelica, Giulia, Chiara, Serena, Silvia, Vittoria, Nicola, Lorenzo Portus, Annalisa, Enrico, Alessio, Francesca, Gianluigi, and Federica, your caring and support are greatly appreciated. I really enjoyed every short coffee break, lazy day, and random stroll after “super heavy” meal. Grazie mille, ragazzi! Ci vediamo quando ci vediamo!

This journey would not be possible without lovely families who allowed me to be part of their lives as well. Oom Fred and Tante Tini Berg deserve special thanks for their ceaseless moral support and hospitalities. Ika and Paul Hoogland, thank you for being great mentors and companies, thank you for every pleasant time and of course for every delicious meal. Jan Peter, Siska, Lauren, and little Killian Hooiveld, I am grateful for letting me to share part of this journey. Thank you for your moral support. Stella and Yovita, my not only food adventure companies, thank you also for our fellowship so that we could encourage and comfort one and another. Many thanks also to the GBI Groningen family.

My last but not least gratitude goes to my father, sisters, brother, and nieces for their wholehearted love and support, as well as their understanding and caring. Thank you for giving me a freedom to choose what I really want to do and for helping me to grow as a person. 感謝你們在我生命的每一條道路上都在那裡，並在你們的祈禱中永遠記得我。我真的感激你們。老爸 (Agus)，姐姐 (Ineke)，哥哥 (Dedy)，妹妹 (Mega)， Jocelyn，和 Michelle，感謝你們。願上帝保佑你們。

Groningen, December 2018,
Meilani Wibowo.

He hath made every thing beautiful in his time.

Ecclesiastes 3:11

Curriculum Vitae

About the author

Meilani Wibowo (1989) was born and raised in Surabaya, Indonesia. After graduating from the Frateran Catholic senior high school in 2007, she studied chemistry at the State University of Surabaya, Indonesia. She completed her undergraduate study in February 2011. While she was finding about her passion, she began working as a teaching assistant in the analytical chemistry laboratory at her alma mater and as a music teacher as her hobby, which she had already started earlier. Seven months later, in September 2011, she was awarded the Taiwanese government scholarship and started her master's degree in the chemistry-chemical engineering programme at the National Taiwan University of Science and Technology. After the completion of her master's degree in July 2013, instead of working in industry, she decided to pursue another master's degree focusing on the theoretical chemistry and computational modelling with the Erasmus Mundus scholarship at the University of Valencia, Spain and gained a distinction in her diploma. In 2015, she was accepted to work on a PhD project in Germany, however in the same year she was also accepted as one of the ITN-EJD-TCCM fellows. The exciting topic and opportunity to work in two different universities made her to choose the ITN-EJD-TCCM programme instead. She began her PhD project in the theoretical chemistry group in the Zernike Institute for Advanced Materials, University of Groningen under the supervision of Ria Broer and Remco Haventih, then she continued her PhD project in the Department of Chemistry and Industrial Chemistry, University of Pisa under the supervision of Maurizio Persico and Giovanni Granucci. During her time at the University of Groningen, she also gave assistances in the quantum chemistry and computational quantum chemistry computer laboratories. Her research interest focuses on the

computational modelling of the photophysical and photochemical processes in the excited states from electronic structure properties to dynamics. In her spare time, she still enjoys playing piano (if there is one), travelling, and dreaming to capture beautiful places around the world.

Publications

1. M. Wibowo, Maurizio Persico, and Giovanni Granucci, Nonadiabatic dynamics simulations of singlet fission in 2,5-bis(fluorene-9-ylidene)-2,5-dihydrothiophene crystals, *Phys. Chem. Chem. Phys.*, 2019, **21**, 692-701.
2. M. Wibowo, Ria Broer, and Remco W. A. Havenith, A rigorous nonorthogonal configuration interaction approach for the calculation of electronic couplings between diabatic states applied to singlet fission, *Comput. Theor. Chem.*, 2017, **1116**, 190-194.
3. M. Garazzi*, M. Wibowo*, H. Gattuso, E. Dumont, D. Roca-Sanjuán, and A. Monari, Hydrogen abstraction by photoexcited benzophenone: Consequences for DNA photosensitization, *Phys. Chem. Chem. Phys.*, 2016, **18**, 7829-7836. *Contributed equally.
4. E. Dumont, M. Wibowo, D. Roca-Sanjuán, M. Garavelli, X. Assfeld, and A. Monari, Resolving the benzophenone DNA-photosensitization mechanism at QM/MM level, *J. Phys. Chem. Lett.*, 2015, **6**, 576-580.

Honours and awards

1. HPC-Europa3 Transnational Access programme award for a short visit in the Donostia International Physics Center, University of the Basque Country, San Sebastian, Spain, working in collaboration with Dr. David Casanova on the combined restricted active space configuration interaction with the short-range density functional theory for understanding the electronic excited state properties: January – March 2019.

2. Marie Skłodowska-Curie Actions Innovative Training Networks (ITN-EJD-TCCM) project of three-year study award for a double doctorate's degree in the University of Groningen and in the University of Pisa: September 2015 – December 2018.
3. Premio Extraordinario de Máster del título de Máster en Erasmus Mundus en Química Teórica y Modelización Computational from the University of Valencia: 11 May 2016.
4. Erasmus Mundus scholarship of two-year study for a master's degree in the Theoretical Chemistry and Computational Modelling programme in the University of Valencia: July 2013 – August 2015.
5. Taiwanese government scholarship of two-year study for a master's degree in chemistry-chemical engineering in the National Taiwan University of Science and Technology: September 2011 – July 2013.
6. The best student award from the chemistry department, the State University of Surabaya, Indonesia: February 2011.
7. The State University of Surabaya scholarship for the top 10 students: August 2009 – February 2011.
8. Directorate General of Higher Education of Indonesia sponsorship for the student project creativity: 2009.